74-15,554

TONG, Kwok-On, 1945-
ON THE UNIFORMITY OF THE FLOW INITIATED
BY A NON-STEADY EXPANSION WAVE.

University of Washington, Ph.D., 1973
Engineering, aeronautical

University Microfilms, A XEROX Company, Ann Arbor, Michigan

ON THE UNIFORMITY OF THE FLOW INITIATED BY A NON-STEADY EXPANSION WAVE

by

KWOK-ON TONG

A dissertation submitted in partial fulfillment

of the requirements for the degree of

DOCTOR OF PHILOSOPHY

UNIVERSITY OF WASHINGTON

1973

Approved by ______________________________
(Chairman of Supervisory Committee)

Department Aeronautics and Astronautics
(Departmental Faculty sponsoring candidate)

Date August 29, 1973

UNIVERSITY OF WASHINGTON

Date: August 17, 1973

We have carefully read the dissertation entitled ON THE UNIFORMITY OF THE FLOW INITIATED BY A NON-STEADY EXPANSION WAVE submitted by Kwok-On Tong in partial fulfillment of the requirements of the degree of Doctor of Philosophy and recommend its acceptance. In support of this recommendation we present the following joint statement of evaluation to be filed with the dissertation.

This dissertation is a study of the flow within a long pressurized tube after activation of a fast-opening valve or rupture of a diaphragm. The effects of the nonsteady turbulent boundary layer as well as initial nonuniformities in pipe diameter and temperature are considered. The approach is to develop closed form analytic expressions for the flow perturbations based on a linearization of the equations of motion and simplifications of the boundary conditions at the two ends of the moving column of gas. Previously developed boundary layer models serve as inputs into the calculation. Pressure time-histories were measured and used to check the theory and its extension to high pipe flow Mach numbers, as well as to the limiting case where the pipe boundary layer has merged to produce a fully developed pipe flow. While the magnitude of many of the effects studied in this work were known for restricted cases from the work of previous authors, this is the first consistent and complete study of what has become an important and timely problem. We find this dissertation satisfactory in all respects.

DISSERTATION READING COMMITTEE: David A Russell
A. Hertzberg
John C Oates

Doctoral Dissertation

In presenting this dissertation in partial fulfillment of the requirements for the doctoral degree at the University of Washington, I agree that the Library shall make its copies freely available for inspection. I further agree that extensive copying of this dissertation is allowable only for scholarly purposes. Requests for copying or reproduction of this dissertation may be referred to University Microfilms, 300 North Zeeb Road, Ann Arbor, Michigan 48106, to whom the author has granted "the right to reproduce and sell (a) copies of the manuscript in microform and/or (b) printed copies of the manuscript made from microform."

Signature Kwoo-On Tong

Date August 29, 1973

TABLE OF CONTENTS

TABLE OF CONTENTS (cont'd.)

FIGURE CAPTIONS

LIST OF SYMBOLS

A	=	Characteristic time of pressure decay.
a	=	Speed of sound.
a_{40}	=	Speed of sound of the gas at x=0 before the opening of the diaphragm.
c_f	=	Drag coefficient.
D	=	Diameter of the tube.
D_0	=	Diameter of the tube at the nozzle inlet (x=0).
D^*	=	Diameter of the nozzle throat.
$f(\xi)$	=	Unknown function.
$f_I(\xi)$	=	$f(\xi)$ due to the boundary layer.
$f_{II}(\xi)$	=	$f(\xi)$ due to the change of diameter.
$f_{III}(\xi)$	=	$f(\xi)$ due to the initial temperature variations.
$g(\eta)$	=	Unknown function.
h	=	Enthalpy.
K	=	The coefficient of the boundary layer thickness (defined in Equation (10)).
L	=	Total length of the supply tube.
ℓ	=	Length of the first section of the supply tube.
M	=	Mach number.
M_0	=	Mach number of the unperturbed flow in the expansion shock fixed coordinate, $\frac{U_0}{a_3} + M_3$.
m	=	The power in the skin friction law used in Appendix C.
n	=	The power in the velocity profile of the boundary layer.
p	=	Static pressure.
p_t	=	Stagnation pressure.
p^*	=	$\bar{p}/p_3$.
q_w	=	Heat transfer at the wall.

Re_{D_0} = Reynolds number based on the unperturbed flow behind the expansion wave and D_0.

r = Radial coordinate.

s = Dimensionless distance behind the expansion shock, $\frac{U_0 t - x}{D_0}$.

T = Temperature.

T_t = Stagnation temperature.

T_{40} = Temperature at x=0 before the opening of the diaphragm.

t = Time after opening of the diaphragm.

$t_{e.s.}$ = Test time based on the expansion shock model.

$t_{e.w.}$ = Test time based on the propagation of the unperturbed expansion wave.

$\bar{t}$ = Dimensionless time, $\frac{U_0 t}{D_0}$.

t^* = $(a_3 - |u_3|)t/L$.

U_0 = Characteristic velocity of the expansion wave.

$U(t)$ = Propagating velocity of the expansion shock at time, t.

u = Velocity component in x direction.

u_{max} = Velocity along the center of the tube.

u^* = $\bar{u}/|u_3|$.

V = Propagating velocity of the discontinuity surface.

v = Velocity component in the r direction.

x = Axial coordinate

x_s = Initial position of each gas particle.

$\bar{x}$ = Dimensionless distance, x/D_0.

$\bar{x}_s$ = x_s/D_0 .

x^* = x/L .

y = Distance from the wall.

α = $-\frac{1 - M_3}{M_0 - 1}$.

β = $\frac{1 + M_3}{M_0 + 1}$.

γ = Ratio of specific heats.

Δ = $\rho_{40}(1 - \frac{\psi}{6})^6 \ tu' - \frac{t}{a_{40}} p'$.

δ = Boundary layer thickness.

δ^* = Boundary layer displacement thickness in the laboratory fixed coordinate.

δ_w^* = Boundary layer displacement thickness in the expansion shock fixed coordinate.

ζ = Slope of the characteristics of the flow behind the expansion shock.

η = Characteristic variable for the flow behind the expansion shock, $\bar{t} - \frac{U_0/a_3}{M_0 + 1}(\bar{t}-\bar{x})$.

Λ = $\rho_{40}(1 - \frac{\psi}{6})^6 \ tu' + \frac{t}{a_{40}} p'$.

u = Coefficient of viscosity.

ν = Kinematic viscosity.

ν_{40} = Kinematic viscosity of the gas at x=0 before the opening of the diaphragm.

ξ = Characteristic variable for the flow behind the expansion shock, $\bar{t} - \frac{U_0/a_3}{M_0 - 1}(\bar{t}-\bar{x})$.

ρ = Density.

ρ_w = Density of the gas at the wall.

ρ_{40} = Density of the gas at x=0 before the opening of the diaphragm.

ρ^* = $\bar{\rho}/\rho_3$.

τ_w = Wall shearing stress.

τ_w^* = τ_w/p_3 .

ψ = Characteristic variable for the flow within the expansion wave, $1 - \frac{x}{a_{40}t}$.

ω = Characteristic variable for the flow within the expansion wave, $t(\frac{5}{6} + \frac{x}{6a_{40}t})^3$.

SUBSCRIPTS:

e = Core flow value (radial variations neglected).

i = Unperturbed flow within the expansion wave.

3 = Unperturbed flow behind the expansion wave.

4 = Initial conditions in the supply tube.

SUPERSCRIPTS:

$(\ )'$ = Perturbation.

$(\bar{\ })$ = Quantity average over the cross-section (except $\bar{x}$, $\bar{x}_s$, and $\bar{t}$).

N.B.: Other symbols are defined as they are used in the text.

ACKNOWLEDGMENT

The author would like to express his special thanks to Professor David A. Russell of the Department of Aeronautics and Astronautics for his advice, guidance and encouragement, without which this investigation could not have been completed. He also wishes to express his gratitude to Professor Abraham Hertzberg for providing the opportunity to work in the exciting environment in the Aerospace Research Laboratory.

The author is greatly indebted to his wife, Lina, for her help in typing the rough draft of this dissertation, and her patience and encouragement throughout these years.

This investigation received financial support from NASA under Grant No. NGL48-002-057 and NGR48-002-107. This support is gratefully acknowledged.

CHAPTER I: INTRODUCTION

This is a study of the effects of boundary layer and axial pipe nonuniformity on the quality of the flow initiated by a non-steady expansion wave in a long tube. Non-steady expansion waves have been employed to generate gas flow in shock tubes and shock tunnels, although in these facilities the test gas is usually the fluid behind the shock wave rather than that behind the expansion wave. Continuous-flow wind tunnels have been invaluable in the past, but it has become increasingly uneconomical and impractical to simulate the high Reynolds number flows around modern aircraft in this type of facility; therefore, quasi-steady testing facilities have achieved renewed importance. Among these short duration flow facilities, Ludwieg tubes offer the most convenient way of producing high Reynolds number and high-mass-flux flow for aerodynamic testing (References 1 and 2).

The Ludwieg tube was first suggested by H. Ludwieg in 1955 as a testing facility (Reference 3). It uses the flow accelerated by a non-steady expansion wave as the test gas. A sketch of such a facility is shown at the bottom of Figure 1. It consists of a long cylindrical tube with one end closed and the other end connected to a nozzle and test section assembly. The test section can either discharge into a large dump tank or into the atmosphere through some muffling device. A diaphragm or quick-opening valve can be located either at the nozzle inlet, as shown in Figure 1, or downstream of the test section. The tube is first pressurized, then by rupturing the diaphragm or opening the valve, a non-steady expansion wave is generated within the tube and propagates towards the closed end while the expanded gas flows into the nozzle. When the expansion wave hits the closed end, it reflects back as another expansion wave.
The available test time of this facility is the time between the opening of the diaphragm and the arrival of the head of the reflected expansion wave at the

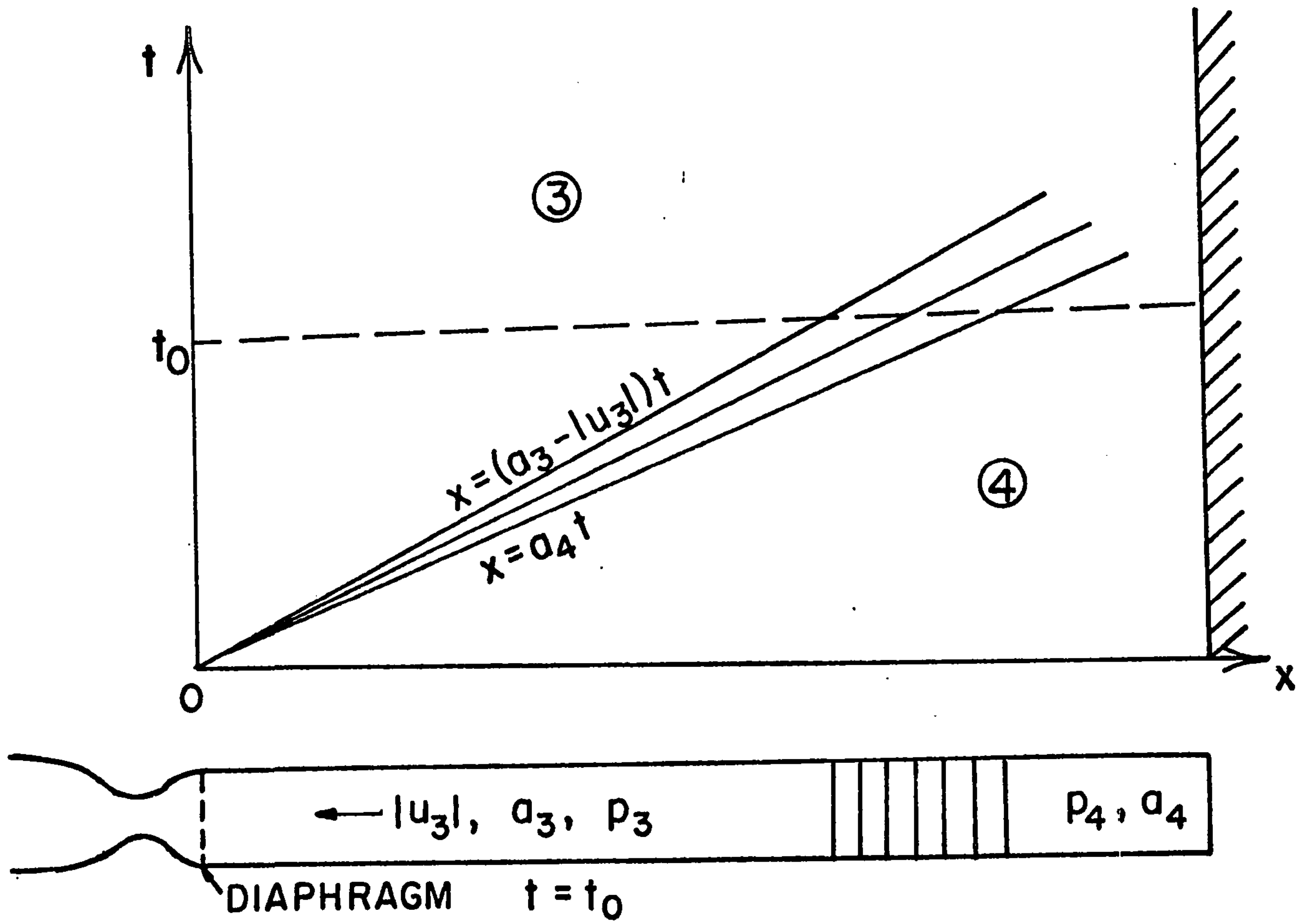

Figure 1: Wave Diagram and Flow Schematic for Ludwieg Tubes.

nozzle inlet. Figure 1 also shows a x-t diagram for the case where the viscosity and heat conductivity of the test gas are neglected. Here x is the position along the tube and t is the time after the opening of the diaphragm. Region 4 is the region in front of the expansion wave and Region 3 is the region behind the expansion wave. There exists a non-steady one dimensional relationship between the two regions: For a given condition in Region 4 the condition in Region 3 depends on the specific heat ratio of the gas and the Mach number in Region 3. This relationship is listed in Appendix A, together with the equation for the available test time of this facility.

In the ideal case the viscosity of the gas is neglected such that Region 3 is a uniform region; in actuality, the viscosity of the gas is non-zero. Because of the viscosity of the gas, a non-steady boundary layer builds up within and behind the expansion wave. The growth of the boundary layer generates secondary waves in the flow external to the boundary layer; the properties of this core flow will be perturbed and become functions of x and t. In this study, the effects of the boundary layer on the flow quality within and behind the expansion wave will be analyzed. Furthermore, it may in practice be difficult to avoid variations in the diameter of the tube and the temperature of gas in Region 4. Such axial nonuniformities introduce further perturbations in the flow behind the expansion wave and their effects on flow quality will also be examined here.

This non-steady boundary layer has received some attention in the past, presumably through the work of Mirels (Reference 4) and Becker (References 5 and 6). Their models for the boundary layer are reviewed in Chapter II, together with a discussion of Becker's analysis (Reference 5) for the effect of the boundary layer on the uniformity of the core flow; the latter was the first detailed attempt to analyze such a problem. It provided the general magnitude of the perturbations at the nozzle inlet. Later, Cable and Cox (Reference 7) calculated the static pressure drop during the test time simply from the shearing stress along the tube wall. Although the results thus obtained were in agreement with their experimental results, both the analytical and the experimental results were for specific conditions and had limited applicability.

In Chapter III, the effects of thin boundary layers and small variations in tube diameter and initial temperature are analyzed, using the general method suggested by Demyanov (Reference 9), Spence and Woods (Reference 10). This method involves the modification of the continuity equation for the core flow to include the displacement effect of the boundary layer, and it uses this thickness as a starting point. The expansion wave is replaced by a fictitious "expansion shock" in order to simplify the analysis. The analysis then yields closed form solutions for the perturbations of the core flow at any point behind the expansion wave.

In Chapter IV, the same basic approach is extended to the effect of the boundary layer on the flow within the non-steady expansion wave. The results thus obtained assist in indicating the validity of the assumption of an expansion shock at high Mach numbers. In Chapter V, the analytical results for the effects of boundary layers and variations in tube diameter obtained in Chapter III are compared with measurements of static pressure in a small Ludwieg tube. Finally, in Chapter VI, the limiting case of fully-developed pipe flow behind an expansion wave is studied. From experiments, the static pressure at the nozzle inlet is found to decay approximately exponentially. It is shown that the characteristic time of the pressure decay can be estimated by a simple method based on the pressure loss in the steady pipe flow.

The simple closed form results obtained in this investigation provide a clear picture of the real condition of the flow initiated by the expansion wave;

they will also be useful in the design of Ludwieg tubes or other facilities using a non-steady expansion wave to generate gas flows.

CHAPTER II: THE BOUNDARY LAYER BEHIND A NON-STEADY EXPANSION WAVE

Most of the perturbations in the core flow can be traced back to the non-steady boundary layer. Mirels (Reference 4) and Becker (Reference 5 and 6) have studied the laminar and turbulent boundary layer behind a non-steady expansion wave. Because the Reynolds number of the flow behind the expansion wave is usually so high that a very large portion of the boundary layer is turbulent, only the turbulent part of Mirels' and Becker's models will be reviewed here.

II-1. Mirels' and Becker's Models for the Boundary Layer

In his analysis, Mirels assumes that the expansion wave is so thin that it can be replaced by a discontinuity propagating with the speed of the head of the expansion wave, $\underline{a}_4$. In a coordinate moving with the discontinuity, the flow is steady, and the growth of the boundary layer behind the discontinuity is described by a steady momentum integral equation. In such a moving coordinate, the fluid velocity relative to the wall is assumed to have a seventh-power profile; the density is given by a polynomial containing the 1/7th and 2/7th power of the distance from the wall. The Blasius relation for the skin friction along a flat plate has been extended to the wave-fixed coordinate and to include the compressibility of the gas. For constant wall temperature, Mirels concludes that the thickness of the boundary layer in the moving coordinate is dependent on the Mach number of the flow and the distance behind the discontinuity surface.

Becker considers the boundary layer within the expansion wave. In the laboratory-fixed coordinate, the boundary layer is described by a non-steady momentum integral equation. Both the velocity and the density relative to the wall are assumed to have a seventh-power law profile. The skin friction law is similar to the one that Mirels uses. If the temperature at the wall is the same as that in Region 4, the thickness of the boundary layer will be a function of the local Mach number and the distance behind the head of the expansion wave.

Becker also considers the boundary layer behind a discontinuity surface moving with speed V. The properties of the gas behind the discontinuity surface are assumed to be the same as those behind the expansion wave. Following the previous procedure, Becker finds the thickness of the boundary layer dependent on the ratio of the velocity outside the boundary layer to the velocity V, and on the distance behind the discontinuity surface. He also concludes that the density can be considered constant across the boundary layer without making any large error in computing its thickness: at $M_3 = 0.5$, the error is only 2%. Assuming that at the tail of the expansion wave the thickness of the boundary layer within the expansion wave is equal to that behind a discontinuity surface with same speed V, Becker finds a single speed V for each M_3. This means, as far as the boundary layer behind the expansion wave is concerned, that the flow can be considered generated by a moving discontinuity surface. The ratio of such V to a_4 for different M_3 is plotted in Figure 2.

Figure 3 is a plot of the displacement thickness of the boundary layer at the origin of the expansion wave, evaluated for nitrogen and $T_4 = 300°K$. In this figure Mirels' result has been converted to a laboratory-fixed coordinate, and the displacement thickness has been nondimensionalized by the diameter of the tube. As might be expected, both models are in agreement at low Mach number, but diverge at high Mach number where neither model can be correct. Recently, Starr and Schueler (Reference 7) have taken measurements which indicate the boundary layer might be thicker than Becker's model predicts. In Appendix C Becker's method has been extended to velocity profiles with different power

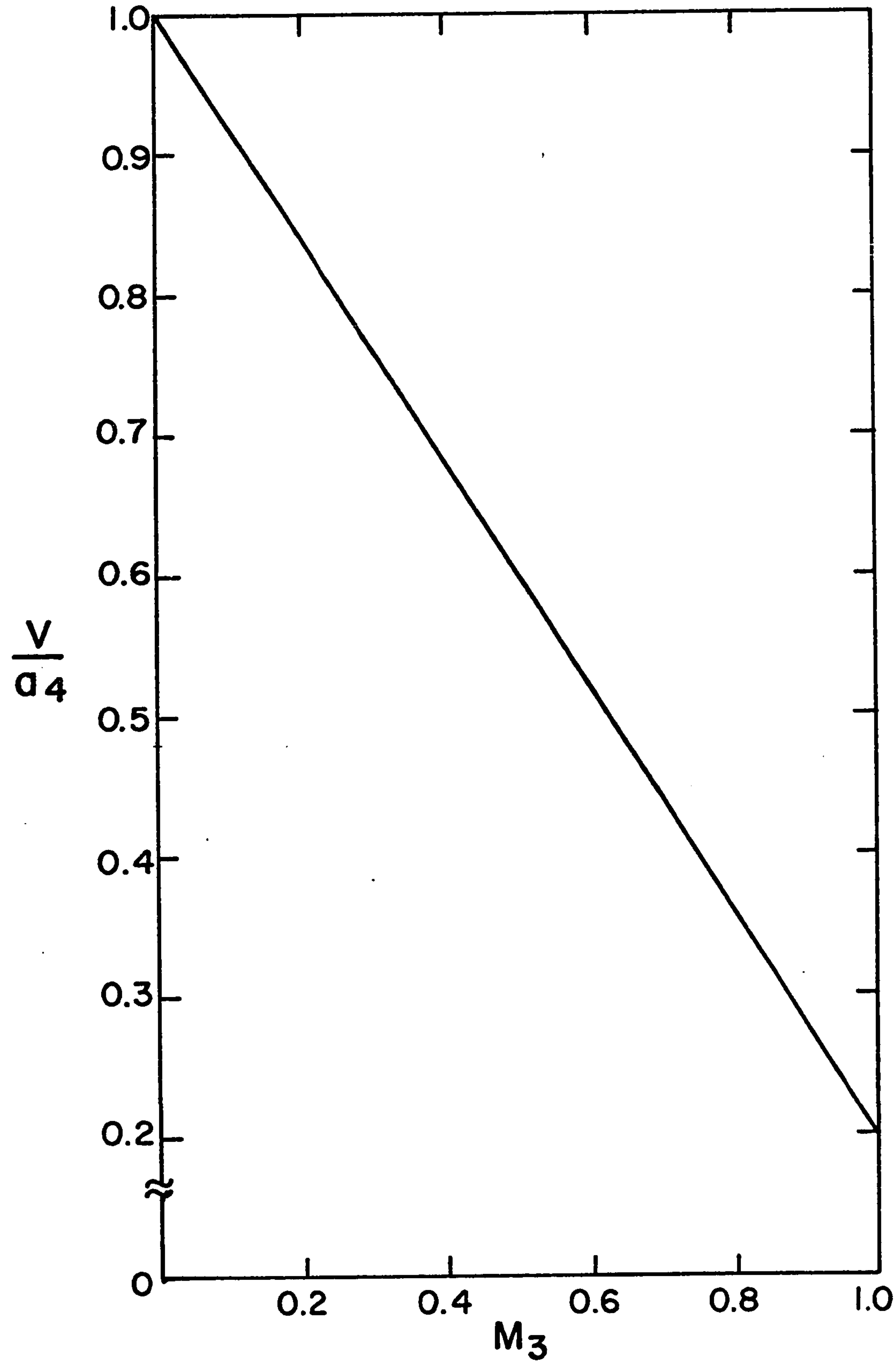

Figure 2: The Velocity of the Discontinuity Surface (V) Based on Becker's Method, γ=1.4.

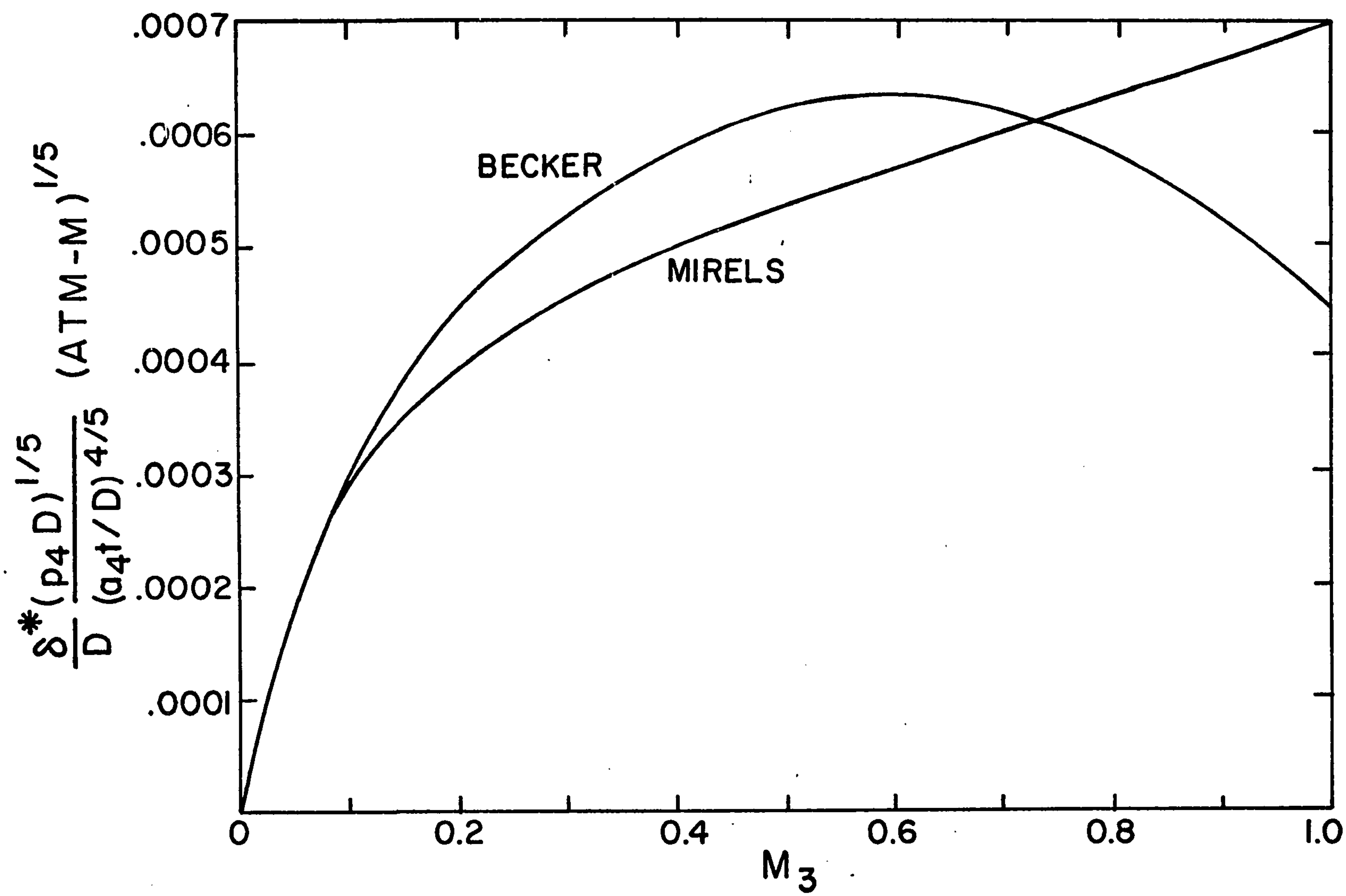

Figure 3: The Thickness of the Turbulent Boundary Layer at the Nozzle Inlet, Nitrogen with T_{40} = 300°K.

laws; however, more experimental results must be obtained before an accurate model for the boundary layer can be established.

II-2. Becker's Treatment of Flow Uniformity

In his treatment of the effect of the boundary layer on the flow behind the expansion wave, Becker (Reference 5) introduces a source term in the continuity equation for the case of thin boundary layers. This source term is assumed to be proportional to the normal velocity at the edge of the boundary layer in the laboratory-fixed coordinate. In evaluating the perturbations at the open end of the tube, Becker assumes that the source term is independent of the position, which is inconsistent with the growth of the boundary layer, especially near the tail of the expansion wave. Furthermore, Becker's results are for the perturbation at the open end of the tube; it will become quite complicated when Becker's method is extended to calculate the perturbations at any point within the tube, and a simple closed form solution may not be obtainable. In the present study, consistent closed form expressions will be developed for the complete core flow.

CHAPTER III: CORE FLOW UNIFORMITY BEHIND THE EXPANSION WAVE

After reviewing several methods used in analyzing the effect of the boundary layer on the flow behind a moving shock wave (Reference 9,10,11,12) the method suggested by Demyanov (Reference 11) and extended by Spence and Woods (Reference 12) was selected as most appropriate for the present study as long as the boundary layers remain thin. This method gives not only a rigorous base for analyzing the effect of the boundary layer (Reference 13), but also provides a simple procedure to obtain closed form solutions.

III-1. Characteristic Velocity of the Expansion Wave (U_0)

In order to simplify the analysis, the non-steady expansion wave is replaced by the "expansion shock" as shown in Figure 4. This is a surface of discontinuity moving with a characteristic velocity of the expansion wave, U_0. The gas is assumed to change from the condition in Region 4 to the condition in Region 3 immediately upon crossing the expansion shock. Although U_0 can be chosen to correspond to the speed of the head (Reference 10) or tail of the expansion wave, or some intermediate speed (Becker uses the mean between the speed of the head and tail of the expansion wave (Reference 5)), U_0 is chosen here based on a physical argument which holds for the complete operation range of M_3 in Ludwieg tubes.

Consider the control volume between the closed end of the tube and the nozzle inlet. As the expansion shock propagates towards the closed end with a speed U_0, the total mass of gas within this control volume decreases with time while the expanded gas flows out of this section. The time rate of mass decreasing for unit cross-sectional area is $(\rho_4 - \rho_3)U_0$ while the mass flux flowing out is $\rho_3|u_3|$. Applying the continuity equation to this control volume,

$$(\rho_4 - \rho_3)U_0 = \rho_3|u_3| \tag{1}$$

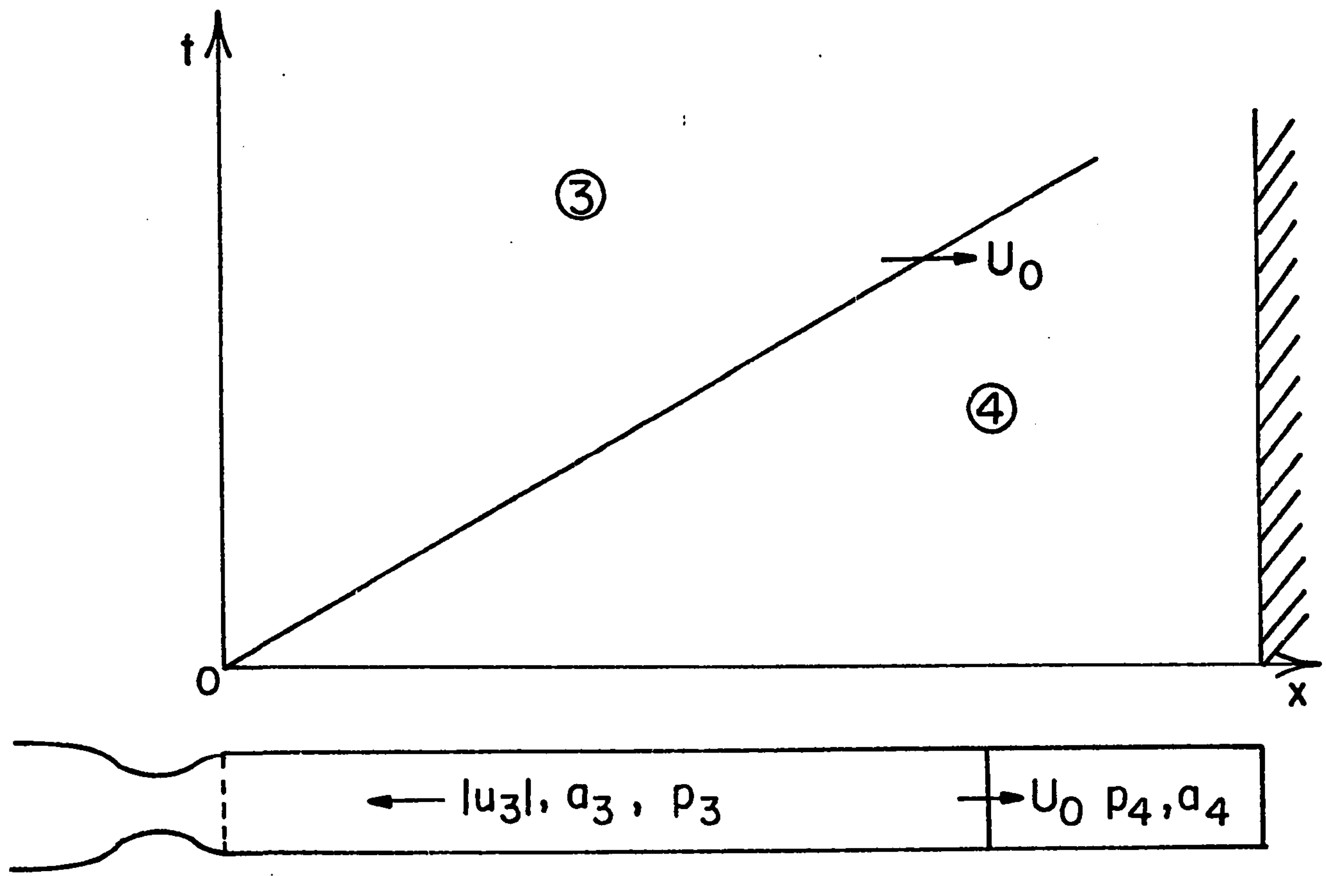

Figure 4: The Wave Diagram and Flow Schematic When the Expansion Wave is Replaced by the Expansion Shock.

or $$U_0 = \frac{|u_3|}{\rho_4/\rho_3 - 1} \quad .$$

Using the non-steady one-dimensional relationship listed in Appendix A,

$$U_0 = \frac{|u_3|}{(a_4/a_3)^{2/\gamma-1} - 1} = \frac{|u_3|}{(1 + \frac{\gamma-1}{2} M_3)^{2/\gamma-1} - 1} \quad ,$$

or $$\frac{U_0}{a_4} = \frac{M_3(1 + \frac{\gamma-1}{2} M_3)^{-1}}{(1 + \frac{\gamma-1}{2} M_3)^{2/\gamma-1} - 1} \quad . \tag{2}$$

Figure 5 shows the ratio U_0/a_4 for different M_3 and the ratio of the speed of the tail of expansion wave $(a - |u_3|)$ to a_4. It can be seen that the speed U_0 based on Equation (2) lies between a_4 and $(a_3 - |u_3|)$, and is always larger than the speed V obtained by Becker (see Figure 2) though both approach a_4 as M_3 approaches zero. The thickness of the boundary layer behind the discontinuity moving with U_0 can be calculated from Becker's model by replacing V by U_0. The result for the region behind the expansion wave agrees very well with that obtained by Becker by matching the thickness of the boundary layer at the tail of expansion wave: even at M_3=0.90, the difference is within 75%. Therefore, as far as the thickness of the boundary layer behind the expansion wave is concerned, replacing the expansion wave by the expansion shock moving with the characteristic velocity U_0 is a good approximation even at high M_3.

III-2. Basic Equations

In order to obtain the basic equations governing the core flow behind the expansion shock propagating with U_0, the method suggested by Spence and Woods is used. The relative thickness of the boundary layer (δ/D_0), and variations in tube diameter and in initial temperature (T_4) are assumed to be small while L/D_0 is >> 1. Here D_0 is the diameter of the tube at the nozzle inlet (i.e. x=0) and L is the tube length.

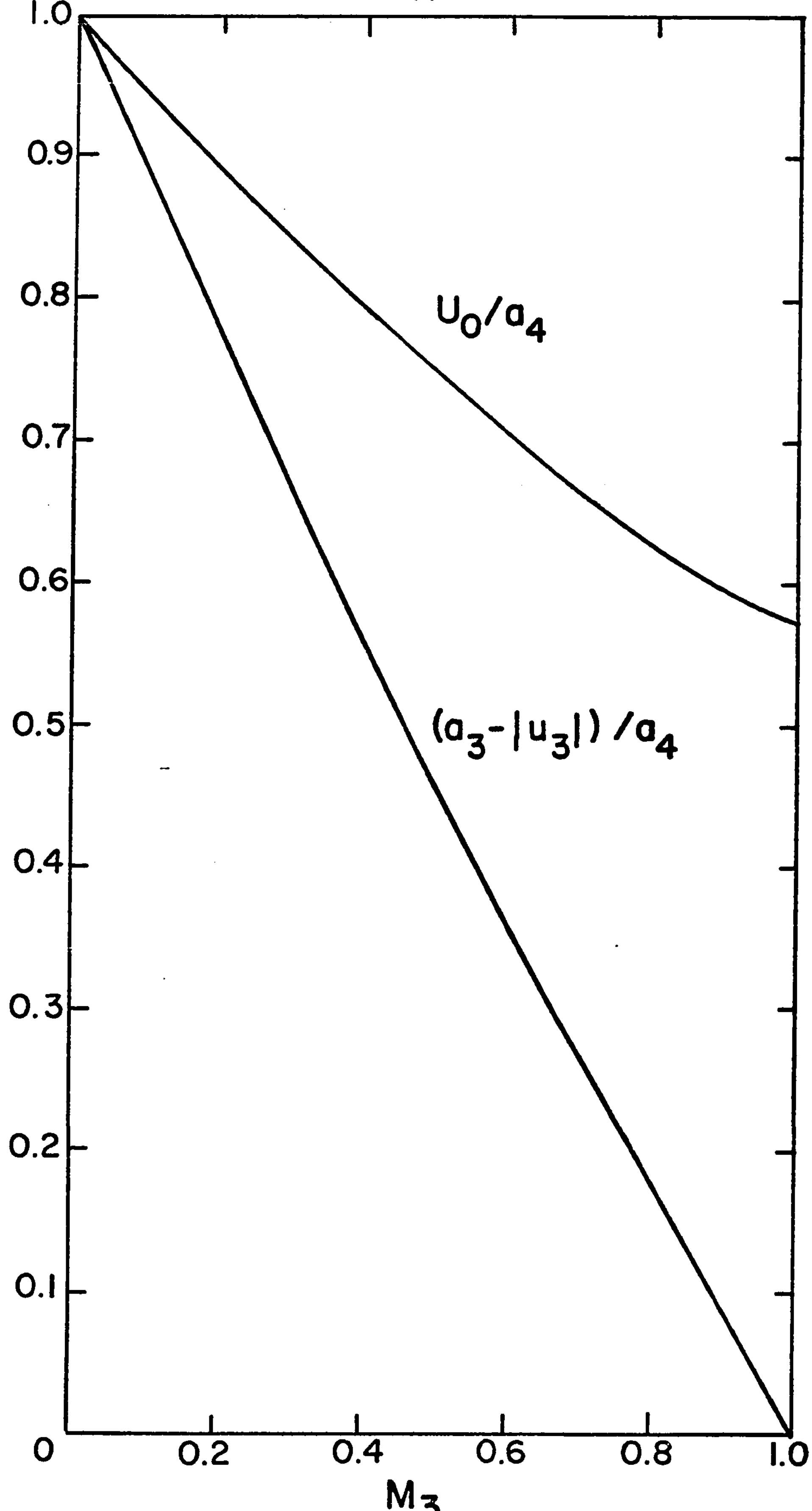

Figure 5: The Characteristic Velocity of the Expansion Wave (U_0) and the Velocity of the Tail of the Expansion Wave, γ=1.4.

Following Spence and Woods, the non-steady continuity equation in cylindrical coordinates can be written as

$$\frac{\partial \rho}{\partial t} + \frac{\partial}{\partial x}(\rho u) + \frac{1}{r}\frac{\partial}{\partial r}(\rho v r) = 0 \quad ,$$

where u and v are the velocity component in the axial and radial directions respectively, and r is the radial coordinate. Multiplying this equation by r and integrating with respect to r from 0 to D/2 yields

$$\int_0^{D/2} r\frac{\partial \rho}{\partial t}\,dr + \int_0^{D/2} r\frac{\partial}{\partial x}(\rho u)dr = -(\rho v r)\Big|_0^{D/2} \quad ,$$

here D is the diameter of the tube at any position. Since at the wall (r = D/2) u=v=0, the above equation can also be written as

$$\frac{\partial}{\partial t}\int_0^{D/2} r\rho dr + \frac{\partial}{\partial x}\int_0^{D/2} r\rho u dr = 0 \quad .$$

For $L/D_0 >> 1$, the properties of the gas outside the boundary layer can be assumed functions x and t only, that is, they are independent of r. If $\delta/D_0 << 1$, D is a function of x only, and $dD/dx \approx O(\delta/D_0)$, the above equation can be integrated into the following form:

$$\frac{\partial \rho_e}{\partial t} + \frac{\partial}{\partial x}(\rho_e u_e) = \frac{4}{D}\frac{\partial}{\partial t}\{\int_0^{\delta}(\rho_e - \rho)dy\} + \frac{4}{D}\frac{\partial}{\partial x}\{\int_0^{\delta}(\rho_e u_e - \rho u)dy\}$$
$$- \rho_e u_e \frac{2}{D}\frac{dD}{dx} \quad , \qquad (3)$$

subscript e denotes the condition of the gas external to the boundary layer; y is the distance from the wall and terms of order $(\delta/D_0)^2$ have been neglected. Equation (3) is the continuity equation for the core flow with mass addition terms due to the boundary layer and diameter changes.

For a given M_3 the thickness of the boundary layer is a function of the distance behind the discontinuity. If

$$\frac{\rho_e - \rho_3}{\rho_3} \approx O(\delta/D_0)$$

then

$$\frac{\partial}{\partial t}\{\int_0^\delta (\rho_e - \rho)dy\} + \frac{\partial}{\partial x}\{\int_0^\delta (\rho_e u_e - \rho u)dy\}$$

$$\approx \frac{\partial}{\partial s}\{\int_0^\delta [\rho_e(U_0 - u_e) - \rho(U_0 - u)]dy\} \quad .$$

Here $s \equiv U_0 t - x$ is the distance behind the surface of discontinuity.

Let $\rho_e(U_0 - u_e)\delta_W^* \equiv \int_0^\delta [\rho_e(U_0 - u_e) - \rho(U_0 - u)]dy$ where δ_W^* is the displacement thickness of the boundary layer in a coordinate moving with U_0. Equation (3) can be simplified into

$$\frac{\partial \rho_e}{\partial t} + \frac{\partial}{\partial x}(\rho_e u_e) = \frac{4}{D}\frac{\partial}{\partial s}[\rho_e(U_0 - u_e)\delta_W^*] - \rho_e u_e \frac{2}{D}\frac{dD}{dx} \quad . \tag{4}$$

The momentum equation for the core flow is

$$\rho_e\left(\frac{\partial u_e}{\partial t} + u_e \frac{\partial u_e}{\partial x}\right) + \frac{\partial p_e}{\partial x} = 0 \quad . \tag{5}$$

For the gas outside the boundary layer, the entropy of each gas particle is assumed constant, that is, the particle path is also the constant entropy line, then

$$\left(\frac{\partial}{\partial t} + u_e \frac{\partial}{\partial x}\right) \ln\left(\frac{p_e}{\rho_e^\gamma}\right) = 0 \quad . \tag{6}$$

Equations (4), (5) and (6) are the basic equations for the properties of the gas external to the boundary layer. It should be emphasized that the effect of the boundary layer is through a source term on the right-hand side of the continuity equation. Physically, when a gas particle moves downstream in the core flow, it is not going to encounter any shearing stress or heat transfer. However, due to the displacement effect of the boundary layer, the effective tube diameter becomes a function of x and t, and this is represented by the source term in the continuity equation.

Combining equations (4) and (6), and assuming the gas is perfect, yields

$$\frac{1}{a_e^2}\left(\frac{\partial p_e}{\partial t} + u_e \frac{\partial p_e}{\partial x}\right) + \rho_e \frac{\partial u_e}{\partial x} = \frac{4}{D}\frac{\partial}{\partial s}\left[\rho_e (U_0 - u_e)\delta_w^*\right]$$

$$- \rho_e u_e \frac{2}{D}\frac{dD}{dx} \quad . \tag{7}$$

Let $D = D_0 + D'$, and $\rho_e = \rho_3 + \rho'$, $p_e = p_3 + p'$, $a_e = a_3 + a'$, $u_e = -|u_3| + u'$, where ρ', p', a' and u' represent their respective perturbed parts. ρ'/ρ_3, p'/p_3, a'/a_3, $u'/|u_3|$ and D'/D_0 are of the order δ/D_0. Simplifying Equations (7) and (5),

$$\frac{1}{a_3^2}\left(\frac{\partial p'}{\partial t} - |u_3| \frac{\partial p'}{\partial x}\right) + \rho_3 \frac{\partial u'}{\partial x} = \frac{4}{D_0}\rho_3 (U_0 + |u_3|)\frac{d\delta_w^*}{dx}$$

$$+ \rho_3 |u_3| \frac{2}{D_0}\frac{dD'}{dx} \quad , \tag{8}$$

$$\rho_3\left(\frac{\partial u'}{\partial t} - |u_3| \frac{\partial u'}{\partial x}\right) + \frac{\partial p'}{\partial x} = 0 \quad . \tag{9}$$

The displacement thickness of the boundary layer in the laboratory-fixed coordinate is assumed to have the form

$$\frac{\delta^*}{D_0} = \frac{5}{16} K (Re_{D_0})^{-1/5} \left(\frac{U_0 t - x}{D_0}\right)^{4/5} \quad . \tag{10}$$

Here K is a coefficient dependent on the value of M_3 and the boundary layer model used, while Re_{D_0} is the Reynolds number based on D_0 and the unperturbed flow of Region 3. The exponents of the Reynolds number and the dimensionless distance $\frac{U_0 t - x}{D_0}$ are the results of the 1/7th power velocity profile. The form of Equation 10 is thus consistent with Mirels' and Becker's models (Section II-1.). As discussed in Chapter II, the density across the boundary layer can be considered constant at least in the limit of low to moderate M_3. From the definition of displacement thickness, it can then be shown that

$$\frac{\delta^*}{\delta^*_w} = \frac{U_0 + |u_3|}{|u_3|}$$

Equations (8), (9) and (10) can be put into the following form:

$$\frac{1}{\rho_3 a_3^2 |u_3|}\left(U_0 \frac{\partial p'}{\partial \bar{t}} - |u_3| \frac{\partial p'}{\partial \bar{x}}\right) + \frac{1}{|u_3|}\frac{\partial u'}{\partial \bar{x}}$$

$$= K(Re_{D_0})^{-1/5}\,(\bar{t}-\bar{x})^{-1/5} + 2\frac{d}{d\bar{x}}\,(D'/D_0) \quad , \tag{11}$$

$$U_0 \frac{\partial u'}{\partial \bar{t}} - |u_3|\frac{\partial u'}{\partial \bar{x}} + \frac{1}{\rho_3}\frac{\partial p'}{\partial x} = 0 \; , \tag{12}$$

where $\bar{x} \equiv x/D_0$ and $\bar{t} \equiv U_0 t/D_0$ are the dimensionless length and time.

III-3. The Characteristics and the General Solutions of the Linearized Equations

Equations (11) and (12) are the linearized equations for the velocity and pressure perturbations of the core flow. They form a system of hyperbolic equations (Reference 14). The characteristics of this system of equations are independent of u' and p', and have slopes $a_3-|u_3|$ and $a_3+|u_3|$ identical to the slopes of the characteristics of the unperturbed flow behind the expansion wave. The characteristic variables are chosen to be

$$\eta \equiv \bar{t} - \frac{U_0/a_3}{M_0+1}\,(\bar{t}-\bar{x}) \qquad \text{and} \qquad \xi \equiv \bar{t} - \frac{U_0/a_3}{M_0-1}\,(\bar{t}-\bar{x}) \tag{13}$$

where $M_0 \equiv U_0/a_3 + M_3$ is the Mach number of the unperturbed flow in the coordinate moving with speed U_0. η refers to the family of characteristics propagating in the -x direction, while ξ is the family propagating in the +x direction. Figure 6 shows the unperturbed path of the expansion shock and the

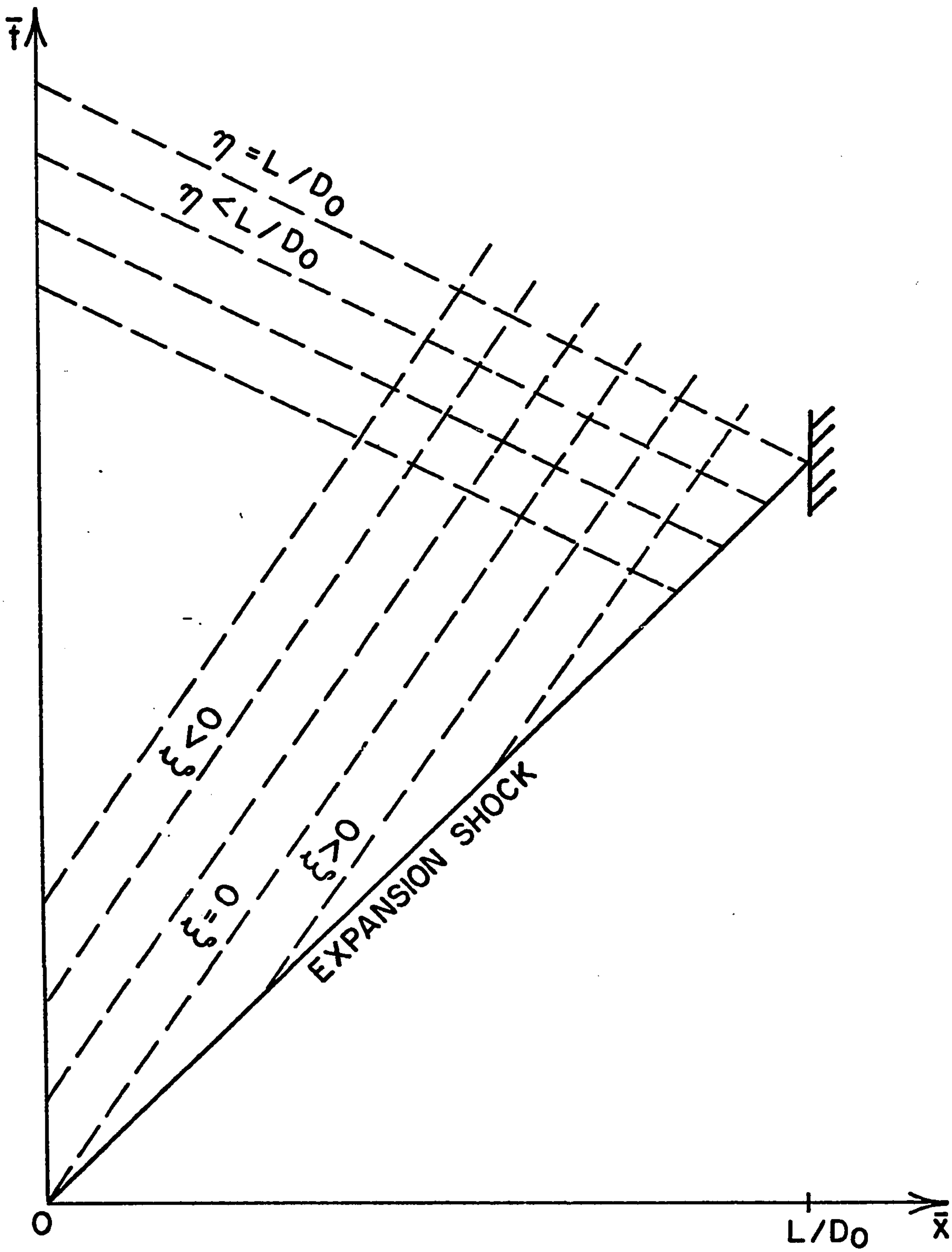

Figure 6: Schematic for the Characteristics of the Flow Behind the Expansion Shock.

two families of characteristics in the $(\bar{x},\bar{t})$ coordinates. It should be pointed out that the ξ=0 characteristic corresponds to the tail of the expansion wave. In the region between the ξ=0 characteristic and the expansion shock, ξ is positive while downstream of the ξ=0 characteristic ξ is negative. The perturbations of the gas in this latter region are studied in this chapter, while Chapter IV considers the perturbations of the flow within the expansion wave.

Since the coefficients in Equations (11) and (12) are constant, u' and p' can be found easily. In dimensionless forms they can be written as

$$\frac{p'}{\rho_3 a_3 |u_3|} = \frac{5}{4} K(Re_{D_0})^{-1/5} \frac{M_0}{M_0^2-1}(\bar{t}-\bar{x})^{4/5} + \frac{2M_3}{1-M_3^2} \frac{D'(\bar{x})}{D_0} + f(\xi) - g(\eta), \tag{14}$$

$$\frac{u'}{|u_3|} = \frac{5}{4} K(Re_{D_0})^{-1/5} \frac{1}{M_0^2-1}(\bar{t}-\bar{x})^{4/5} + \frac{2}{1-M_3^2} \frac{D'(\bar{x})}{D_0} + f(\xi) + g(\eta), \tag{15}$$

where $f(\xi)$ and $g(\eta)$ are two unknown functions resulting from the integration process. These two functions can be found by applying the boundary conditions at the two ends of the gas column. (The derivations of Equations (13), (14) and (15) can be found in Appendix B).

III-4. The Boundary Condition at the Expansion Shock

In order to calculate U_0, it is obvious from Equation (1) that ρ_3 and $|u_3|$ must be known first. In other words, U_0 depends on the conditions of the gas in front of and behind the expansion shock. When there are variations in T_4, the gas in front of the expansion shock is not uniform even though p_4 is constant. The condition of the gas behind the expansion shock is disturbed due to the effects of the boundary layer and of pipe axial nonuniformities. Hence, the propagation speed of the expansion shock is also perturbed. Letting U(t) denote the speed of the expansion shock at any instant of time, Equation (1) can be generalized into

$$U(\bar{t})[\rho_e(\bar{t}) - \rho_4(\bar{t})] = u_e(\bar{t})\rho_e(\bar{t}) \quad . \tag{16}$$

Here ρ_4 is the density of the gas in front of the expansion shock, while ρ_e and u_e are the density and velocity of the gas behind the expansion shock. Since they are functions of t, they are also functions of $\bar{t}$ which is a dimensionless time. Equation (16) becomes Equation (1) when $\rho_e = \rho_3$ and $u_e = -|u_3|$.

If the differences between ρ_4, ρ_e, u_e and their respective unperturbed values are small, U will be close to U_0, and the real path of the expansion shock will be very close to the unperturbed path. To the first approximation, the difference between the perturbed and unperturbed path of the expansion shock can be neglected, that is, Equation (16) holds along the path $x = U_0 t$ (or $\bar{x} = \bar{t}$). Equation (16) can be rewritten in the following form,

$$\begin{aligned} u_e(\bar{t}) &= U(\bar{t})[1 - \rho_4(\bar{t})/\rho_e(\bar{t})] \\ &= U(\bar{t})\left[1 - \frac{p_4}{p_e(\bar{t})}\left(\frac{a_e(\bar{t})}{a_{40}(\bar{t})}\right)^2\right] \quad . \end{aligned} \tag{16a}$$

Taking the pressure of the gas in Region 4 to be constant, it follows that

$$\begin{aligned} du_e = dU\left[1 - \frac{p_4}{p_e}\left(\frac{a_e}{a_4}\right)^2\right] - U\Bigg[&- \frac{p_4}{p_e^2}\left(\frac{a_e}{a_4}\right)^2 dp_e \\ &+ 2\frac{p_4}{p_e}\frac{a_e}{a_4^2}da_e - 2\frac{p_4}{p_e}\left(\frac{a_e}{a_4}\right)^2\frac{da_4}{a_4}\Bigg] \quad . \end{aligned} \tag{17}$$

Let

$$a_4(\bar{t}) = a_{40} + a_4'(\bar{t}),$$

$$\rho_4(\bar{t}) = \rho_{40} + \rho_4'(\bar{t}),$$

$$p_e(\bar{t}) = p_3 + p'(\bar{t}),$$

$$a_e(\bar{t}) = a_3 + a'(\bar{t}),$$

$$U(\bar{t}) = U_0 + U'(\bar{t}),$$

a_{40} and ρ_{40} are the values of a_4 and ρ_4 at x=0 while the order of a_4'/a_{40}, ρ_4'/ρ_{40}, p'/p_3, a'/a_3 and U'/U_0 is < 1. Since $du_e \approx u'$, $dp_e \approx p'$ and $dU_0 \approx U'$, Equation (17) becomes

$$u' \approx U'[1 - \frac{p_4}{p_3}(\frac{a_3}{a_{40}})^2] - U_0\Big\{- \frac{p_4}{p_3^2}(\frac{a_3}{a_{40}})^2 p' + 2\frac{p_4}{p_3}\frac{a_3}{a_{40}^2}a' - 2\frac{p_4}{p_3}(\frac{a_3}{a_{40}})^2\frac{a_4'}{a_{40}}\Big\}. \tag{18}$$

The entropies of the gas particles in front of and behind the expansion shock are assumed to be the same, so that

$$\frac{p'}{p_3} = \frac{2\gamma}{\gamma-1}\left(\frac{a'}{a_3} - \frac{a_4'}{a_{40}}\right). \tag{19}$$

Recalling the Riemann Invariants

$$a_e - \frac{\gamma-1}{2}u_e = a_4,$$

and remembering in the ideal case

$$a_3 + \frac{\gamma-1}{2}|u_3| = a_{40},$$

then

$$a' - \frac{\gamma-1}{2}u' = a_4'. \tag{20}$$

Combining Equations (18), (19), (20), (2), and (A1) and (A4) in Appendix A, the boundary conditions for u' and p' along the unperturbed path of the expansion shock are obtained:

$$\frac{p'}{\rho_3 a_3 |u_3|} = \frac{\frac{U'}{U_0} - \frac{U_0}{a_3}\left(\frac{a_{40}}{a_3}\right)^{2/\gamma-1}\frac{a_4'}{a_{40}}}{\left[\frac{U_0}{a_3}\left(\frac{a_{40}}{a_3}\right)^{2/\gamma-1} - 1\right]} + \frac{a_4'}{a_{40}} \quad , \tag{21a}$$

$$\frac{u'}{|u_3|} = \frac{\frac{U'}{U_0} - \frac{U_0}{a_3}\left(\frac{a_{40}}{a_3}\right)^{2/\gamma-1}\frac{a_4'}{a_{40}}}{\left[\frac{U_0}{a_3}\left(\frac{a_{40}}{a_3}\right)^{2/\gamma-1} - 1\right]} \quad . \tag{21b}$$

Evaluating Equations (14) and (15) at the unperturbed path of the expansion shock (i.e. $\bar{x} = \bar{t}$, $\xi = \eta = \bar{t}$),

$$\frac{p'}{\rho_3 a_3 |u_3|} = \frac{2M_3}{1-M_3}\frac{D'(\bar{t})}{D_0} + f(\bar{t}) - g(\bar{t}) \quad , \tag{22a}$$

$$\frac{u'}{|u_3|} = \frac{2}{1-M_3}\frac{D'(\bar{t})}{D_0} + f(\bar{t}) + g(\bar{t}) \quad . \tag{22b}$$

Substituting Equations (21) into (22) gives

$$f(\bar{t}) = \frac{\frac{U'(\bar{t})}{U_0} - \frac{U_0}{a_3}\left(\frac{a_{40}}{a_3}\right)^{2/\gamma-1}\frac{a_4'(\bar{t})}{a_{40}}}{\left[\frac{U_0}{a_3}\left(\frac{a_{40}}{a_3}\right)^{2/\gamma-1} - 1\right]} + \frac{1}{2}\frac{a_4'(t)}{a_{40}} - \frac{1}{1-M_3}\frac{D'(t)}{D_0} \quad ,$$

$$g(\bar{t}) = -\frac{1}{2}\frac{a_4'(\bar{t})}{a_{40}} - \frac{1}{1+M_3}\frac{D'(\bar{t})}{D_0} \quad .$$

or

$$f(\xi) = \frac{\frac{U'(\xi)}{U_0} - \frac{U_0}{a_3}\left(\frac{a_{40}}{a_3}\right)^{2/\gamma-1}\frac{a_4'(\xi)}{a_{40}}}{\left[\frac{U_0}{a_3}\left(\frac{a_{40}}{a_3}\right)^{2/\gamma-1} - 1\right]} + \frac{1}{2}\frac{a_4'(\xi)}{a_{40}} - \frac{1}{1-M_3}\frac{D'(\xi)}{D_0} \quad , \tag{23}$$

$$g(\eta) = -\frac{1}{2}\frac{a_4'(\eta)}{a_{40}} - \frac{1}{1+M_3}\frac{D'(\eta)}{D_0} \quad . \tag{24}$$

Since $g(\eta)$ is constant along η = constant, it is easily seen from Figure 6 that $g(\eta)$ must have the form shown in Equation (24) for the region behind the expansion wave (i.e. in the $\xi \leq 0$ region).

III-5. The Boundary Conditions at the Nozzle Inlet (i.e. x=0)

The unknown function $f(\xi)$ for the region behind the expansion wave (i.e. $\xi \leq 0$ region) must be solved before u' and p' can be obtained. This function $f(\xi)$ can be obtained by applying the appropriate boundary conditions at the nozzle inlet. Because the basic equations are linear, the effects of boundary layer, of tube diameter change, and of initial temperature distribution on the boundary conditions can be considered separately and then superimposed to obtain the total effect.

Effect of the Boundary Layer $f_I(\xi)$

As the boundary layer grows, the effective diameters at the nozzle inlet and at the throat of the nozzle decrease with time, and the effective Mach number at the nozzle inlet will also become time dependent. If the nozzle is much shorter than the tube, then at any instant in time, the Mach number at the nozzle inlet can be calculated from the ratio of the effective cross-section area at the nozzle inlet to that at the throat of the nozzle by the one-dimensional steady channel flow relationship. In general, the relationship between the growth of the boundary layer at the nozzle inlet and that at the throat depends on the contour of the nozzle, and is quite complicated. In the case of low M_3 and thin boundary layer at the nozzle inlet, however, the thickness of the boundary layer at the nozzle throat can be neglected. In this case, the Mach number at the nozzle inlet depends only on the local displacement thickness of the boundary layer. If the Mach number at the nozzle throat is always 1, then from the one-dimensional steady channel flow relationship, one obtains

$$\frac{dA}{A} = - \frac{1-M_3^2}{1 + \frac{\gamma-1}{2} M_3^2} \frac{dM_e}{M_3} , \tag{25}$$

where A is the geometric cross-sectional area at the nozzle inlet. Since

$$\frac{dA}{A} \approx - 4\delta^*/D_0$$

where δ^* is the displacement thickness at the nozzle inlet, and

$$\frac{dM_e}{M_3} \approx \frac{M'}{M_3} \approx -\left(\frac{u}{|u_3|} + \frac{\gamma-1}{2\gamma}\frac{p'}{p_3}\right),$$

the entropy of the gas being constant, Equation (25) becomes

$$-4\,\delta^*/D_0 = \frac{1-M_3^2}{1+\frac{\gamma-1}{2}M_3}\left(\frac{u'}{|u_3|} + \frac{\gamma-1}{2}\frac{p'}{p_3}\right). \tag{26}$$

Referring back to Equation (10),

$$\frac{\delta^*}{D_0} = \frac{5}{16}K(Re_{D_0})^{-1/5}\,\bar{t}^{\,4/5}, \tag{27}$$

Applying Equations (14) and (15) at the nozzle inlet where

$$\xi = -\frac{1-M_3}{M_0-1}\bar{t} \equiv \alpha\bar{t},$$

$$\eta = \frac{1+M_3}{M_0+1}\bar{t} \equiv \beta\bar{t},$$

and considering only the boundary layer effect,

$$\frac{p'}{\rho_3 a_3|u_3|} = \frac{5}{4}K(Re_{D_0})^{-1/5}\frac{M_0}{M_0^2-1}\bar{t}^{\,4/5} + f_I(\alpha\bar{t}) = \frac{1}{\gamma M_3}\frac{p'}{p_3},$$

$$\frac{u'}{|u_3|} = \frac{5}{4}K(Re_{D_0})^{-1/5}\frac{1}{M_0^2-1}\bar{t}^{\,4/5} + f_I(\alpha\bar{t}).$$

Combining these two equations with Equations (26) and (27) one obtains,

$$f_I(\alpha\bar{t}) = -\frac{5}{4}K(Re_{D_0})^{-1/5}\,\bar{t}^{\,4/5}$$

$$\cdot \frac{(1+\frac{\gamma-1}{2}M_3^2)(M_0^2-1) + (1-M_3^2)(1+\frac{\gamma-1}{2}M_3M_0)}{(1+\frac{\gamma-1}{2}M_3)(M_0^2-1)(1-M_3^2)},$$

or $$f_I(\xi) = -\frac{5}{4} K(Re_{D_0})^{-1/5} (\frac{\xi}{\alpha})^{4/5}$$

$$\cdot \frac{(1 + \frac{\gamma-1}{2} M_3^2)(M_0^2-1) + (1-M_3^2)(1 + \frac{\gamma-1}{2} M_3 M_0)}{(1 + \frac{\gamma-1}{2} M_3)(M_0^2-1)(1-M_3^2)} , \text{ for } \xi \leq 0 . \quad (28)$$

It should be noted that $f_I(\xi)$ is a function of M_3, p_4 and T_{40} only.

Effect of the Change of Diameter $f_{II}(\xi)$

When the effect of the boundary layer is neglected, the ratio of the cross-sectional area at the nozzle inlet to that at the throat of the nozzle is constant, therefore, the Mach number at the nozzle inlet is constant. In other words,

$$\frac{u'}{|u_3|} = -\frac{a'}{a_3} , \quad (29)$$

the negative sign is due to the fact that in the unperburbed case the gas flows in the -x direction. Since the change in T_4 is also neglected here, the entropy of each gas particle is the same. From

$$\frac{a_e}{a_3} = \left(\frac{p_e}{p_3}\right)^{\gamma-1/2\gamma} ,$$

it follows that

$$\frac{a'}{a_3} \approx \frac{\gamma-1}{2\gamma} \frac{p'}{p_3} . \quad (30)$$

From Equations (14), (15) and (24), p' and u' become

$$\frac{p'}{\rho_3 a_3 |u_3|} = f_{II}(\alpha\bar{t}) + \frac{1}{1+M_3} \frac{D'(\beta\bar{t})}{D_0} = \frac{1}{\gamma M_3} \frac{p'}{p_3} ,$$

and $$\frac{u'}{|u_3|} = f_{II}(\alpha\bar{t}) - \frac{1}{1+M_3} \frac{D'(\beta\bar{t})}{D_0} . \quad (31)$$

Combining Equations (29), (30) and (31), one obtains

$$f_{II}(\alpha\bar{t}) = \frac{1 - \frac{\gamma-1}{2} M_3}{(1 + \frac{\gamma-1}{2} M_3)(1+M_3)} \frac{D'(\beta\bar{t})}{D_0} ,$$

or $$f_{II}(\xi) = \frac{1 - \frac{\gamma-1}{2} M_3}{(1 + \frac{\gamma-1}{2} M_3)(1+M_3)} \frac{D'(\frac{\beta}{\alpha}\xi)}{D_0} . \tag{32}$$

The function $f_{II}(\xi)$ depends not only on M_3 but also on the distribution of diameter along the axis of the tube.

Effect of Initial Temperature Variations $f_{III}(\xi)$

In this case, the Mach number at the nozzle inlet (x=0) is a constant, but the entropy of the gas is not because the initial temperature (T_4) varies. Since the entropy of each gas particle is constant, the particle paths are also the constant entropy paths. For small perturbations, the actual particle path is very close to the unperturbed particle path. If the expansion wave is replaced by an expansion shock, the unperturbed particle path passing any point (x,t) can be shown to be

$$(x - x_s) = (-|u_3|)(t - \frac{x_s}{U_0}) ,$$

or $$\bar{x}_s = \frac{U_0}{U_0 + |u_3|}\left(\bar{x} + \frac{|u_3|}{U_0}\bar{t}\right) , \tag{33}$$

where x_s is the initial position of the gas particle passing x at t (see Figure 7), and $\bar{x}_s = x_s/D_0$. For $x = \bar{x} = 0$,

$$\bar{x}_s = \frac{|u_3|}{U_0 + |u_3|}\bar{t} = \frac{M_3}{M_0}\bar{t} . \tag{34}$$

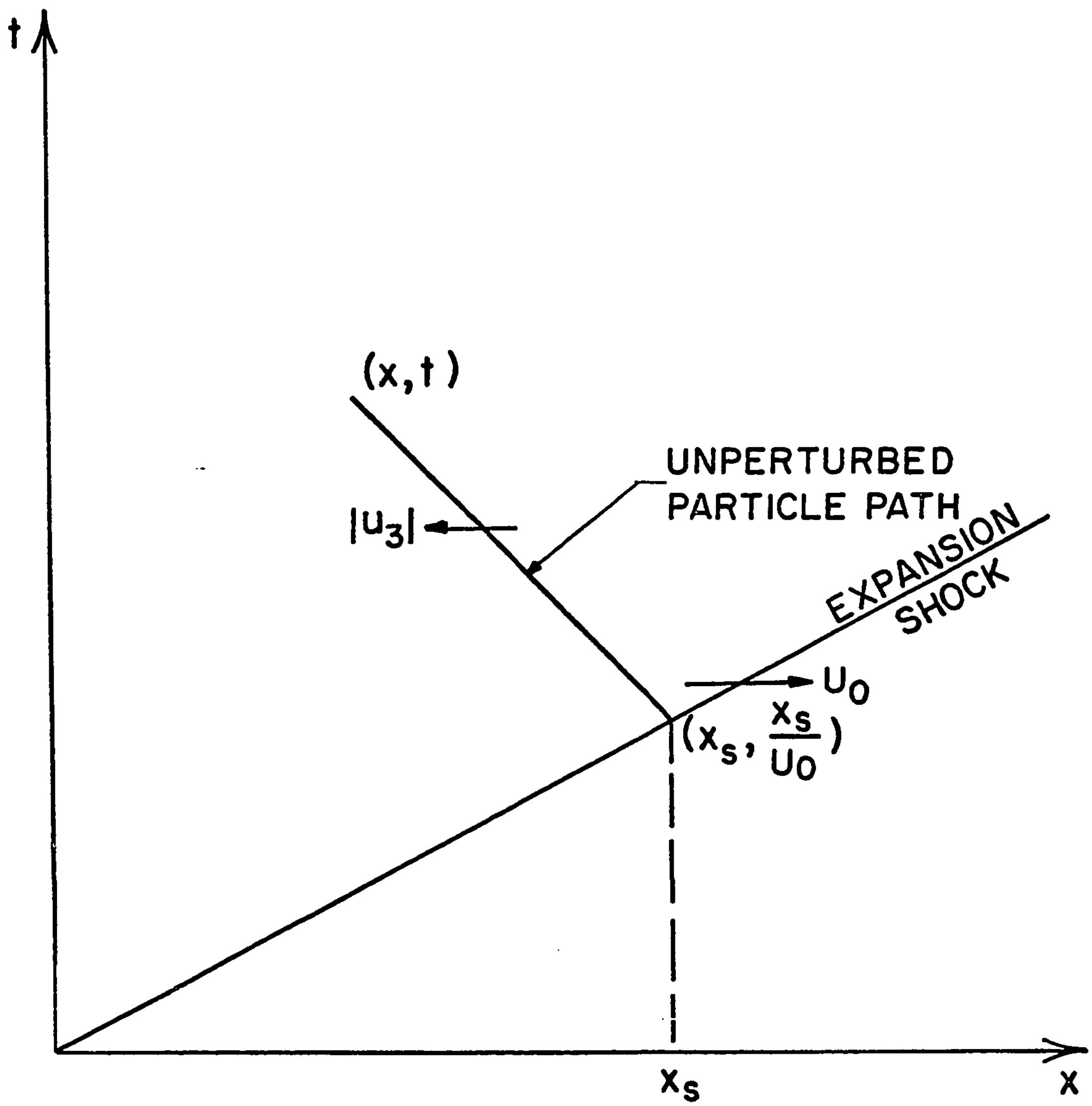

Figure 7: Schematic for the Unperturbed Particle Path.

From the relationship

$$\frac{p_e}{p_4} = \left(\frac{a_e}{a_4} \right)^{2\gamma/\gamma-1} ,$$

it follows

$$\frac{p'}{p_3} \approx \frac{2\gamma}{\gamma-1} \left(\frac{a'}{a_3} - \frac{a_4'(\bar{x}_s)}{a_{40}} \right) , \tag{35}$$

where the last term on the right-hand side represents the difference in the entropy of the gas due to T_4' at $\bar{x}_s$.

From Equations (14), (15) and (24), p' and u' become

$$\frac{p'}{\rho_3 a_3 |u_3|} = f_{III}(\alpha\bar{t}) + \tfrac{1}{2} \frac{a_4'(\beta\bar{t})}{a_{40}} = \frac{1}{\gamma M_3} \frac{p'}{p_3} , \tag{36}$$

$$\frac{u'}{|u_3|} = f_{III}(\alpha\bar{t}) - \tfrac{1}{2} \frac{a_4'(\beta\bar{t})}{a_{40}} .$$

By combining Equations (29), (35) and (36),

$$f_{III}(\alpha\bar{t}) = \tfrac{1}{2} \frac{1 - \frac{\gamma-1}{2} M_3}{1 + \frac{\gamma-1}{2} M_3} \frac{a_4'(\beta\bar{t})}{a_{40}} - \frac{1}{1 + \frac{\gamma-1}{2} M_3} \frac{a_4'\left(\frac{M_3}{M_0}\bar{t}\right)}{a_{40}} ,$$

or

$$f_{III}(\xi) = \tfrac{1}{2} \frac{1 - \frac{\gamma-1}{2} M_3}{1 + \frac{\gamma-1}{2} M_3} \frac{a_4'\left(\frac{\beta}{\alpha}\xi\right)}{a_{40}} - \frac{1}{1 + \frac{\gamma-1}{2} M_3} \frac{a_4'\left(\frac{M_3}{M_0}\frac{\xi}{\alpha}\right)}{a_{40}} . \tag{37}$$

III-6. Results and Discussions

With $f_I(\xi)$, $f_{II}(\xi)$ and $f_{III}(\xi)$ given by Equations (28), (32) and (37) respectively, the pressure and velocity perturbations of the flow behind the expansion wave are given by:

$$\frac{p'}{\rho_3 a_3 |u_3|} = \underbrace{\frac{5}{4} K(Re_{D_0})^{-1/5} \frac{M_0}{M_0^2-1} (\bar{t}-\bar{x})^{4/5} - (\frac{\xi}{\alpha})^{4/5} \frac{(1+\frac{\gamma-1}{2}M_3^2)(M_0^2-1) + (1-M_3^2)(1+\frac{\gamma-1}{2}M_3 M_0)}{(1+\frac{\gamma-1}{2}M_3)(M_0^2-1)(1-M_3^2)}}_{\text{due to boundary layer}}$$

$$+ \underbrace{\frac{2M_3}{1-M_3^2}\frac{D'(\bar{x})}{D_0} + \frac{1-\frac{\gamma-1}{2}M_3}{(1+\frac{\gamma-1}{2}M_3)(1+M_3)}\frac{D'(\frac{\beta}{\alpha}\xi)}{D_0} + \frac{1}{1+M_3}\frac{D'(\eta)}{D_0}}_{\text{due to change of diameter}}$$

$$+ \underbrace{\frac{1}{2}\frac{1-\frac{\gamma-1}{2}M_3}{1+\frac{\gamma-1}{2}M_3}\frac{a_4'(\frac{\beta}{\alpha}\xi)}{a_{40}} - \frac{1}{1+\frac{\gamma-1}{2}M_3}\frac{a_4'(\frac{M_3}{M_0}\frac{\xi}{\alpha})}{a_{40}} + \frac{1}{2}\frac{a_4'(\eta)}{a_{40}}}_{\text{due to variation in } T_4}, \qquad (38)$$

$$\frac{u'}{|u_3|} = \underbrace{\frac{5}{4} K(Re_{D_0})^{-1/5} \frac{1}{M_0-1} (\bar{t}-\bar{x})^{4/5} - (\frac{\xi}{\alpha})^{4/5} \frac{(1+\frac{\gamma-1}{2}M_3^2)(M_0^2-1) + (1-M_3^2)(1+\frac{\gamma-1}{2}M_3 M_0)}{(1+\frac{\gamma-1}{2}M_3)(M_0^2-1)(1-M_3^2)}}_{\text{due to boundary layer}}$$

$$
\underbrace{+ \frac{2}{1-M_3^2}\frac{D'(\bar{x})}{D_0} + \frac{1 - \frac{\gamma-1}{2}M_3}{(1+\frac{\gamma-1}{2}M_3)(1+M_3)}\frac{D'(\frac{\beta}{\alpha}\xi)}{D_0} - \frac{1}{1+M_3}\frac{D'(\eta)}{D_0}}_{\text{due to change of diameter}}
$$

$$
\underbrace{+ \tfrac{1}{2}\frac{1 - \frac{\gamma-1}{2}M_3}{1+\frac{\gamma-1}{2}M_3}\frac{a_4'(\frac{\beta}{\alpha}\xi)}{a_{40}} - \frac{1}{1+\frac{\gamma-1}{2}M_3}\frac{a_4'(\frac{M_3}{M_0}\frac{\xi}{\alpha})}{a_{40}} - \tfrac{1}{2}\frac{a_4'(\eta)}{a_{40}}}_{\text{due to variation in } T_4} \quad . \tag{39}
$$

It is obvious from the derivation that Equations (38) and (39) are valid for $\xi \le 0$ (i.e. behind the expansion wave) and $t \le L/U_0$ (i.e. before the expansion shock reaches the closed end). As the temperature is almost constant across the boundary layer, the waves propagating in the -x direction have a maximum speed in the core flow. Therefore, when the expansion wave is replaced by the expansion shock, the test time, $t_{e.s.}$, is determined by the intersection of the η = constant characteristic passing through $(L, L/U_0)$ and $x=0$. In other words

$$
t_{e.s.} = \frac{L}{U_0}\frac{1}{\beta} \quad ,
$$

or

$$
\bar{t}_{e.s.} = \frac{U_0 t_{e.s.}}{D_0} = \frac{1}{\beta}\frac{L}{D_0} \quad . \tag{40}
$$

The ratio of $t_{e.s.}$ to $t_{e.w.}$ is shown in Figure 8 for different M_3, where $t_{e.w.}$ is the test time calculated from the propagation of the unperturbed expansion wave. It can be seen that even at $M_3 = 0.5$, the difference is only 17%.

The fact that the tube is closed will not modify the flow at any position along the tube until the $\eta = L/D_0$ characteristic reaches that particular

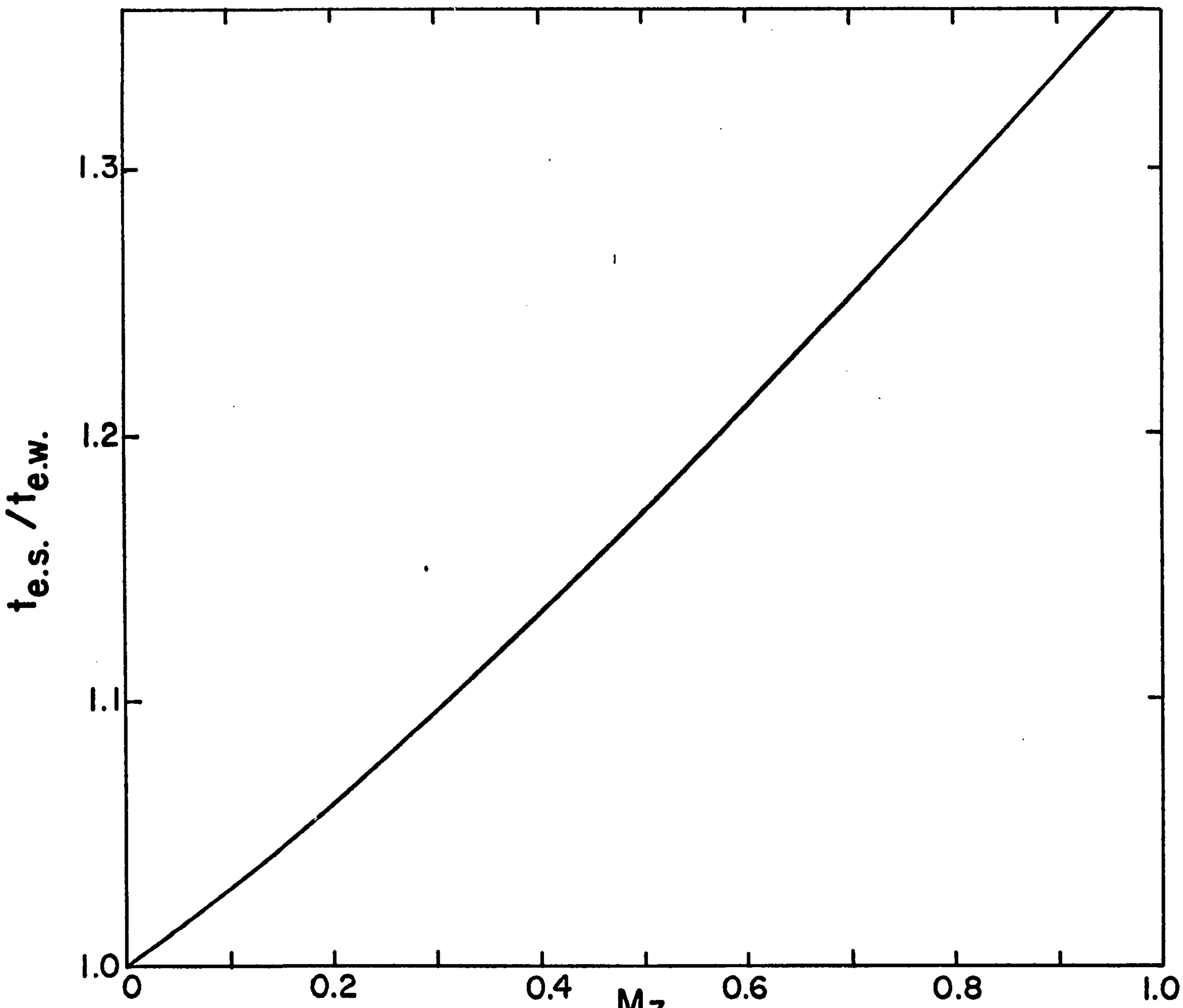

Figure 8: The Ratio of $t_{e.s.}/t_{e.w.}$, γ=1.4.

position; therefore, Equations (38) and (39) are valid for the whole region bounded by the ξ=0 and $\eta = L/D_0$ characteristics and $\bar{x}$=0, (Figure 6).

Once the pressure and velocity perturbations are known, the perturbations of speed of sound, Mach number, stagnation pressure and stagnation temperature can be calculated. The perturbation due to the boundary layer, change of diameter and variation of T_4 will be discussed separately below.

Effect of Boundary Layer

The set of equations for the perturbations in the core flow are as follows:

$$\frac{p'}{\rho_3 a_3 |u_3|} = \frac{5}{4} K(Re_{D_0})^{-1/5} \frac{M_0}{M_0^2-1} (\bar{t}-\bar{x})^{4/5} - \left(\frac{\xi}{\alpha}\right)^{4/5} \frac{(1+\frac{\gamma-1}{2}M_3^2)(M_0^2-1)+(1-M_3^2)(1+\frac{\gamma-1}{2}M_3M_0)}{(1+\frac{\gamma-1}{2}M_3)(M_0^2-1)(1-M_3^2)} \quad , \tag{41}$$

$$\frac{u'}{|u_3|} = \frac{5}{4} K(Re_{D_0})^{-1/5} \frac{1}{M_0^2-1} (\bar{t}-\bar{x})^{4/5} - \left(\frac{\xi}{\alpha}\right)^{4/5} \frac{(1+\frac{\gamma-1}{2}M_3^2)(M_0^2-1)+(1-M_3^2)(1+\frac{\gamma-1}{2}M_3M_0)}{(1+\frac{\gamma-1}{2}M_3)(M_0^2-1)(1-M_3^2)} \quad , \tag{42}$$

$$\frac{a'}{a_3} = \frac{\gamma-1}{2\gamma}\frac{p'}{p_3} \quad , \tag{43}$$

$$\frac{M'}{M_3} = -\frac{u'}{|u_3|} + \frac{a'}{a_3} \quad , \tag{44}$$

$$\frac{T'}{T_3} = 2\frac{a'}{a_3} \quad , \tag{45}$$

$$\frac{T_t'}{T_{t3}} = \frac{T_3}{T_{t3}}(\gamma-1)M_3^2\left(\frac{M'}{M_3}\right) + \frac{T'}{T_3} \quad , \tag{46}$$

$$\frac{p_t'}{p_{t3}} = \frac{\gamma}{\gamma-1}\left(\frac{T_t'}{T_{t3}} - \frac{T'}{T_3}\right) + \frac{p'}{p_3} = \frac{\gamma}{\gamma-1}\frac{T_t'}{T_{t3}} \quad . \tag{47}$$

It should be noted that only terms of first order in the perturbations have been retained.

The first term on the right-hand sides of Equations (41) and (42) represent the perturbations caused by the local displacement thickness. This causes a positive pressure and velocity perturbation and a negative Mach number perturbation. On the other hand, the boundary condition at the nozzle inlet require that the Mach number increases according to the one-dimensional steady channel flow relationship. Therefore, secondary non-steady expansion waves are sent back from the nozzle inlet to satisfy this boundary condition, and the effect of these waves is represented by the second term in Equations (41) and (42).

Figures 9a and 9b show the profile of the pressure perturbation in the flow behind the expansion wave at a given instant of time for different M_3. Here the abscissa, $x/[(a_3 - |u_3|)t]$, which is equal to 1 at the tail of the expansion wave and 0 at the nozzle inlet. The ordinate is

$$\frac{p'}{p_3} \frac{(Re_{D_0})^{1/5}}{[(a_3 - |u_3|)t/D_0]^{4/5}} \;.$$

While Figure 9a is for low to moderate Mach numbers, Figure 9b is for high Mach numbers. Figure 10a and Figure 10b are similar plots for the velocity perturbation. It can be seen that for any given M_3 both pressure and velocity perturbations are positive at the tail of expansion wave, decrease as x decreases, and become negative at the nozzle inlet. This is due to the fact that the characteristics behind the expansion wave are parallel to the tail of the expansion wave. Therefore, while the perturbations at the nozzle inlet are governed by the boundary condition, they are governed only by the local displacement thickness at the tail of the expansion wave. It should be mentioned

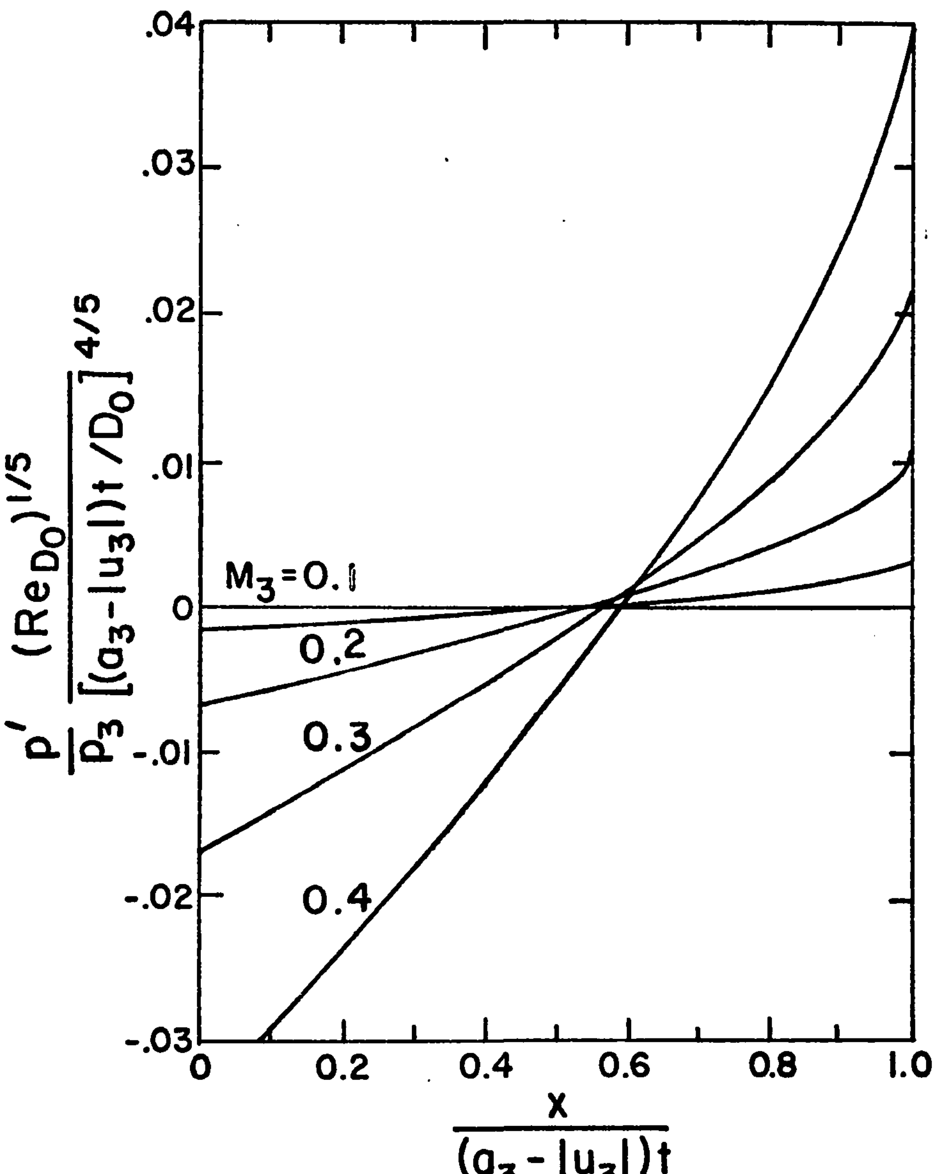

Figure 9a: Boundary Layer Induced Static Pressure Perturbations Behind the Expansion Wave, γ=1.4.

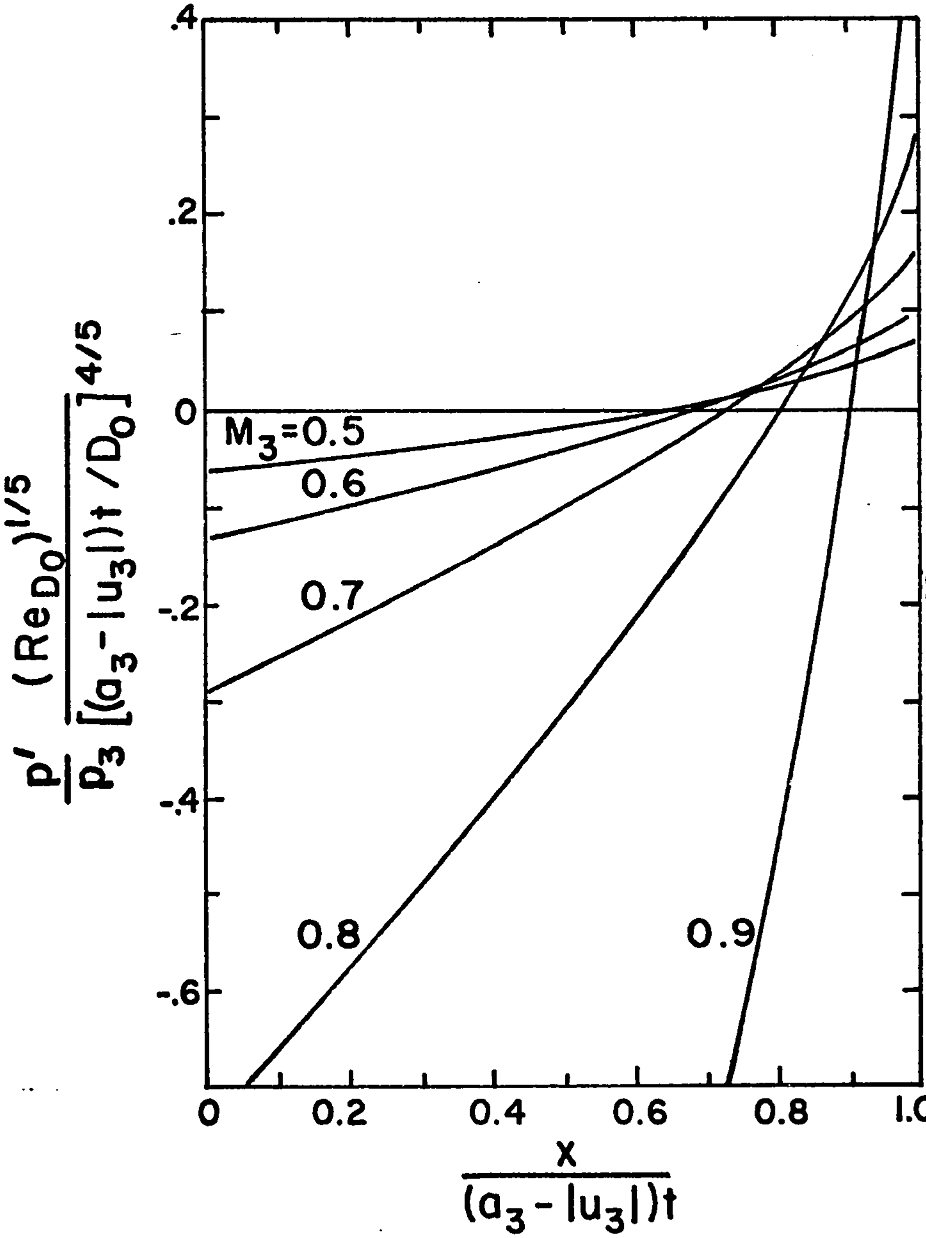

Figure 9b: Boundary Layer Induced Static Pressure Perturbations Behind the Expansion Wave, γ=1.4.

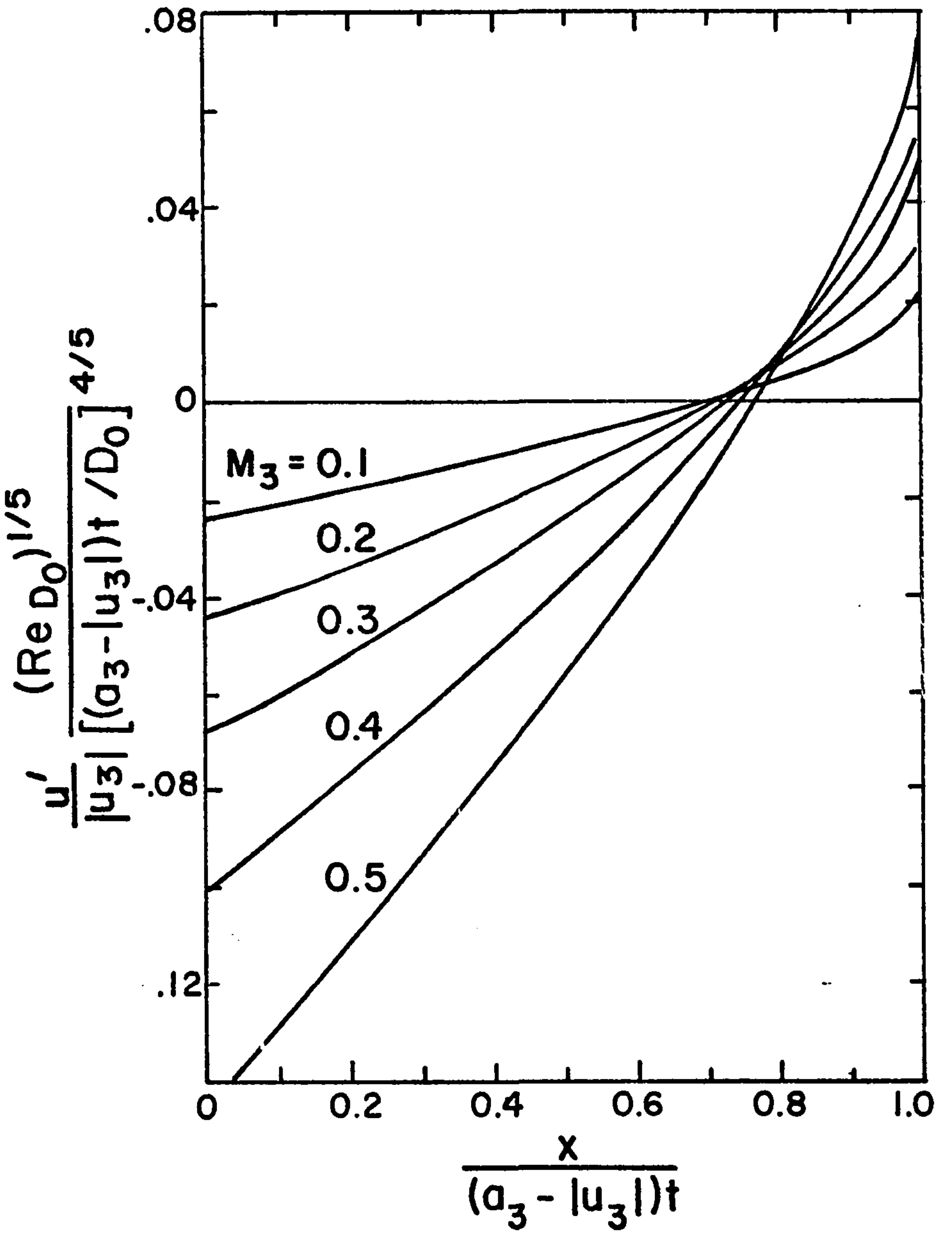

Figure 10a: Boundary Layer Induced Velocity Perturbations Behind the Expansion Wave, γ=1.4.

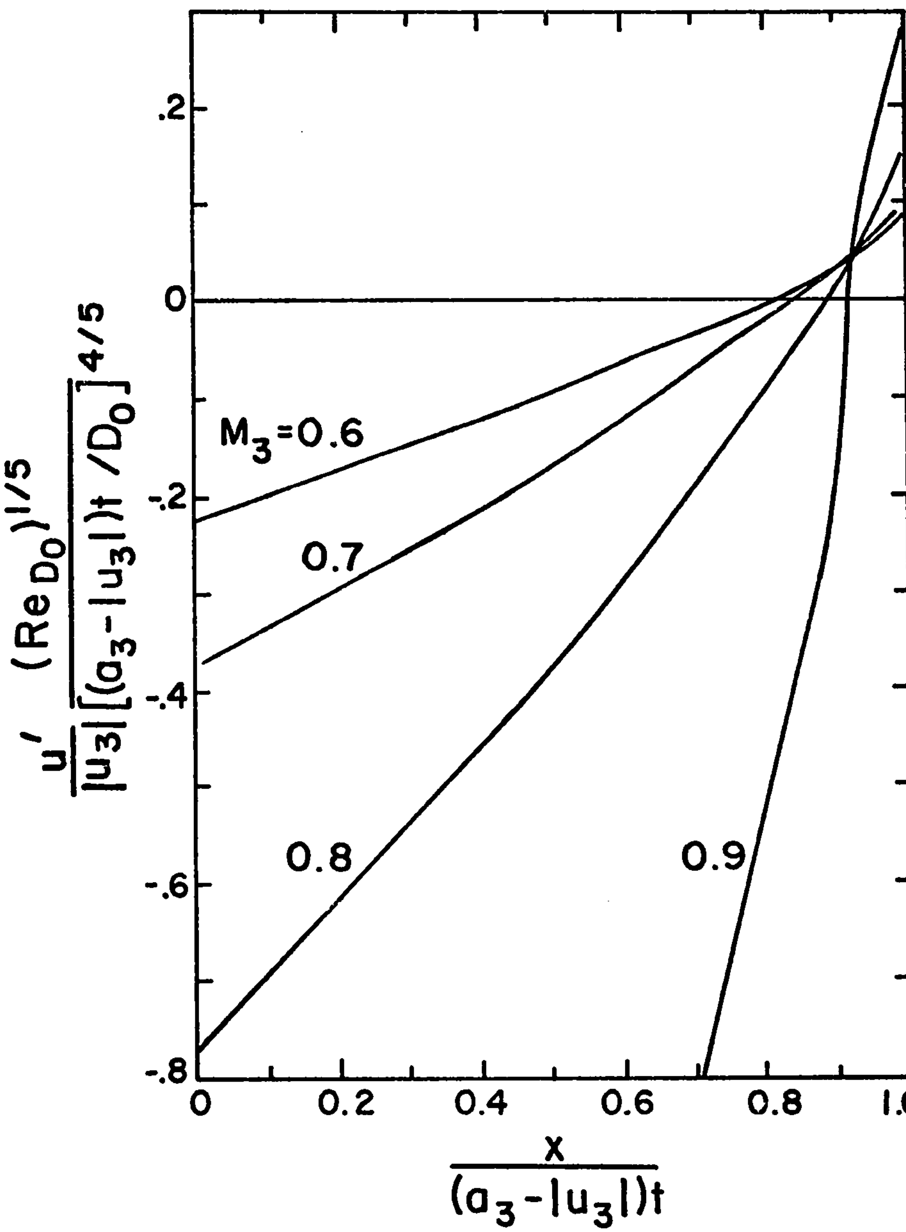

Figure 10b: Boundary Layer Induced Velocity Perturbations Behind the Expansion Wave.

that for a given time t, $(a_3 - |u_3|)t$ decreases as M_3 increases, therefore, the slopes, $\frac{\partial p'}{\partial x}$ and $\frac{\partial u'}{\partial x}$, are steeper at higher M_3 than that at lower M_3.

The static pressure and velocity perturbation at the nozzle inlet at the end of the test time are shown in Figure 11 for different M_3. These results are for nitrogen with T_{40} = 300°K, and the test time is taken to be $\frac{1}{\beta}\frac{L}{U_0}$. It can be seen that the static pressure perturbation has a stronger M_3 dependence than the velocity perturbation, and for most M_3, $-u'/|u_3|$ is larger than $-p'/p_3$. Since the second terms in Equations (41) and (42) contain $(1-M_3^2)$ in the denominator, both $-u'/|u_3|$ and $-p'/p_3$ approach ∞ as M_3 approaches 1. The perturbations of Mach number, stagnation pressure and stagnation temperature at the nozzle inlet at the end of test time are shown in Figure 12. The Perturbation of the stagnation temperature is smaller than that of stagnation pressure which is always smaller than that of the static pressure.

By comparison, Becker's results cannot be represented in forms as convenient as Equations (41) and (42). In Figure 13, the static pressure, velocity and stagnation pressure perturbations at the nozzle inlet have been plotted against M_3. These results are for nitrogen at T_{40} = 300°K with δ^*/D = 0.06 at the nozzle inlet. Under such condition, the nozzle inlet is nearly filled with boundary layer. The solid lines are based on Becker's results, while the dotted lines are the results of the present analysis. The stagnation pressure perturbation based on the present analysis is higher than that predicted by Becker's result, however, the opposite is true for the velocity and static pressure perturbations. The agreement between these two different analyses are relatively close, this may be due to the fact that since only the perturbations at the nozzle inlet are considered, the assumption which Becker made concerning the dependence of the source term is fairly accurate (see Section II-2). It should be mentioned that even with this thick boundary layer, the perturbation in stagnation pressure is only a few percent of its unperturbed value.

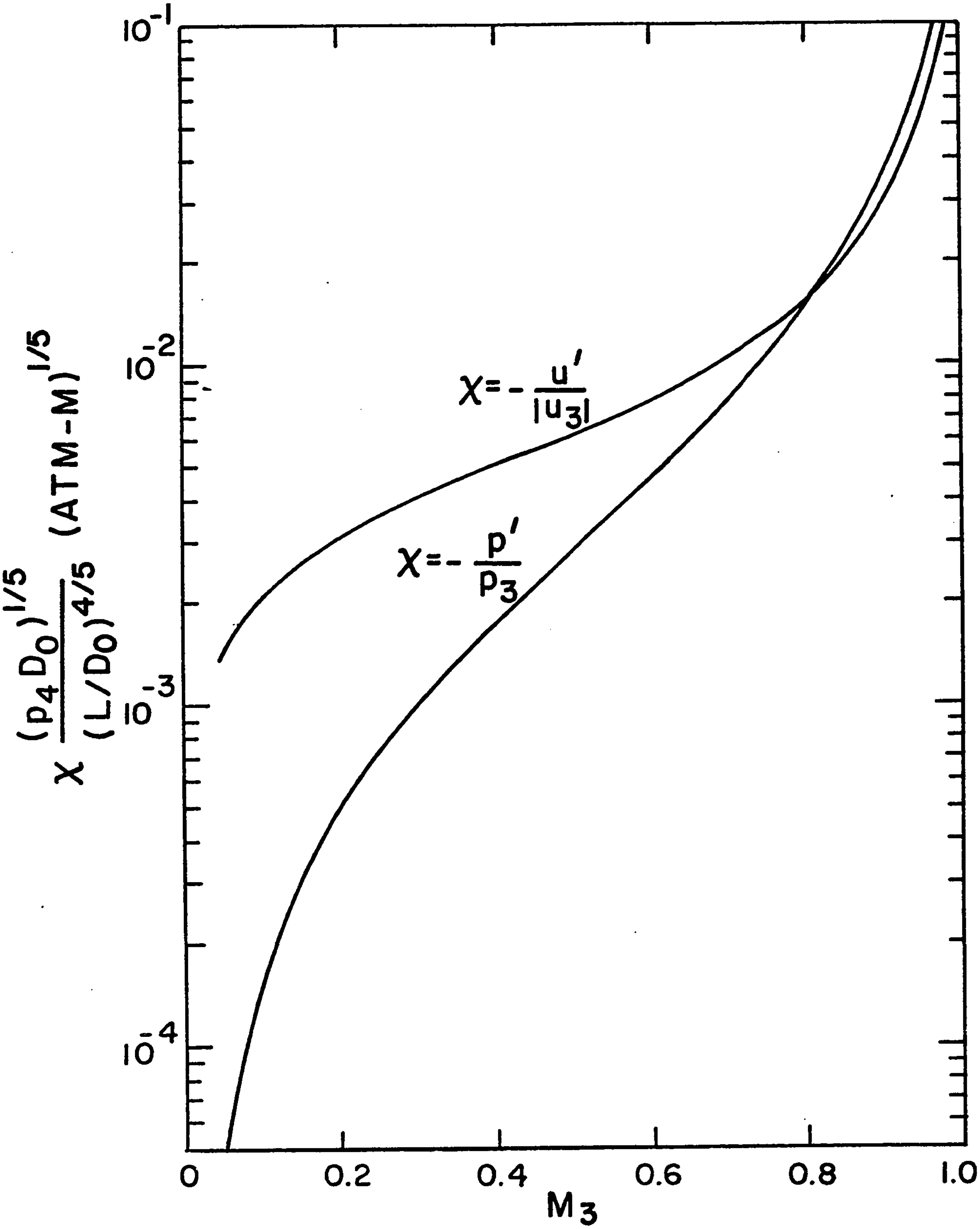

Figure 11: Boundary Layer Induced Velocity and Pressure Perturbations at the Nozzle Inlet and the End of Test Time, Nitrogen with T_{40} = 300°K.

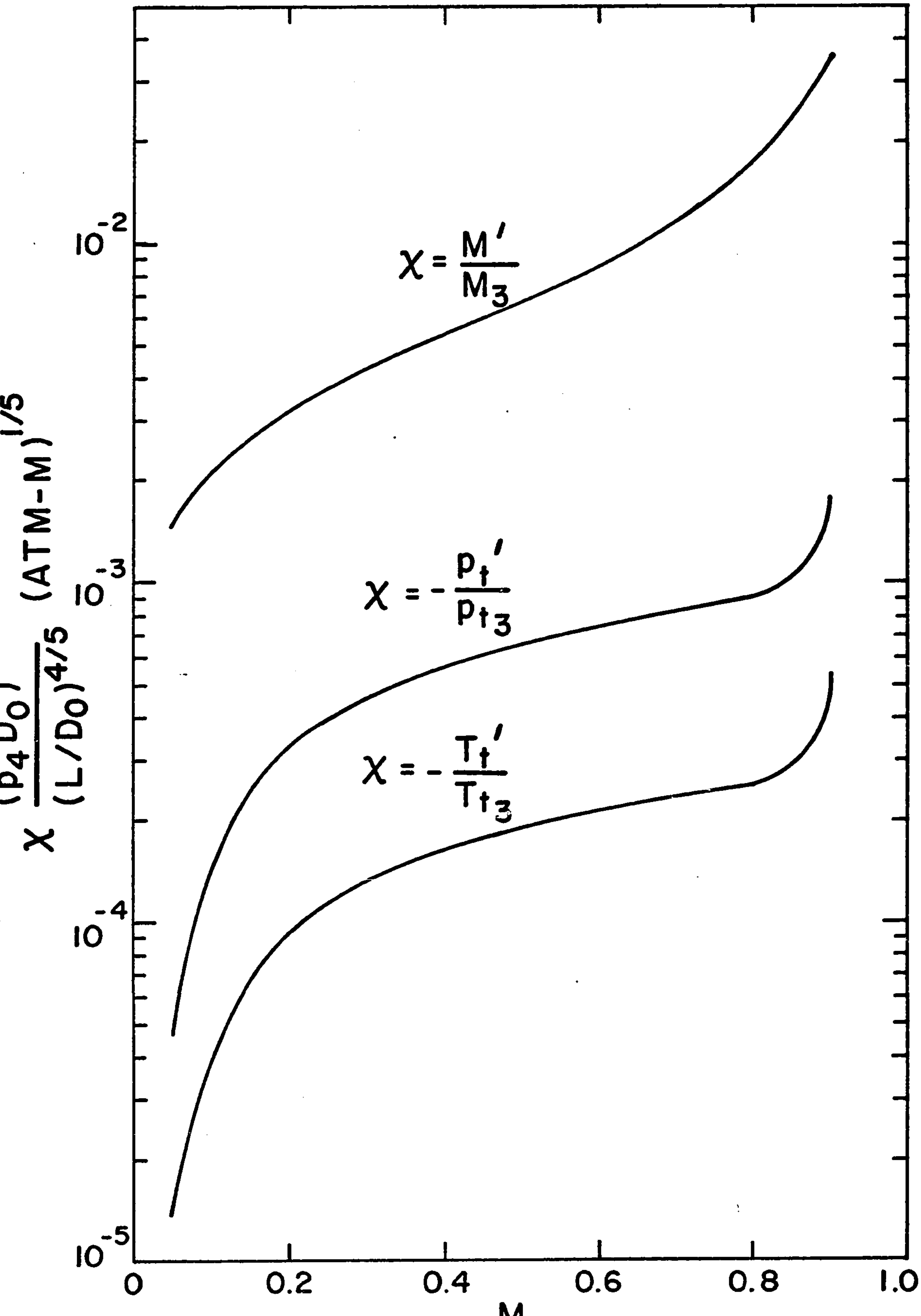

Figure 12. Boundary Layer Induced Mach Number, Stagnation Pressure and Stagnation Temperature Perturbations at the Nozzle Inlet and the End of Test Time, Nitrogen with T_{40} = 300°K.

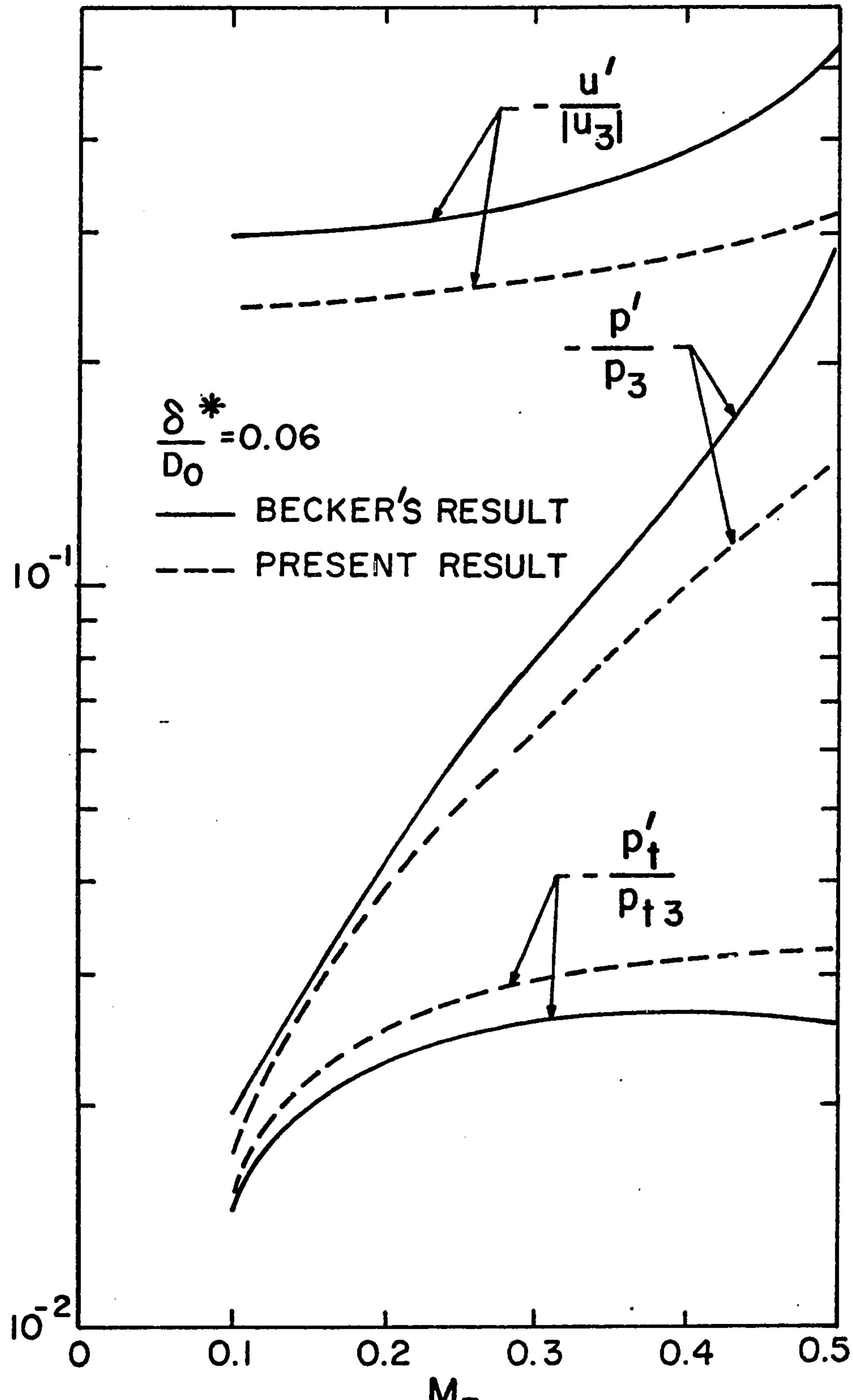

Figure 13: Comparison of the Boundary Layer Induced Perturbations at the Nozzle Inlet Predicted by Two Different Analyses, δ^*/D_0 at the Nozzle Inlet Equals 0.06, γ= 1.4.

For a given boundary layer thickness at the nozzle inlet, as M_3 increases, the thickness of boundary layer at the nozzle throat also increases. At high M_3 the boundary layer thickness at the throat should not be neglected. From the one-dimensional steady channel flow relationship, it can be shown that if this boundary layer thickness is taken into consideration, the perturbation of Mach number at the nozzle inlet is smaller than if this boundary layer thickness is neglected, and hence Equations (41) to (45) overestimate the perturbations at high M_3. Therefore the boundary condition in this chapter is valid only for low M_3 and thin boundary layer at the nozzle inlet. In general, the appropriate boundary condition for high M_3 will be difficult to obtain in closed form. The growth of the boundary layer between the nozzle inlet and nozzle throat depends on the geometry of the nozzle and is obtainable by numerical analysis (e.g. Reference 15). Such calculations were not carried out in the present study because of the other inconsistencies in the analysis at high M_3.

In an earlier paper (Reference 16), Equation (41) was simplified at low M_3 by neglecting all the terms of M_3^2 and higher order. This is equivalent to replacing Equation (26) with:

$$-4\delta^*/D_0 \;=\; -\frac{dM_e}{M_3} \;\approx\; \frac{u'}{|u_3|} + \frac{\gamma-1}{2\gamma}\frac{p'}{p_3} \quad . \tag{26a}$$

The static pressure perturbations thus obtained were found to agree very well with the experimental results even at high M_3 (see also Chapter V). At high M_3, for the same δ^*/D_0 at the nozzle inlet, the simplified boundary condition given by Equation (26a) yields a smaller perturbation in Mach number than that given by Equation (26). As explained earlier, if the throat boundary layer thickness is taken into consideration at high M_3, this perturbation is expected to be smaller. Therefore, while Equation (26) is valid only for low M_3, Equation (26a) is consistent at low M_3 and more appropriate at high M_3.

Although this analysis for the perturbations in the core flow is based on the assumption that the boundary layer has a 1/7th power velocity profile, boundary layers with 1/7th to 1/9th profiles have been observed in other experiments (Reference 8). In Appendix C, the present analysis is extended to boundary layers with 1/nth power velocity profiles. When Becker's approach to the growth of the boundary layer behind a discontinuity surface moving with velocity V is extended to a 1/nth power velocity profile, the displacement thickness of the boundary layer turns out to be similar to Equation (10), with K and the exponents of the Reynolds number and $\frac{U_0 t-x}{D_0}$ dependent on n; the density across the boundary layer can be considered constant. Expressions similar to Equations (41) and (42) are derived for static pressure and velocity perturbations. Figure 14 plots the static pressure and velocity perturbations at the nozzle inlet at the end of test time for n=7 and 10. m is the power in skin friction law as discussed in Appendix C. It can be seen that the effect of n on the perturbations is small.

Effect of the Change of Diameter

When the effects of boundary layer and variations in T_4 are neglected, the static pressure and velocity perturbations at any point $(\bar{x},\bar{t})$ are

$$\frac{p'}{\rho_3 a_3 |u_3|} = \frac{2M_3}{1-M}\frac{D'(\bar{x})}{D_0} + \frac{1-\frac{\gamma-1}{2}M_3}{(1+\frac{\gamma-1}{2}M_3)(1+M_3)}\frac{D'(\frac{\beta}{\alpha}\xi)}{D_0} + \frac{1}{1+M_3}\frac{D'(\eta)}{D_0} \quad , \tag{48}$$

$$\frac{u'}{|u_3|} = \frac{2}{1-M_3^2}\frac{D'(\bar{x})}{D_0} + \frac{1-\frac{\gamma-1}{2}M_3}{(1+\frac{\gamma-1}{2}M_3)(1+M_3)}\frac{D'(\frac{\beta}{\alpha}\xi)}{D_0} - \frac{1}{1+M_3}\frac{D'(\eta)}{D_0} \quad . \tag{49}$$

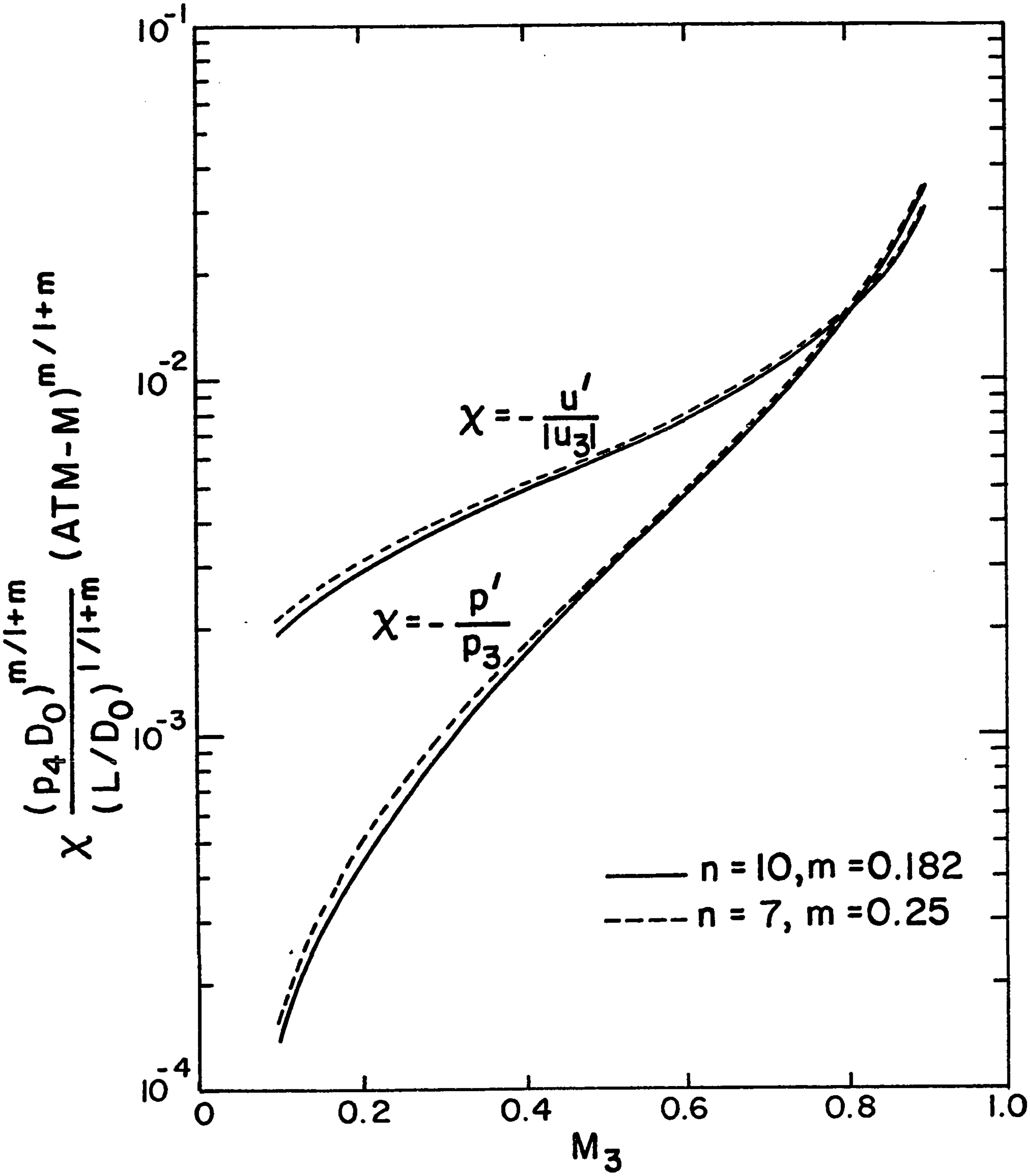

Figure 14: Velocity and Static Pressure Perturbations Induced by Boundary Layers with Different Velocity Profile, Nitrogen with T_{40} = 300°K.

Since the entropy of the gas is constant, the relations for the perturbations in speed of sound, Mach number, temperature, stagnation temperature and stagnation pressure are the same as given by Equations (43) to (47).

When applied to the nozzle inlet (i.e. $\bar{x}=0$), Equations (48) and (49) can be simplified into

$$\frac{p'}{\rho_3 a_3 |u_3|} = \frac{2}{(1 + \frac{\gamma-1}{2} M_3)(1+M_3)} \frac{D'(\beta\bar{t})}{D_0} \quad , \tag{48a}$$

$$\frac{u'}{|u_3|} = - \frac{(\gamma-1)M_3}{(1 + \frac{\gamma-1}{2} M_3)(1+M_3)} \frac{D'(\beta\bar{t})}{D_0} \quad . \tag{49a}$$

Hence at any given time $\bar{t}$, the perturbations at the nozzle inlet depend only on the variations from D_0 of the diameter at $\bar{x}=\beta\bar{t}$.

It can be seen from Equations (48) and (49) that the perturbations at any point $(\bar{x},\bar{t})$ consist of three parts: the local value of D', the effect of the boundary condition at the nozzle inlet, and the difference of diameter at some point upstream of $\bar{x}$. These effects are illustrated in Figure 15. Generally, it is impossible to draw any conclusion about the perturbations without specifying the distribution of diameter. However, the perturbations at the nozzle inlet are linearly dependent on the diameter at some specific point along the tube, and can be calculated in term of D'/D_0. The perturbations in static pressure, velocity, and temperature thus obtained at the nozzle inlet for $\gamma=1.4$ are shown in Figure 16. The perturbations are seen to be 0.1 - 1 times D'/D_0 for moderate M_3. Because the Mach number at x=0 is constant, p'/p_3 and T'/T_3 are identical to p_t'/p_{t3} and T_t'/T_{t3}, respecticely, at the nozzle inlet.

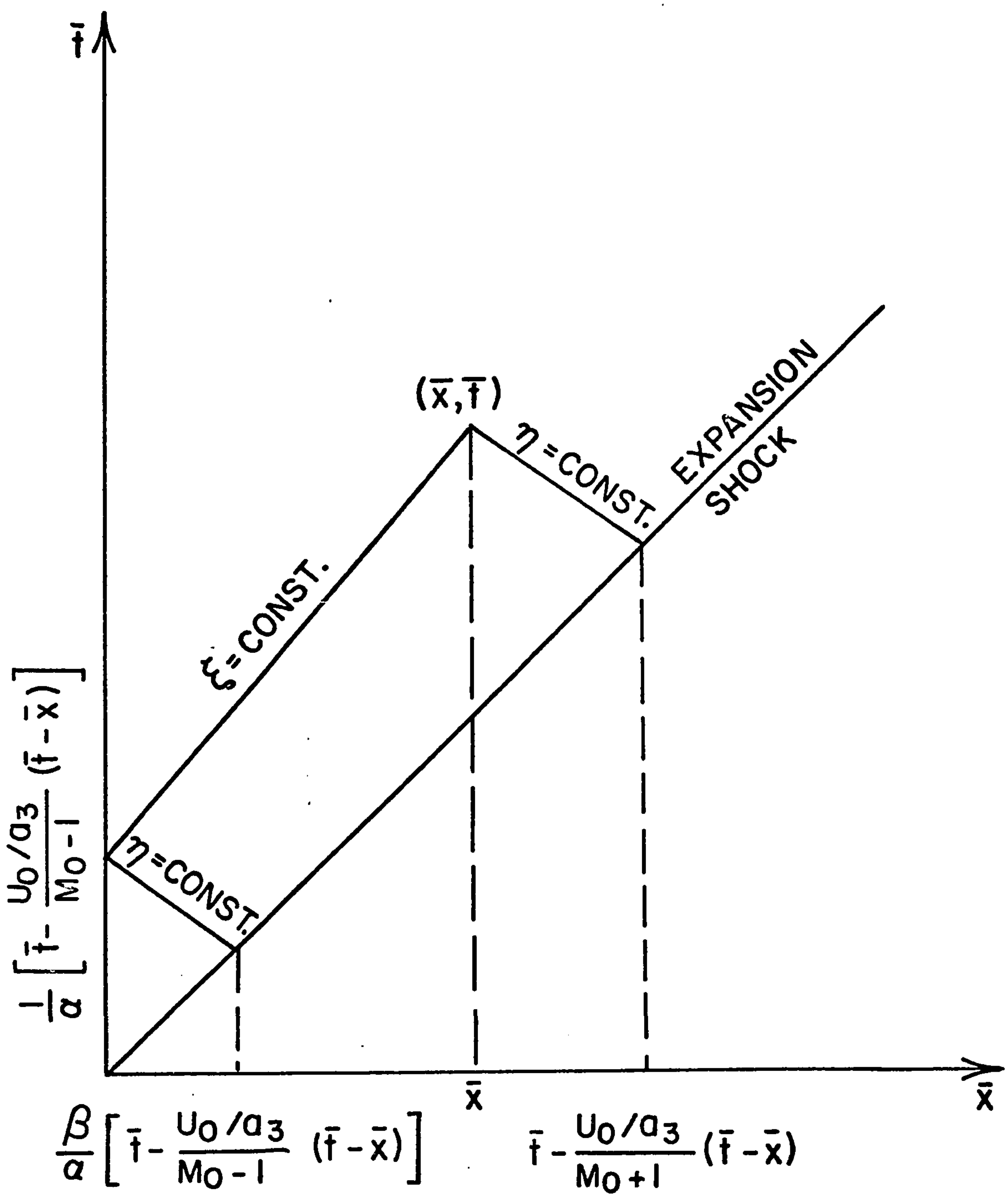

Figure 15: Relationship Between the Distribution of Tube Diameter and Perturbations at Arbitrary Point.

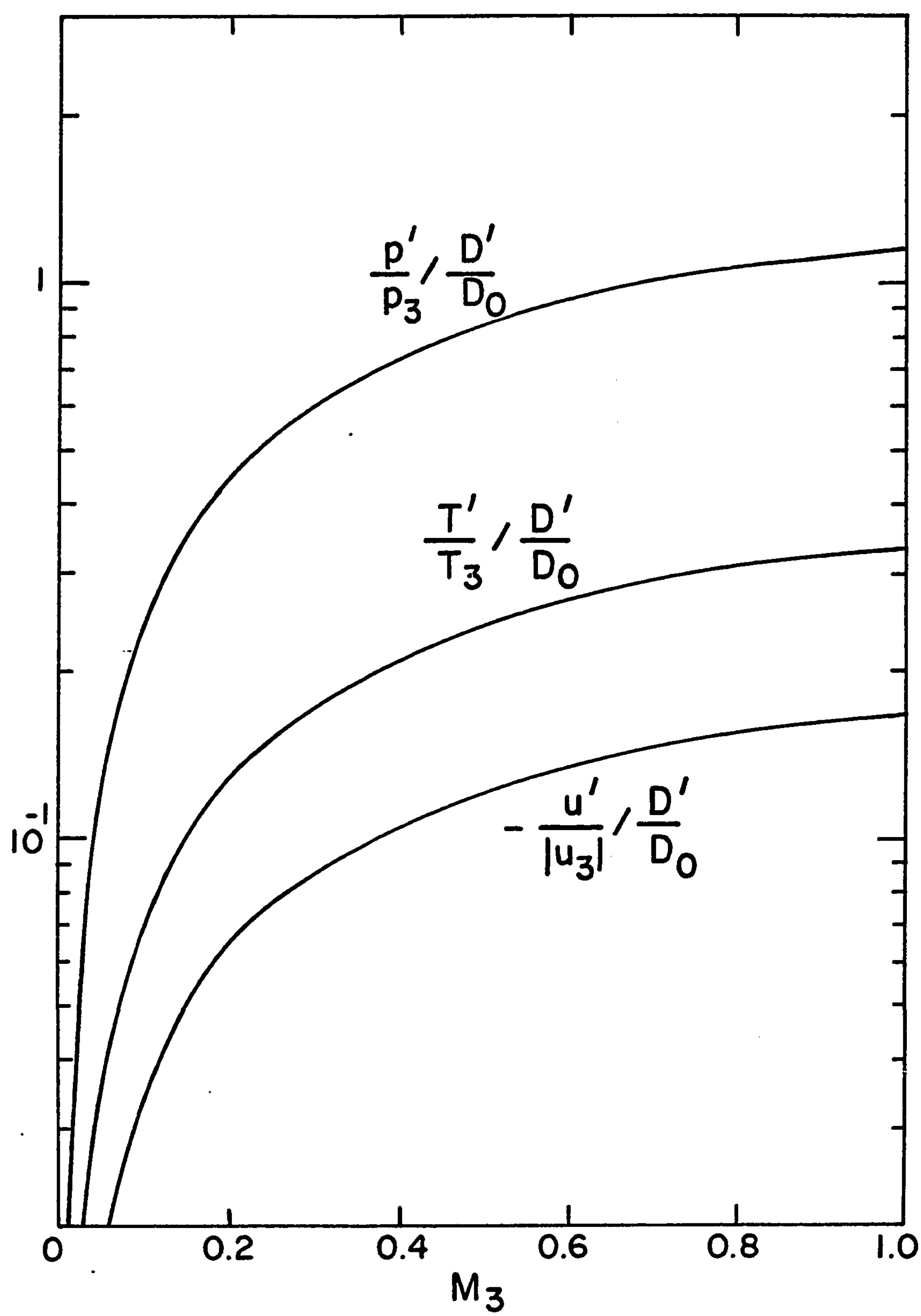

Figure 16: Effect of Changes in Tube Diameter on the Core Flow Perturbations at the Nozzle Inlet, γ=1.4.

Effect of Initial Temperature Variations

For this case, Equations (38) and (39) can be simplified into

$$\frac{p'}{\rho_3 a_3 |u_3|} = -\frac{1}{1+\frac{\gamma-1}{2}M_3}\frac{a_4'\left(\frac{M_3}{M_0}\frac{\xi}{\alpha}\right)}{a_{40}} + \frac{1}{2}\frac{1-\frac{\gamma-1}{2}M_3}{1+\frac{\gamma-1}{2}M_3}\frac{a_4'\left(\frac{\beta}{\alpha}\xi\right)}{a_{40}}$$

$$+ \frac{1}{2}\frac{a_4'(\eta)}{a_{40}} \quad , \tag{50}$$

$$\frac{u'}{|u_3|} = -\frac{1}{1+\frac{\gamma-1}{2}M_3}\frac{a_4'\left(\frac{M_3}{M_0}\frac{\xi}{\alpha}\right)}{a_{40}} + \frac{1}{2}\frac{1-\frac{\gamma-1}{2}M_3}{1+\frac{\gamma-1}{2}M_3}\frac{a_4'\left(\frac{\beta}{\alpha}\xi\right)}{a_{40}}$$

$$- \frac{1}{2}\frac{a_4'(\eta)}{a_{40}} \quad . \tag{51}$$

In Equations (50) and (51), the static pressure and velocity perturbations are written in terms of the variations of initial speed of sound (a_4'), which bears the relationship $a_4'/a_{40} = \frac{1}{2} T_4'/T_{40}$ with the variation of initial temperature (T_4). Although the entropy is constant for individual gas particles, it is different for different particles. The perturbations in the speed of sound and the stagnation pressure are

$$\frac{a'}{a_3} = \frac{\gamma-1}{2\gamma}\frac{p'}{p_3} + \frac{a_4'(\bar{x}_s)}{a_{40}} \quad , \tag{52}$$

$$\frac{p_t'}{p_{t3}} = \frac{\gamma}{\gamma-1}\left(\frac{T_t'}{T_{t3}} - \frac{T'}{T_3}\right) + \frac{p'}{p_3} = \frac{\gamma}{\gamma-1}\frac{T_t'}{T_{t3}} - 2\frac{a_4'(\bar{x}_s)}{a_{40}} \tag{53}$$

Expressions for the perturbations in Mach number, temperature and stagnation temperature are the same as given in Equations (44), (45) and (46).

For x=0, Equations (50), (51) and (52) become

$$\frac{p'}{\rho_3 a_3 |u_3|} = -\frac{1}{1+\frac{\gamma-1}{2}M_3}\frac{a_4'\left(\frac{M_3}{M_0}\bar{t}\right)}{a_{40}} + \frac{1}{1+\frac{\gamma-1}{2}M_3}\frac{a_4'(\beta\bar{t})}{a_{40}} \quad , \tag{50a}$$

$$\frac{u'}{|u_3|} = -\frac{1}{1+\frac{\gamma-1}{2}M}\frac{a_4'\left(\frac{M_3}{M_0}\bar{t}\right)}{a_{40}} - \frac{\frac{\gamma-1}{2}M_3}{1+\frac{\gamma-1}{2}M_3}\frac{a_4'(\beta\bar{t})}{a_{40}} \quad , \tag{51a}$$

$$\frac{a'}{a_3} = \frac{\gamma-1}{2}\frac{p'}{p_3} + \frac{a_4'\left(\frac{M_3}{M_0}\bar{t}\right)}{a_{40}} \quad . \tag{52a}$$

The term $\frac{a_4'\left(\frac{M_3}{M_0}\bar{t}\right)}{a_{40}}$ represents the variation of entropy of the gas particle occupying the nozzle inlet at $\bar{t}$. The perturbations at the nozzle inlet at any time $\bar{t}$ depend on the variations of initial temperature at $M_3/M_0\bar{t}$ and $\beta\bar{t}$ along the tube, as shown in Figure 17a; the perturbations at any other point $(\bar{x},\bar{t})$, however, depend on the variations of initial temperature at four points (viz. $\frac{M_3}{M_0}\frac{\xi}{\alpha}$, $\frac{\beta}{\alpha}\xi$, η and $\bar{x}_s$) along the tube as shown in Figure 17b.

Figure 18 shows the perturbations in static pressure, velocity, and temperature at the nozzle inlet at the end of test time for a linear initial temperature distribution. Here $\Delta T_4/T_4$ is the variation of T_4 at the closed end It is obvious that the perturbations are 0.1 - 1 times $\Delta T_4/T_4$ for moderate M_3. Because the Mach number at the nozzle inlet is constant, p'/p_3 and T'/T_3 at that position are identical to p_t'/p_{t3} and T_t'/T_{t3}, respectively.

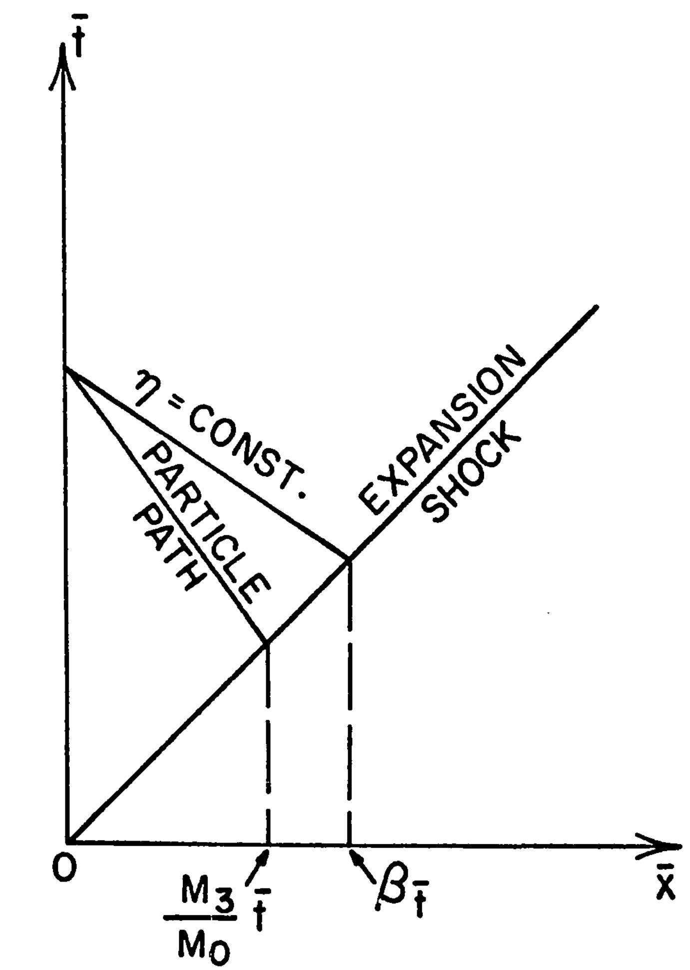

Figure 17a: Relationship Between Initial Temperature Distribution and the Nozzle Inlet Perturbations.

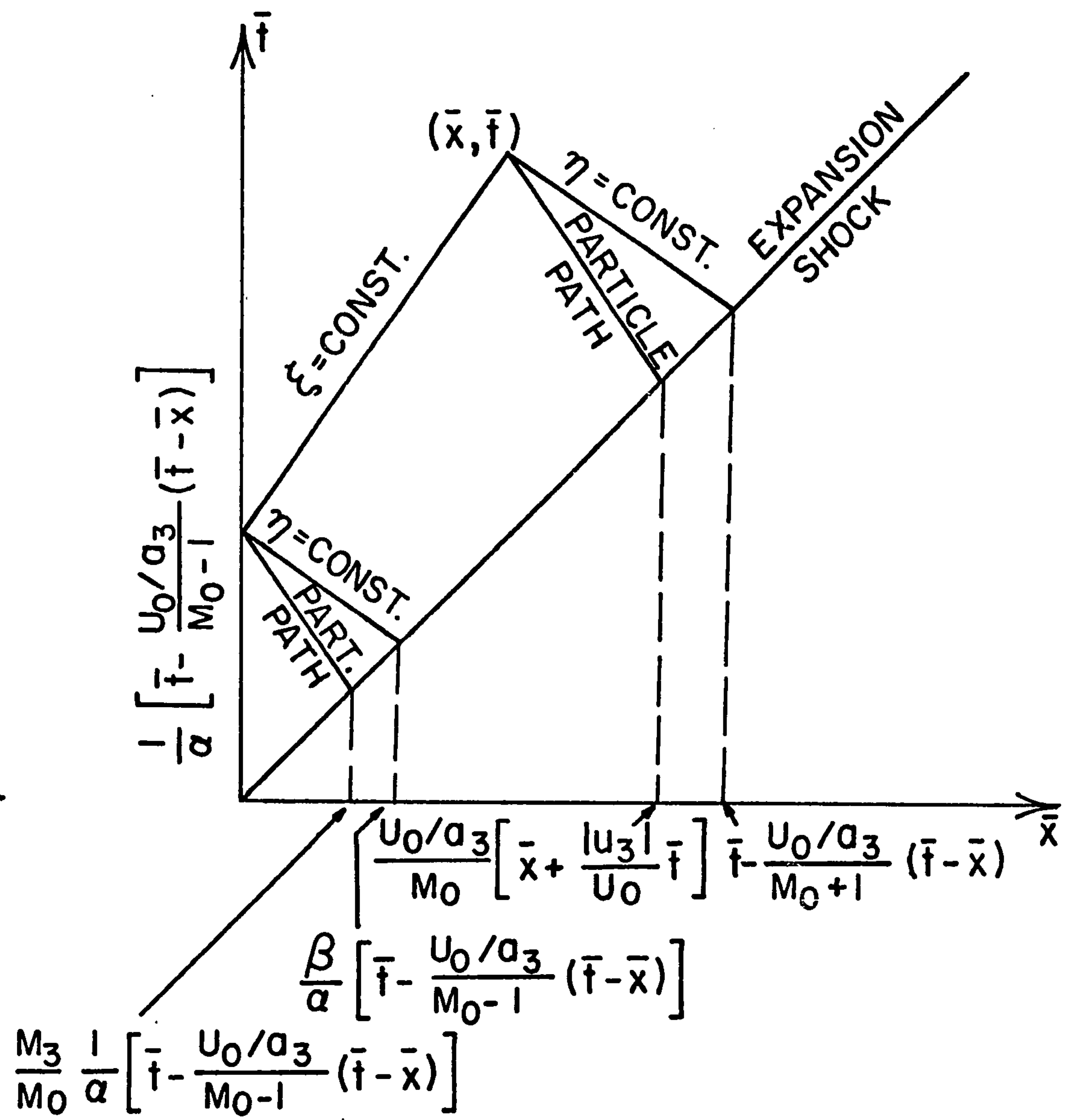

Figure 17b: Relationship Between Initial Temperature Distribution and Perturbations at Arbitrary Point.

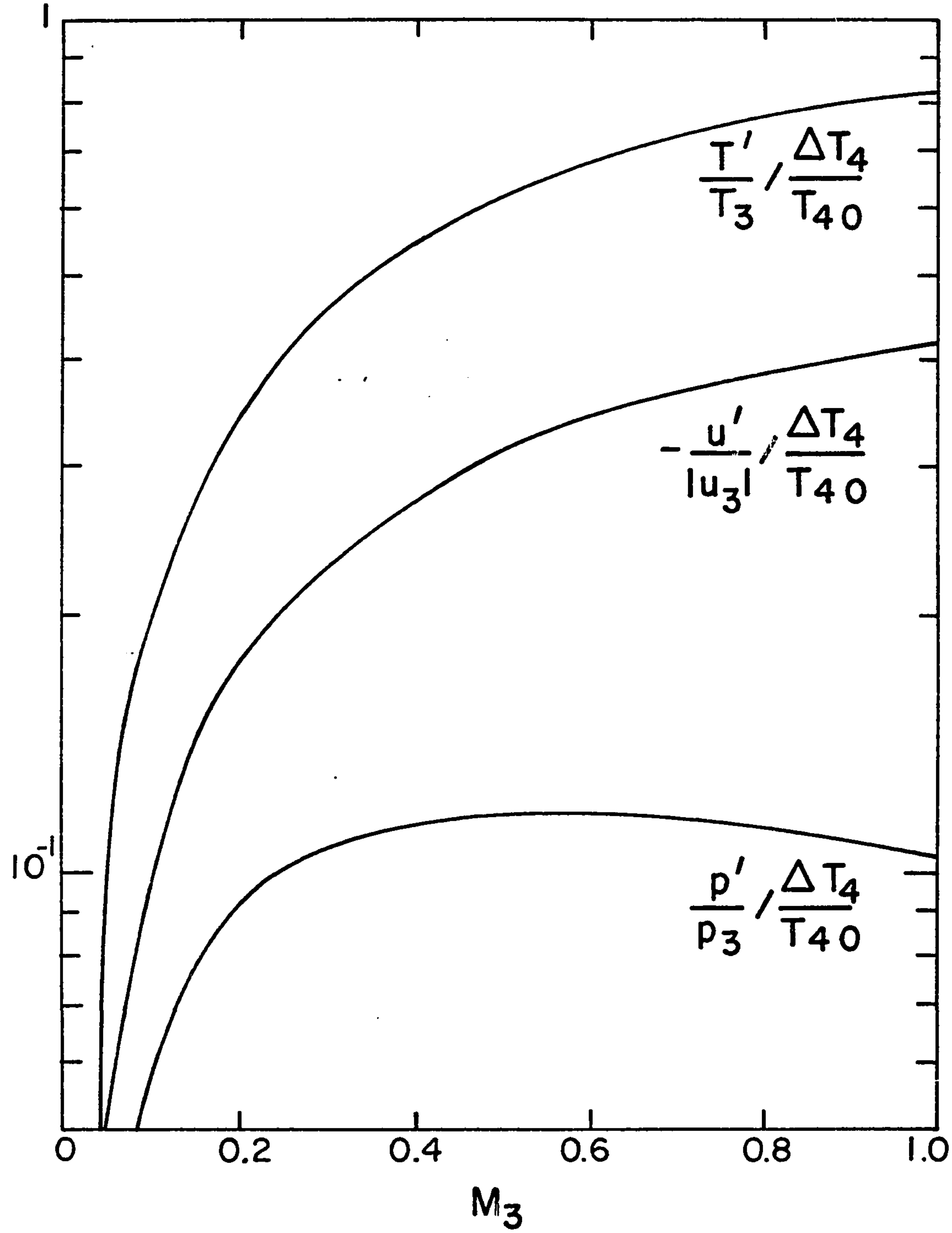

Figure 18: Effect of a Linear Initial Temperature Distribution on the Core Flow Perturbations at the Nozzle Inlet, $\gamma = 1.4$.

CHAPTER IV: CORE FLOW UNIFORMITY WITHIN THE EXPANSION WAVE

As mentioned in Chapter I, Becker pioneered the study of the viscous effect within the Ludwieg tube, however, he did not consider the effect of the boundary layer on the flow within the expansion wave. In a recent paper, such an effect was considered by Hall (Reference 18), but his emphasis was on the effect of laminar boundary layer. In this chapter, the effect of the non-steady turbulent boundary layer on the uniformity of the core flow within the expansion wave is studied. The basic approach is the same as in the previous chapter. Besides being an extension of the work in Chapter III, the result of this study will be useful for assessing the validity of the expansion shock assumption at high Mach number.

IV-1. Equations for the Flow Within the Expansion Wave

Even in the ideal case, the flow within the expansion wave is non-steady and the method of characteristics must be used in order to calculate the properties of the flow. Following Becker (Reference 5), one can define $\psi \equiv 1 - \frac{x}{a_{40}t}$ as dimensionless distance between any point x and the head of the expansion wave at time t, then along each ψ = constant line, the unperturbed properties of the flow remain constant (Reference 5, 14, 17). In other words, for a given condition in Region 4, the flow properties are a function of ψ only. For centered waves, the condition of isentropy leads to:

$$a_i = a_{40}\left(1 - \frac{\gamma-1}{\gamma+1}\psi\right) = a_{40}\left(1 - \frac{\psi}{6}\right) , \tag{54}$$

$$T_i = T_{40}\left(1 - \frac{\gamma-1}{\gamma+1}\psi\right)^2 = T_{40}\left(1 - \frac{\psi}{6}\right)^2 \approx T_{40}\left(1 - \frac{\psi}{3}\right) , \tag{55}$$

$$\rho_i = \rho_{40}\left(1 - \frac{\gamma-1}{\gamma+1}\psi\right)^{2/\gamma-1} = \rho_{40}\left(1 - \frac{\psi}{6}\right)^5 , \tag{56}$$

$$p_i = p_4(1 - \frac{\gamma-1}{\gamma+1}\psi)^{2\gamma/\gamma-1} = p_4(1 - \frac{\psi}{6})^7 \quad , \tag{57}$$

$$u_i = - a_{40}(\frac{2}{\gamma+1}\psi) = - a_{40}(\frac{5}{6}\psi) \quad , \tag{58}$$

$$M_i = \frac{\frac{2}{\gamma+1}\psi}{1 - \frac{\gamma-1}{\gamma+1}} = \frac{5\psi}{6 - \psi} \quad . \tag{59}$$

where the subscript i refers to the unperturbed conditions in the flow within the expansion wave, and the right-hand expressions in Equations (54) to (59) are for $\gamma = 1.4$.

IV-2. Linearized Equations

Since only the effect of the boundary layer is considered, the continuity equation takes a similar form to Equation (3),

$$\frac{\partial \rho_e}{\partial t} + \frac{\partial}{\partial x}(\rho_e u_e) = \frac{4}{D_0}\frac{\partial}{\partial t}\int_0^\delta (\rho_e - \rho)dy + \frac{4}{D_0}\frac{\partial}{\partial x}\int_0^\delta (\rho_e u_e - \rho u)dy \quad . \tag{3a}$$

The momentum equation is the same as Equation (5),

$$\rho_e\left(\frac{\partial u_e}{\partial t} + u_e\frac{\partial u_e}{\partial x}\right) + \frac{\partial p_e}{\partial x} = 0 \quad . \tag{5}$$

And the condition of particle isentropy also holds, that is,

$$\left(\frac{\partial}{\partial t} + u_e\frac{\partial}{\partial x}\right)\ln\frac{p_e}{\rho_e^{\gamma}} = 0 \quad . \tag{6}$$

Equations (3a) and (6) can be combined to give

$$\frac{1}{a_e^2}\left(\frac{\partial p_e}{\partial t} + u_e \frac{\partial p_e}{\partial x}\right) + \rho_e \frac{\partial u_e}{\partial x} = \frac{4}{D_0}\frac{\partial}{\partial t}\int_0^\delta (\rho_e - \rho)\,dy + \frac{4}{D_0}\frac{\partial}{\partial x}\int_0^\delta (\rho_e u_e - \rho u)\,dy \quad . \tag{60}$$

Assuming

$$\frac{U}{u_e} = (y/\delta)^{1/7} \quad , \text{ and } \frac{\rho}{\rho_e} = \frac{\rho_w}{\rho_e} + \left(1 - \frac{\rho_w}{\rho_e}\right)\left(\frac{y}{\delta}\right)^{1/7} , \quad \text{(Reference 5)}$$

where ρ_w is the density at the wall, then

$$\int_0^\delta (\rho_e - \rho)\,dy = \rho_e \left(1 - \frac{\rho_w}{\rho_e}\right)\frac{\delta}{8} \quad ,$$

$$\int_0^\delta (\rho_e u_e - \rho u)\,dy = \rho_e u_e \left(\frac{2}{9} - \frac{7}{72}\frac{\rho_w}{\rho_e}\right)\delta \quad .$$

Substituting the above into Equation (60), the governing equations become

$$\frac{1}{a_e^2}\left(\frac{\partial p_e}{\partial t} + u_e \frac{\partial p_e}{\partial x}\right) + \rho_e \frac{\partial u_e}{\partial x} = \frac{4}{D_0}\frac{\partial}{\partial t}\left[\rho_e\left(1 - \frac{\rho_w}{\rho_e}\right)\frac{\delta}{8}\right] + \frac{4}{D_0}\frac{\partial}{\partial x}\left[\rho_e u_e\left(\frac{2}{9} - \frac{7}{72}\frac{\rho_w}{\rho_e}\right)\delta\right] \quad , \tag{61}$$

$$\rho_e\left(\frac{\partial u_e}{\partial t} + u_e \frac{\partial u_e}{\partial x}\right) + \frac{\partial p_e}{\partial x} = 0 \quad . \tag{62}$$

As discussed In Chapter II, the thickness of the turbulent boundary layer within the expansion wave was given by Becker (Reference 5) as

$$\delta = (a_{40}t)^{4/5}\left(\frac{\nu_{40}}{a_{40}}\right)^{1/5}\left[\frac{0.196}{3}\left(1 - 0.193\psi - 0.006\psi^2\right)\right]^{4/5} \cdot \psi^{7/5} \approx (a_{40}t)^{4/5}\left(\frac{\nu_{40}}{a_{40}}\right)^{1/5}\left(\frac{0.196}{3}\right)^{4/5}\psi^{7/5} \quad . \tag{63}$$

At $\psi = 1$ (i.e. $M_i = 1$) the value of δ as given by the second expression is 20% less than that given by the first expression; for simplicity, the second expression is used in this analysis.

The properties of the core flow within the expansion wave, similar to those behind the expansion wave, can be separated into the perturbed and the unperturbed parts, except in this case the latter part is a function of x and t. If the wall temperature remains as T_{40}, then

$$\frac{\rho_w}{\rho_e} = \frac{T_e}{T_{40}} \quad .$$

For small perturbations, Equations (61) and (62) can be simplified into

$$\frac{1}{a_i^2}\left(\frac{\partial p'}{\partial t} + u_i \frac{\partial p'}{\partial x} + u' \frac{\partial p_i}{\partial x}\right) - \frac{\gamma-1}{\gamma}\frac{1}{a_i^2}\frac{p'}{p_i}\left(\frac{\partial p_i}{\partial t} + u_i \frac{\partial p_i}{\partial x}\right)$$

$$+ \rho_i \frac{\partial u'}{\partial x} + \rho' \frac{\partial u_i}{\partial x} = \frac{4}{D_0}\left\{\frac{1}{8}\frac{\partial}{\partial t}\left[\rho_i \left(1 - \frac{T_i}{T_{40}}\right)\delta\right]\right.$$

$$\left. + \frac{\partial}{\partial x}\left[\rho_i u_i \delta\left(\frac{2}{9} - \frac{7}{72}\frac{T_i}{T_{40}}\right)\right]\right\} \quad , \tag{64a}$$

$$\rho_i\left(\frac{\partial u'}{\partial t} + u_i \frac{\partial u'}{\partial x} + u' \frac{\partial u_i}{\partial x}\right) + \frac{p'}{a_i^2}\left(\frac{\partial u_i}{\partial t} + u_i \frac{\partial u_i}{\partial x}\right)$$

$$+ \frac{\partial p'}{\partial x} = 0 \quad . \tag{64b}$$

Here all the terms of order $(\delta/D_0)^2$ and higher are neglected. (The details of the derivation of Equations (64a) and (64b) can be found in Appendix D).

IV-3. Solutions of the Linearized Equations

Equations (64a) and (64b) form a system of partial differential equations essentially similar to Equations (11) and (12), but the present equations are quasi-linear with coefficients which are known functions of x and t. It can be shown easily that this system of equations is hyperbolic (Reference 14) with characteristic directions given by $(a_i + u_i)$ and $(-a_i + u_i)$. Following References 5 and 14, the two characteristic variables are chosen as

$$\psi = 1 - \frac{x}{a_{40}t} \quad , \tag{65}$$

and
$$\omega = t\left(\frac{5}{6} + \frac{x}{6a_{40}t}\right)^3 \quad , \quad \text{for } \gamma = 1.4 \tag{66}$$

ψ as defined earlier, is a dimensionless distance between any point x and the head of the expansion wave at time t, while ω represents the time when a ω = constant characteristic intersects the head of the expansion wave. In terms of these two characteristic variables, Equations (64a) and (64b) become

$$\Lambda_\omega + \frac{2}{3}\frac{\Delta}{\omega} - \frac{4a_{40}}{D_0}\left(\frac{0.196}{3}\right)^{4/5} \rho_{40}a_{40}{}^{4/5}\left(\frac{\nu_{40}}{a_{40}}\right)^{4/5} \omega^{4/5}\left(1 - \frac{\psi}{6}\right)^{3/5}$$
$$\cdot \ \psi^{7/5}\left(\frac{7}{20} - \frac{401}{72 \times 36}\psi + \frac{13}{60 \times 27}\psi^2\right) = 0 \tag{67}$$

$$\Delta_\psi + \frac{1}{1 - \frac{\psi}{6}}\left(\frac{\Delta}{2}\right) + \frac{2a_{40}}{D_0}\left(\frac{0.196}{3}\right)^{4/5} \rho_{40}a_{40}{}^{4/5}\left(\frac{\nu_{40}}{a_{40}}\right)^{1/5} \omega^{9/5}$$
$$\cdot \left(1 - \frac{\psi}{6}\right)^{-2/5} \psi^{7/5}\left(\frac{7}{20} - \frac{401}{72 \times 36}\psi + \frac{13}{60 \times 27}\psi^2\right) = 0 \tag{68}$$

Here

$$\Lambda \equiv \rho_{40}\left(1 - \frac{\psi}{6}\right)^6 tu' + \frac{t}{a_{40}}p' \tag{69a}$$

$$\Delta \equiv \rho_{40}\left(1 - \frac{\psi}{6}\right)^6 tu' - \frac{t}{a_{40}}p' \tag{69b}$$

(The derivation of Equations (67) and (68) can be found in Appendix D).

From Equation (68) it follows that

$$\Delta = C(\omega)(1 - \frac{\psi}{6})^3 - (1 - \frac{\psi}{6})^3 \frac{2a_{40}}{D_0} (\frac{0.196}{3})^{4/5} \rho_{40} a_{40}^{4/5}$$

$$\cdot (\frac{\nu_{40}}{a_{40}})^{1/5} \omega^{9/5} \int (1 - \frac{\psi}{6})^{-17/5} \psi^{7/5} \left(\frac{7}{20} - \frac{401}{72 \times 36} \psi \right.$$

$$\left. + \frac{13}{60 \times 27} \psi^2 \right) d\psi \quad .$$

Along the head of the expansion wave, (i.e. $\psi = 0$) u' and p' are zero, and the second term in the above equation is also zero. Hence $C(\omega)$ must equal to zero for any value of ω. If $(1 - \frac{\psi}{6})^{-17/5}$ is expanded by a binomial series, i.e.

$$(1 - \frac{\psi}{6})^{-17/5} = 1 + \frac{17}{30} \psi + \ldots,$$

then

$$\Delta = -10(\frac{0.196}{3})^{4/5} \frac{\rho_{40} a_{40}^{9/5}}{D_0} (\frac{\nu_{40}}{a_{40}})^{1/5} (1 - \frac{\psi}{6})^3 \omega^{9/5} \psi^{12/5}$$

$$\cdot (\frac{0.35}{12} + \frac{0.04363}{17} \psi - \frac{0.00692}{22} \psi^2) \quad . \qquad (70)$$

From Equation (67), one obtains

$$\Lambda = \frac{20}{9} (\frac{0.196}{3})^{4/5} \frac{\rho_{40} a_{40}^{9/5}}{D_0} (\frac{\nu_{40}}{a_{40}})^{1/5} \omega^{9/5} \left[\frac{5}{3} (1 - \frac{\psi}{6})^3 (\frac{0.35}{12} \right.$$

$$+ \frac{0.04363}{17} \psi - \frac{0.00692}{22} \psi^2) + (1 - \frac{\psi}{6})^{3/5} \omega^{7/5} (\frac{7}{20}$$

$$\left. - \frac{401}{72 \times 36} \psi + \frac{13}{60 \times 27} \psi^2) \right] \quad . \qquad (71)$$

The constant of integration is zero because both u' and p' approach zero as t approaches zero.

Combining Equations (70) and (71) to solve for p´ and u´,

$$\frac{p'}{p_4} = 14\left(\frac{0.196}{3}\right)^{4/5} \left(\frac{a_{40}t}{D_0}\right)^{4/5} \left(\frac{\nu_{40}}{a_{40}D_0}\right)^{1/5} \left(1 - \frac{\psi}{6}\right)^{6}$$

$$\cdot\ \psi^{7/5} \left[\frac{37}{54}\left(1 - \frac{\psi}{6}\right)^{12/5} \psi \left(\frac{0.35}{12} + \frac{0.04363}{17}\psi - \frac{0.00692}{22}\psi^2\right)\right.$$

$$\left. + \frac{1}{9}\left(\frac{7}{20} - \frac{401}{72 \times 36}\psi + \frac{13}{60 \times 27}\psi^2\right)\right] , \tag{72}$$

$$\frac{u'}{a_4} = 10\left(\frac{0.196}{3}\right)^{4/5} \left(\frac{a_{40}t}{D_0}\right)^{4/5} \left(\frac{\nu_{40}}{a_{40}D_0}\right)^{1/5} \psi^{7/5}\left[-\frac{17}{54}\left(1\right.\right.$$

$$\left. - \frac{\psi}{6}\right)^{12/5} \psi \left(\frac{0.35}{12} + \frac{0.04363}{17}\psi - \frac{0.00692}{22}\psi^2\right)$$

$$\left. + \frac{1}{9}\left(\frac{7}{20} - \frac{401}{72 \times 36}\psi + \frac{13}{60 \times 27}\psi^2\right)\right] \tag{73}$$

IV-4. <u>Results and Discussion</u>

Equations (72) and (73) can be rewritten in the following form:

$$\frac{p'}{p_i} = 14\left(\frac{0.196}{3}\right)^{4/5} \left(\frac{a_{40}t}{D_0}\right)^{4/5} \left(\frac{\nu_{40}}{a_{40}D_0}\right)^{1/5} \frac{\psi^{7/5}}{1 - \frac{\psi}{6}} \left[\frac{37}{54}\left(1\right.\right.$$

$$\left. - \frac{\psi}{6}\right)^{12/5} \psi \left(\frac{0.35}{12} + \frac{0.04363}{17}\psi - \frac{0.00692}{72}\psi^2\right)$$

$$\left. + \frac{1}{9}\left(\frac{7}{20} - \frac{401}{72 \times 36}\psi + \frac{13}{60 \times 27}\psi^2\right)\right] , \tag{72a}$$

$$\frac{u'}{|u_i|} = 12\left(\frac{0.196}{3}\right)^{4/5} \left(\frac{a_{40}t}{D_0}\right)^{4/5} \left(\frac{\nu_{40}}{a_{40}D_0}\right)^{1/5} \psi^{2/5}\left[-\frac{17}{54}\left(1\right.\right.$$

$$\left. - \frac{\psi}{6}\right)^{12/5} \psi \left(\frac{0.35}{12}\right) + \frac{0.04363}{17}\psi - \frac{0.00692}{22}\psi^2)$$

$$\left. + \frac{1}{9}\left(\frac{7}{20} - \frac{401}{72 \times 36}\psi + \frac{13}{60 \times 27}\psi^2\right)\right] . \tag{73a}$$

The perturbations of other properties in the core flow are:

$$\frac{a'}{a_i} = \frac{1}{2}\frac{T'}{T_i} = \frac{\gamma-1}{2}\frac{\rho'}{\rho_i} = \frac{\gamma-1}{2\gamma}\frac{p'}{p_i} \quad , \tag{74}$$

$$\frac{M'}{M_i} = -\left(\frac{u'}{|u_i|} + \frac{a'}{a_i}\right) \quad , \tag{75}$$

$$\frac{T_t'}{T_{ti}} = \frac{T_i}{T_{ti}}(\gamma-1)M_i^2\left(\frac{M'}{M_i}\right) + \frac{T'}{T_i} = \frac{\gamma-1}{\gamma}\frac{p_t'}{p_{ti}} \quad . \tag{76}$$

When $0 \leq \psi \leq 1$, the p' and u' given by Equations (72a) and (73a) are positive. Thus, the effect of boundary layer is to reduce the basic changes in pressure, velocity, temperature, etc. The same conclusion has been drawn by Hall (Reference 18) for the case of laminar boundary layer.

From the derivation of Equations (72) and (73), it is obvious that the perturbations at any point within the expansion wave are functions of ψ and t only, and are independent of the flow downstream. This is because the characteristics for the linearized equations are the same as that for the unperturbed flow in which the characteristics are divergent. The perturbations at the tail of expansion wave are independent of the boundary condition at the nozzle inlet; similar results have been obtained in the previous chapter.

The perturbations in static pressure and velocity at the tail of the expansion wave can be evaluated from Equations (72a) and (73a) by replacing ψ with ψ_3, $|u_i|$ with $|u_3|$, and p_i with p_3. Here ψ_3 is given by

$$\psi_3 = \frac{6M_3}{5 + M_3}$$

Figure 19 shows such perturbations for nitrogen at T_{40} = 300°K. The pressure perturbation increases as M_3 increases, while the velocity perturbation peaks at about M_3 = 0.4. Equivalent perturbations based on the results of the

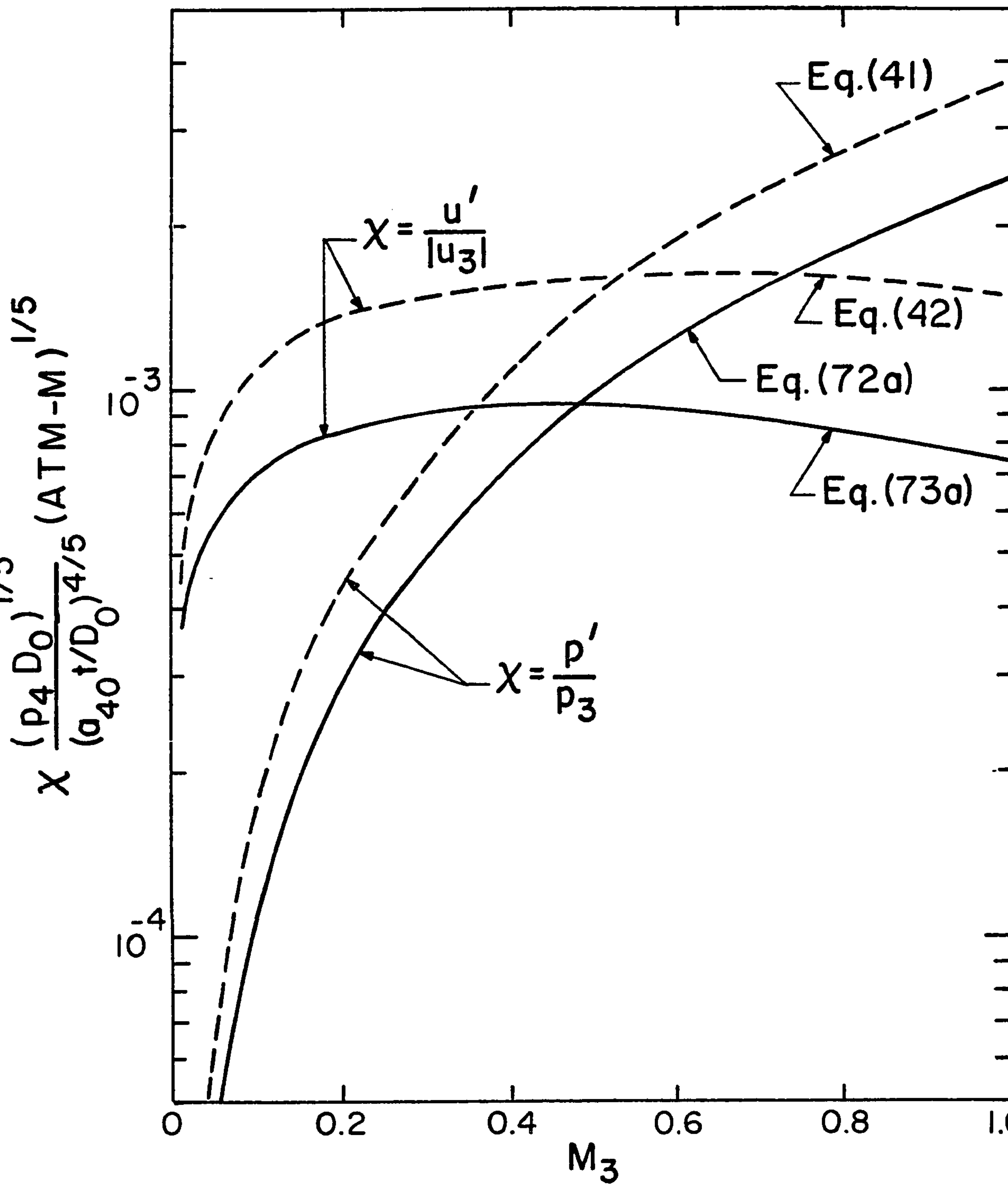

Figure 19. Boundary Layer Induced Velocity and Static Pressure Perturbations at the Tail of the Expansion Wave, Nitrogen with T_{40} = 300°K.

previous chapter are also shown in Figure 19. Here the velocity perturbation has a maximum value at around $M_3 = 0.7$. Although the perturbations based on the expansion shock model are consistently larger, the two models are generally in agreement: even at $M_3 = 0.9$, the difference in static pressure perturbation is just 55%, while there is a factor of two difference in the two velocity perturbations. From this comparison, it can be concluded that the expansion shock model is still reasonably accurate even at high Mach number.

IV-5. Matching the Perturbations at the Tail of the Expansion Wave

An attempt has been made to calculate an effective U_0 by matching p' and u' at the unperturbed tail of the expansion wave. For the flow behind the expansion wave, the non-steady expansion wave is replaced by an expansion shock moving with unknown velocity U_0. The static pressure and velocity perturbation at any point behind the expansion wave are given by Equations (14) and (15). When evaluated at the unperturbed tail of expansion wave, i.e. $\xi = 0$ and $\eta = 2\bar{t}/(M_0 + 1)$, these perturbations are

$$\frac{p'}{p_3} = \gamma M_3 \Big[\frac{5}{4} K(Re_{D_0})^{-1/5} \frac{M_0}{M_0^2 - 1} \left(\frac{M_0 - 1}{U_0/a_3}\right)^{4/5} \bar{t}^{\,4/5} + f(0) - g\left(\frac{2\bar{t}}{M_0 + 1}\right) \Big] \quad , \tag{77}$$

$$\frac{u'}{|u_3|} = \frac{5}{4} K(Re_{D_0})^{-1/5} \frac{1}{M_0^2 - 1} \left(\frac{M_0 - 1}{U_0/a_3}\right)^{4/5} \bar{t}^{\,4/5} + f(0) + g\left(\frac{2\bar{t}}{M_0 + 1}\right) \quad ; \tag{78}$$

$f(0)$ can be set equal to zero without losing generality. K has the same functional dependence on M_3 and $|u_3|/U_0$ as in Becker's model. The static pressure and velocity perturbation at the same position can also be calculated from Equations (72a) and (73a); they are set equal to Equations (77) and (78). Thus, two equations of unknown U_0 and $g(\frac{2\bar{t}}{M_0 + 1})$ are obtained. The U_0 obtained by solving these two equations turns out to be larger than a_{40}, with the ratio U_0/a_{40} ranging from 1.12 at $M_3 = 0.1$ to 1.25 at $M_3 = 0.9$. The displacement thickness of the boundary layer based on this value of U_0 is much larger than that obtained by Becker (Reference 5; see also Chapter II): even at $M_3 = 0.1$ there is a factor of two differences in the displacement thickness at the tail of the expansion wave.

The evident failure of this attempt may be due to the fact that only the first order terms are considered. Under such conditions, the divergence of the characteristics from their unperturbed positions are neglected; the governing equations change from quasi-linear to linear across the unperturbed tail of the expansion wave. Taking into consideration the second and higher order terms, not only will the tail of expansion wave be perturbed, but the governing equations will change gradually from one form to another in this region. In other words, the second order terms are expected to be important at the tail of expansion wave. Unfortunately, the governing equations become non-linear when these terms are included; closed form solution may not be obtainable.

CHAPTER V: EXPERIMENTS ON THE EFFECTS OF THE BOUNDARY LAYER AND INITIAL PIPE NONUNIFORMITY

Experiments were carried out in order to check the analysis in Chapter III and their extrapolation to high M_3, thick boundary layers and large pipe nonuniformities. These involved the measurement of the static pressure perturbation at the nozzle inlet throughout the test period.

V-1. Experiments for the Effect of Boundary Layer

The apparatus consisted mainly of a supply tube made up of sections of cold drawn seamless carbon steel pipe with 2.5 cm i.d. and 1.59 cm wall. Two of these sections were 3.56 m long and a third was 6.5 m. Various combinations were used in order to vary the overall length. One end of the supply tube was connected to gas bottles while the other end was connected to the nozzle-diaphragm assembly and then to a stainless steel dump tank 1 m in diameter and 1 m long. Figure 20 depicts the apparatus.

The nozzles used here were not contoured nozzles but were plates 1.25 cm thick with either many small holes located within 1.25 cm from the center or a single large hole at the center. The Mach number behind the expansion wave was altered by changing the plates. For $M_3 \leq 0.5$, four plates of different specifications were used: one plate with twenty-seven 2 mm holes, one with sixty-five 2 mm holes, one with one 2 cm hole, and the fourth with one 2.08 cm hole. They correspond to $M_3 = 0.106$, 0.24, 0.4, and 0.5, respectively. For a reason which will be explained later, two extra plates were used: one with a 1.07 cm hole and the other with a 1.64 cm hole; these correspond to $M_3 = 0.106$ and 0.24. For $M_3 > 0.5$, because the difference between the area at the nozzle inlet and at the nozzle throat is very small, a plate with a single hole of 2.54 cm diameter was used, and the open area of the diaphragm served as the nozzle throat. The diaphragms were made of soft aluminum 1.59 mm thick and

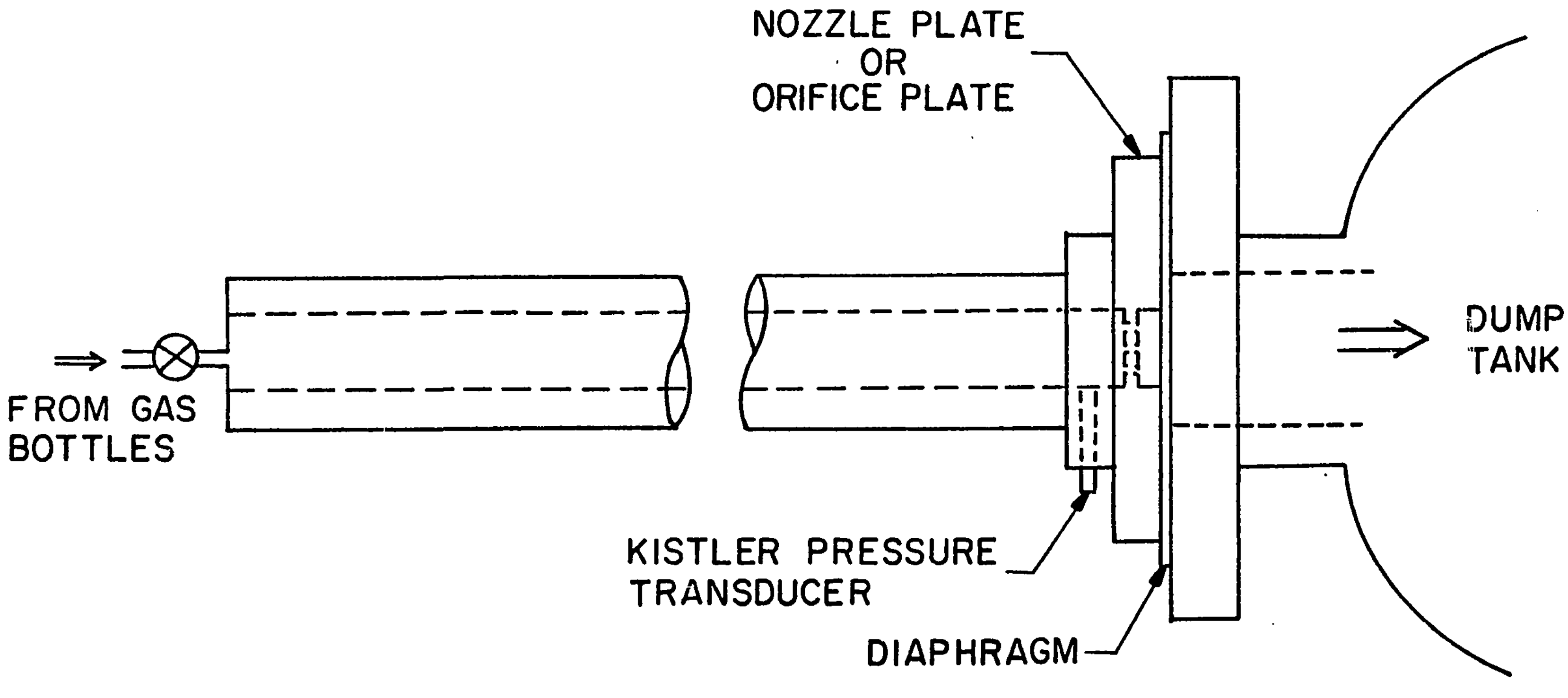

Figure 20: Schematic for the Experimental Apparatus.

were placed between the nozzle plate and the dump tank. They were scribed and then ruptured by pressurizing the supply tube.

A Model 603A Kistler Pressure Transducer was used for the measurement of static pressure. This transducer was mounted on a flange 1.25 cm thick with a 2.54 cm hole at the center. The flange was located upstream of the nozzle. The distance between the centerline of the transducer and the upstream edge of the holes on the nozzle plate was approximately 1 cm. The signal from the transducer was first amplified by a Kistler Charge Amplifier and then displayed on the screen of an oscilloscope; an accelerometer was used as a triggering device for the oscilloscope.

Results. A sample static pressure trace obtained for nitrogen with p_4 = 60 atm, T_{40} = 300°K, M_3 = 0.106 and L/D_0 = 280 is shown in Figure 21. Trace A was a reference trace taken at a known pressure level close to the nominal p_3 value. The expansion wave is seen to clear the gauge in the first millisecond of run time, dropping the pressure to the nominal p_3 value. The expanded vertical scale of the trace shows that the subsequent decline in pressure is nearly linear, in approximate agreement with $t^{4/5}$ dependence predicted by Equation (41). Similar measurement have been made at different M_3 and also at L/D_0 = 540, with p_4 ranging from 30 atm to 130 atm.

For fixed M_3 and L/D_0, the shape of the static pressure trace did not show any pressure dependence. When M_3 was equal to or exceeded 0.4, the static pressure was nearly constant for the first 5 to 7 milliseconds and then declined linearly. This may be due to the finite opening time of the diaphragm. Because the diaphragm did not open instantaneously, the expansion wave became non-centered, and the static pressure at the nozzle inlet dropped to a value slightly higher than p_3 within a millisecond and then decreased gradually to p_3 within the next few milliseconds. For L/D_0 = 540 and at high Mach numbers, the rate of pressure decline decreased during the last part of the test time,

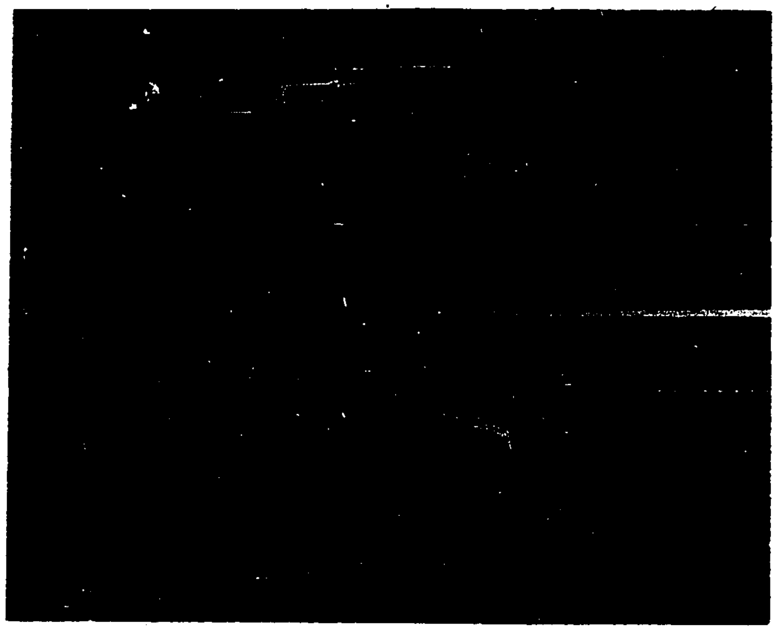

→ 1% p_3/div.

→ 5 msec/div.

Figure 21: Static Pressure Trace for the Effect of the Boundary Layer.

because the boundary layer was so thick that a small part of the flow became fully developed pipe flow. For M_3 = 0.106 and 0.24, the results obtained with nozzle plates with a single hole were similar to those with nozzle plate having many small holes; this indicating that the pressure decline is independent of the flow details in the neighborhood of the gauge station.

The results of the static pressure perturbation at the end of the test time are shown in Figure 22. For M_3 equal to or less than 0.5, p_3 is calculated from p_4, while for M_3 larger that 0.5, p_3 is measured from the static pressure trace with an error of less than 4%. When the results are presented in a normalized fashion such as Figure 22, no dependence on L/D_0 can be observed, as expected from the analysis. The circular symbols are for individual runs, while the bars on some symbols represent the extreme limits of the results of at least ten separate experiments at fixed M_3. The magnitude of p'/p_3 ranges from 1% at M_3 = 0.106 and L/D_0 = 280 to 20% at high M_3 and L/D_0 = 540.

In some of the experiments, thin-film heat transfer gauges were located at different positions along the tube to measure T_4. Although they showed that small axial temperature gradients could be setup in the gas due to compression heating during the charging process, the perturbations in T_4 were at most 1% and its effect on these experiments could generally be neglected (see Figure 18).

The static pressure perturbation predicted by Equation (41) is shown as curve A in Figure 22. The agreement between the experimental results and curve A is good at low M_3; as M_3 increases, the agreement becomes poorer, with curve A consistently giving larger perturbations. As M_3 = 0.5, the predicted value is nearly double the experimental result. The simplified form of Equation (41) for small M_3 (Reference 16) is also shown in Figure 22 as curve B. The agreement between curve B and the experimental results are surprisingly good even at high Mach number. The reason for such good agreement has been discussed in Section III-6.

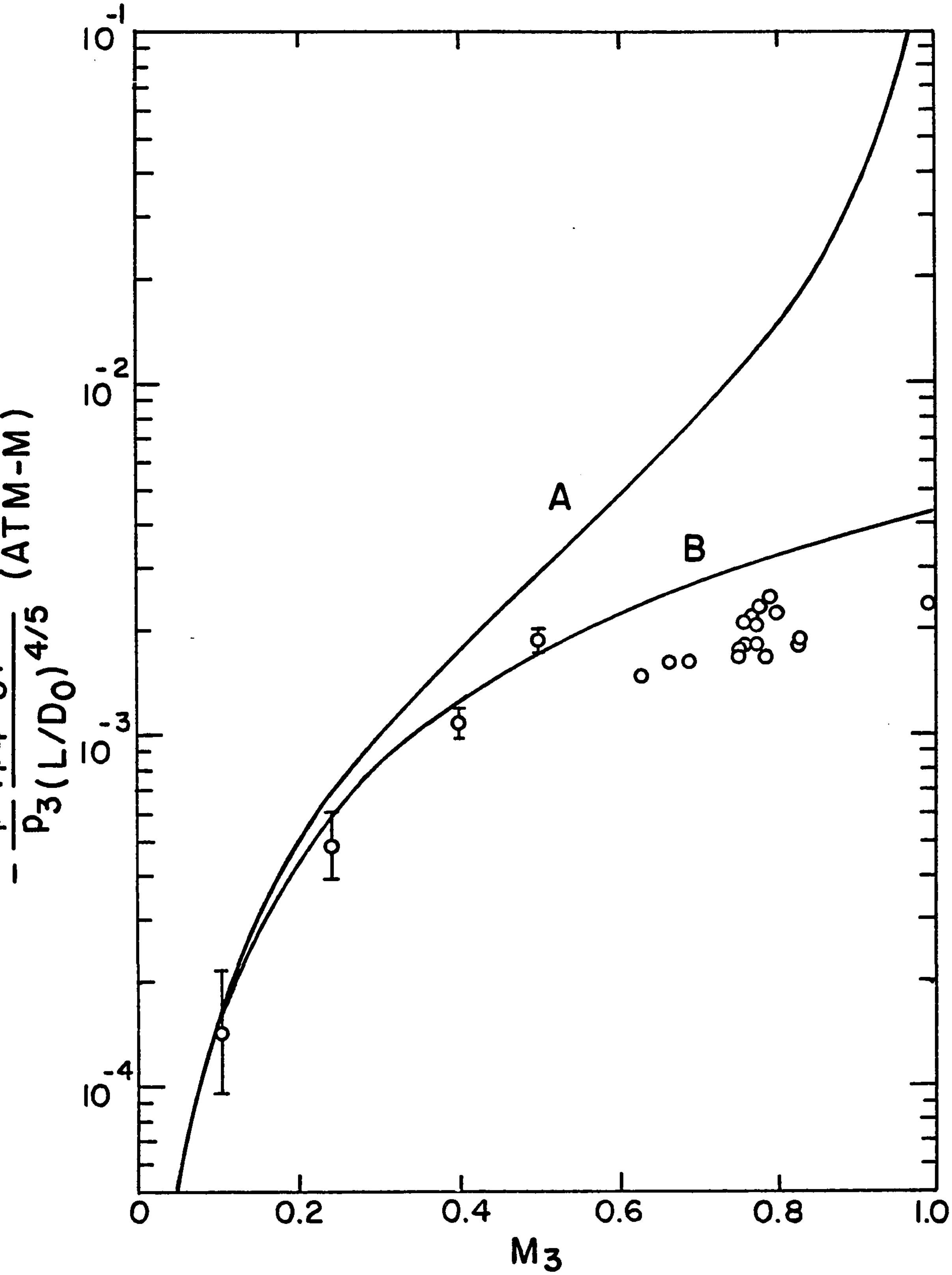

Figure 22: Experimental Results of Boundary Layer Induced Static Pressure Perturbations.

V-2. Experiment for the Effect of Initial Pipe Nonuniformity

Effects of the Change of Diameter.

The experimental setup was similar to the one used in the previous section, except in this case the supply tube consisted of two sections of tube with different internal diameters. The first section was the 3.56 m long tube used in the previous experiments while the second section, located upstream of the first, was 3.16 m long cold drawn seamless steel pipe with either 2.86 cm i.d. and 1.59 cm wall, or 3.18 cm i.d. and 1.59 cm wall, or 3.81 cm i.d. and 1.59 cm wall. When the expansion wave enters the second section of the supply tube, a compression wave will be reflected back due to the increase of the diameter; hence the static pressure trace at the nozzle inlet shows a sudden rise when the reflected compression wave arrives. This rise in static pressure has been measured for different M_3 and changes in tube diameter.

Results. Figure 23 is a sample static pressure trace obtained for nitrogen with p_4 = 70 atm, T_{40} = 300°K, and M_3 = 0.106; the internal diameter of the second section of the supply tube was 3.18 cm. Trace A was a reference trace taken at a known pressure level close to the nominal p_3 value. It can be seen that the reflected compression wave arrived at the nozzle inlet at 18 msec causing a jump in the static pressure. Similar measurements have been made at different M_3 and tube diameter, with p_4 ranging from 30 atm to 130 atm. The results of this set of experiments are presented in Figure 24. Each of the circular, triangular or cross symbol represents a single run, while the bar on some symbols represent the experimental limits of at least 5 runs at fixed M_3. The predicted value given by Equation (48a) in Chapter III are also shown. The experimental value of the static pressure perturbation are not only lower than the predicted value but also have a different dependence on M_3: for a fixed change in diameter, the experimental results show a maximum value between

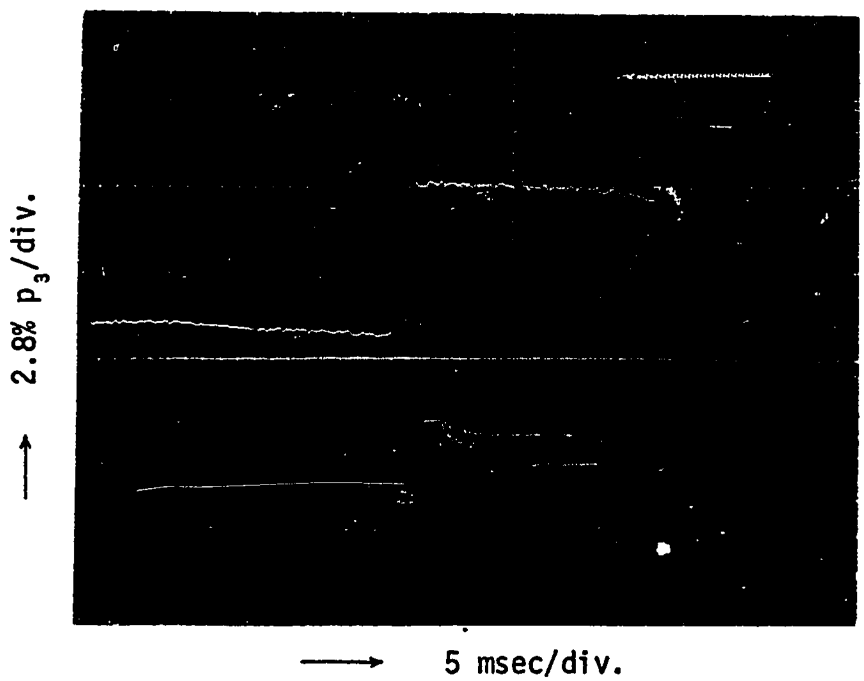

Figure 23: Static Pressure Trace for the Effect of Changes in Tube Diameter.

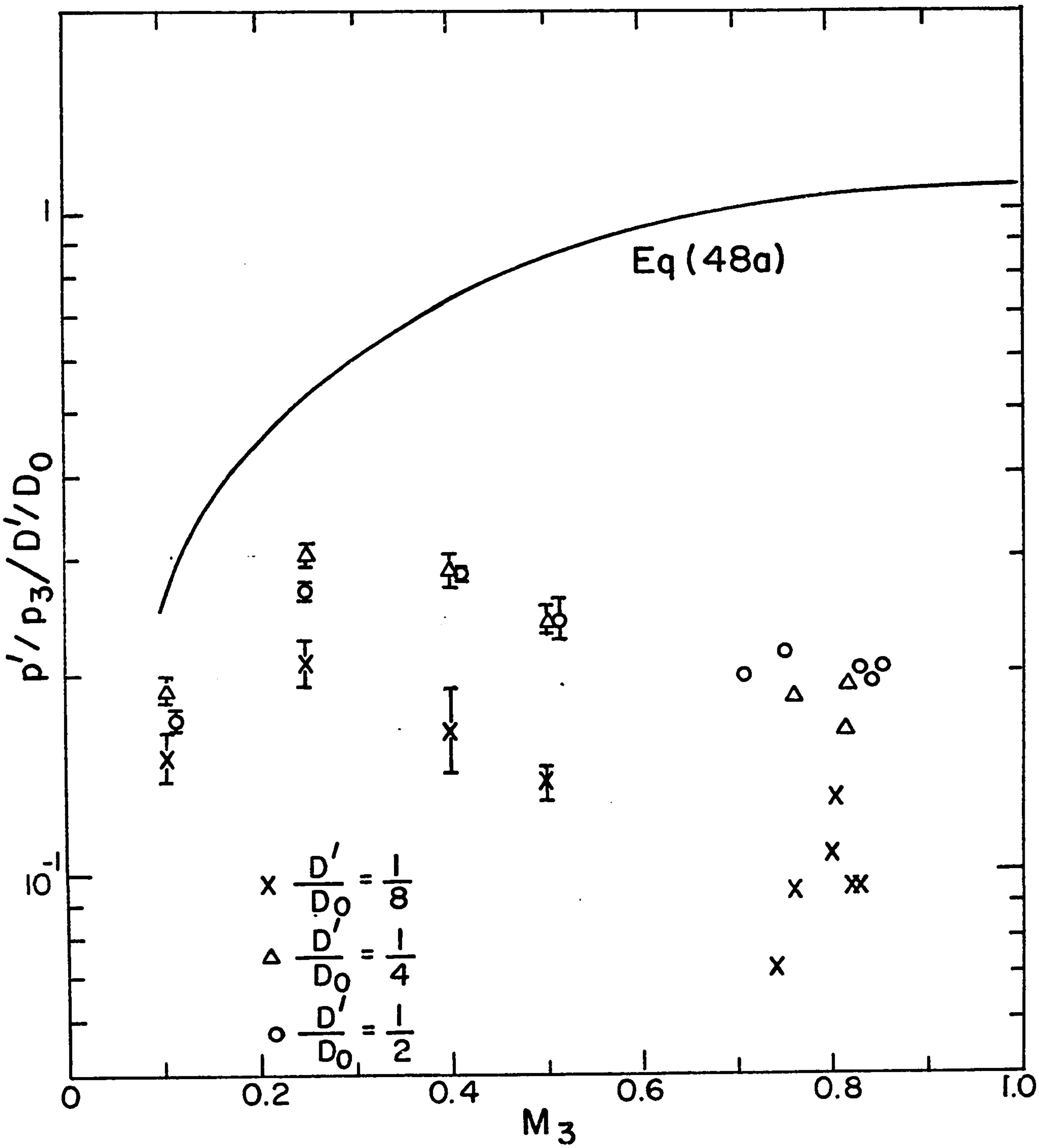

Figure 24: Experimental Results of Static Pressure Perturbations Induced by a Change in Tube Diameter Located 3.56 m Downstream.

M_3 = 0.2 and 0.4 while the predicted value increases with M_3. This discrepancy between the experimental and analytical results is due to the boundary layer in the first section of the supply tube. As far as the effect of change in diameter on the perturbation of the flow is concerned, this boundary layer will introduce two effects. First, when the reflected compression wave due to the change of diameter propagates downstream, it will propagate into a convergent tube rather than a tube with constant area; the compression wave is expected to become stronger (Reference 19). Also, due to the growth of the boundary layer, the Mach number at the nozzle inlet increases with time, and this will reduce the static pressure perturbation given in Equation (48a).

In order to show that this discrepancy between experimental and analytical results is indeed due to the effect of the boundary layer, a second set of experiments has been performed with the length of the first section of the supply tube cut down to 0.915 m, while the second section can be either the tube of 2.86 cm i.d. or 3.18 cm i.d. The results of the second set of experiments are presented in Figure 25a and 25b together with the corresponding results from the first set of experiments. Figure 25a is for the case where the change of diameter is one-eighth of D_0, while Figure 25b is for a change of diameter of one-fourth of D_0. ℓ/D_0 is the ratio of the length of the first section of the supply to its diameter tube. Since Equation (48a) corresponds to zero boundary layer thickness, its values are designated as the case of ℓ/D_0 = 0 in Figures 25a and 25b. The results from the second set of experiments are closer to the prediction of Equation (48a) than the corresponding results from the first set of experiments, and it is seen that the results from the second set of experiments level off at high M while the corresponding reuults from the first set decreases with M . Since the only difference between these two set of experiments is the length of the first section of supply tube, or to be precise, the thicknesses of the boundary layer at the nozzle inlet, it is safe to conclude

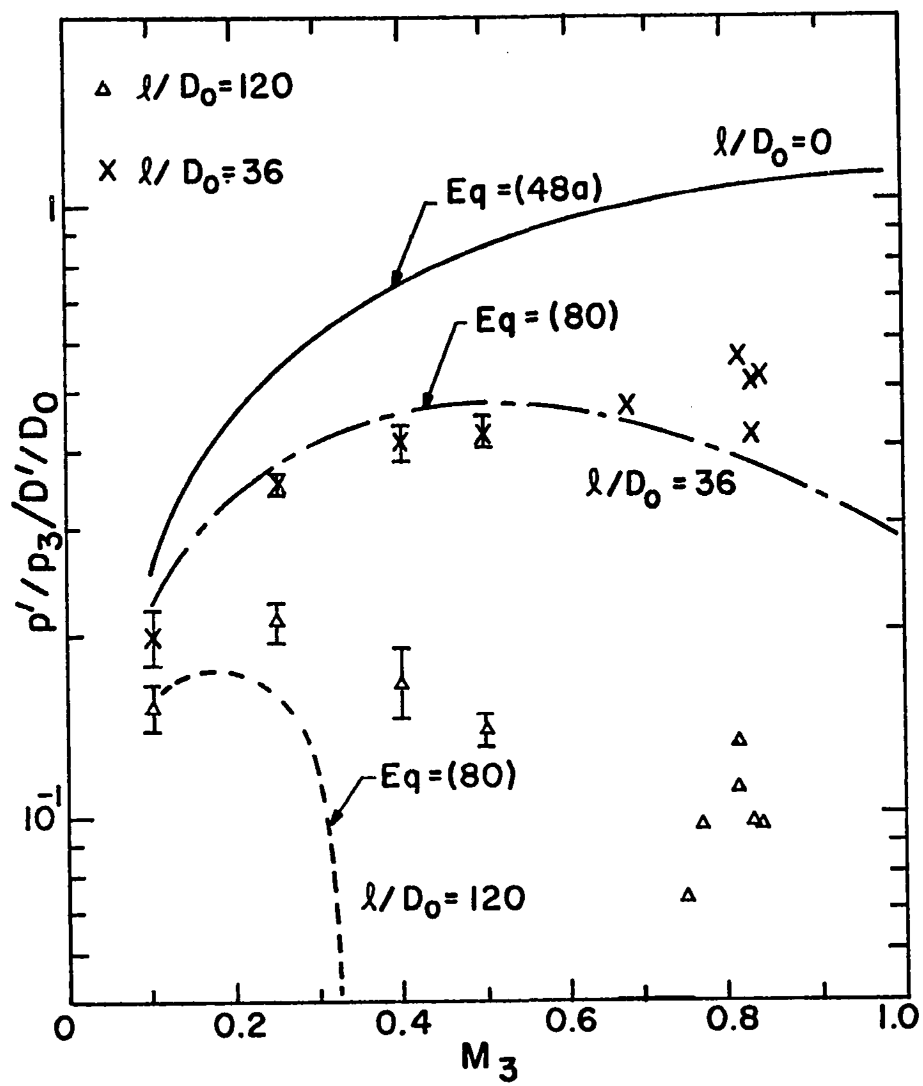

Figure 25a: Results of Static Pressure Perturbations Induced by a Change in Tube Diameter Located 0.915 m Downstream, $D'/D_0 = 1/8$.

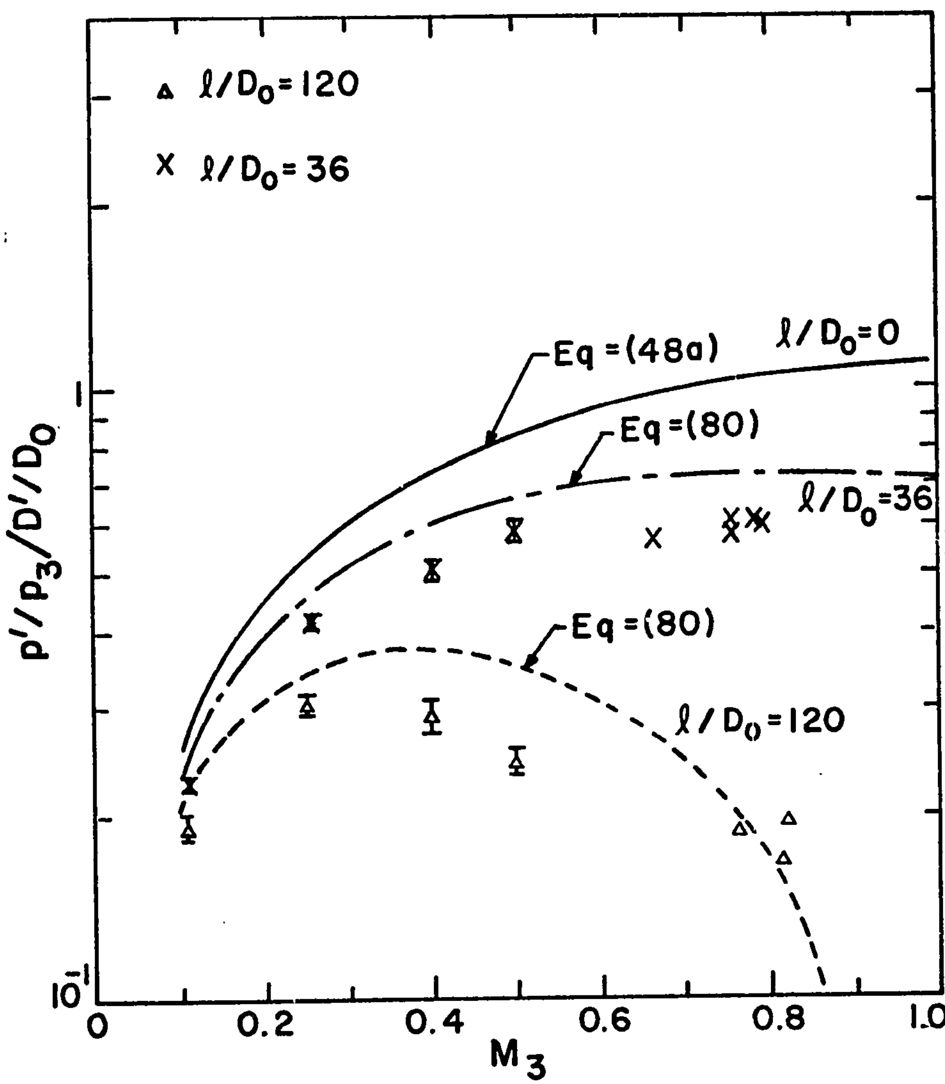

Figure 25b: Results of Static Pressure Perturbations Induced by a Change in Tube Diameter Located 0.915 m Downstream, $D'/D_0 = 1/4$.

that the discrepancy between the results of the first set of experiments and the analytical results is due to the boundary layer.

An attempt has been made to modify the analysis in order to include the effect of the boundary layer in the first section of the supply tube. Instead of using the boundary condition of constant Mach number at the nozzle inlet, the boundary condition

$$- 4\delta^*/D_0 = - \frac{dM_e}{M_3} = \left(\frac{u'}{|u_3|} + \frac{\gamma-1}{2\gamma}\frac{p'}{p_3}\right) \tag{79}$$

is used. It has been discussed in Section III-6 that this boundary condition gives a good prediction of the effect of the boundary layer on the core flow static pressure perturbations even at high M_3. Here

$$\frac{\delta^*}{D_0} = \frac{5}{4} K(Re_{D_0})^{-1/5}\, \bar{t}^{4/5}$$

and u'/u_3 and p'/p_3 are given by Equation (31). The pressure perturbation at the nozzle inlet is given by

$$\frac{p'}{p_3} = - \gamma M_3 \frac{5}{4} K(Re_{D_0})^{-1/5}\, \bar{t}^{4/5} \frac{1}{1 + \frac{\gamma-1}{2} M_3} + \frac{2\gamma M_3}{1 + \frac{\gamma-1}{2} M_3} \cdot \frac{1}{1 + M_3} \frac{D'(\beta\bar{t})}{D_0} \quad . \tag{80}$$

It is obvious that for fixed M_3 and D'/D_0, the static pressure perturbation at the nozzle inlet given by Equation (80) is a weak function of p_4. The pressure perturbation is shown in Figures 25a and 25b for p_4 = 81 atm. For D'/D_0 = 1/8, the results of the first set of experiments agrees with the predicted value given by Equation (80) only at very low M_3; at moderate or high M_3, the experimental results are higher. The predicted values given by Equation (80) are slightly higher than the results of the second set of experiments up to M_3 = 0.7. For D'/D_0 = 1/4, the agreement between the predicted and experimental values are better than for $D'/D_0 = 1/8$. It should be emphasized that Equation (80) includes only the effect of the change of Mach number at the nozzle inlet due to the boundary layer; no attempt has been made to estimate the change of the strength of the reflected wave caused by the change of diameter as it propagates downstream. The neglect of such effect is the reason why at high M_3 the predicted values of Equation (80) corresponding to the first set of experiments are negative while the experimental values are positive.

Effect of Initial Temperature Variations

Detailed experimental study has not been carried out to measure the effect of initial temperature variations on the core flow static pressure perturbation. Several problems arise in setting up a known initial temperature distribution in the gas. First, the axial initial temperature distribution must be measured accurately because the static pressure perturbation is expected to be proportional to the initial temperature variation. Secondly, as the heat conduction in the gas is slow, the gas must be held stationary within the tube long enough to provide uniform temperature at each position along the tube; this requires both the use of steady temperature heating elements for the gas and a mechanically or electrically activated puncher to rupture the diaphragm. Finally, mixing of the gas caused by the temperature differences must be minimized. Although a systematic experimental study of the effect of initial temperature variation was not undertaken, a few experiments established that the predicted magnitude are of the right general order.

CHAPTER VI: UNIFORMITY OF FULLY-DEVELOPED PIPE FLOW BEHIND AN EXPANSION WAVE

In Chapter III and IV, the causes of flow non-uniformity, i.e. the thickness of the boundary layer, the change of diameter and initial temperature, are assumed to be small, their analytical results are compared with experimental results in Chapter V. In this chapter, the case where the flow is dominated by large viscous effects is considered, i.e. the fully-developed pipe flow behind a non-steady expansion wave.

VI-1. Experiment

A series of experiments were carried out wherein the static pressure was measured at the exit of very long aspect ratio tubes. The apparatus was similar to that used in Chapter V, except in this case, the supply tube consisted of 304 stainless steel high pressure tubing with 6.35 mm i.d. and 1.65 mm wall. The total length of the supply tube was 13.9 m. M_3 was varied by using different nozzle plates each with a single hole at the center. A 1.27 cm thick flange with a single hole of 2.54 cm diameter was located between the nozzle plate and the diaphragm, allowing the use of the same diaphragm as in the study of Chapter V. The Kistler Pressure Transducer was located upstream of the nozzle plate as in Chapter V. The pressure in the supply tube ranged from 30 to 130 atm. Based on Becker's results, the boundary layer at the nozzle inlet will occupy the whole tube when the head of the expansion wave is just a few meters downstream; this distance is about 4 m at M_3 = 0.1, decreases to 1.7 m at M_3 = 0.5. Although fully-developed pipe flow will not occur instantly when δ/D = 0.5, there is no doubt that a very large portion of the flow behind the expansion wave will become fully-developed during most of the test time for the present experiments.

Results. Figure 26a is a sample static pressure trace for nitrogen with p_4 = 57 atm, T_{40} = 300°K, and M_3 = 0.1. The expansion wave clears the gauge in the first two milliseconds, dropping the pressure to the nominal p_3 value. The pressure then declines almost linearly until the reflected expansion wave arrives at 84 msec, a time that is about 13% larger than $t_{e.w.}$. This reflected expansion wave is weaker than the unperturbed reflected wave. Figure 26b and 26c are similar static pressure traces for M_3 = 0.235 and 0.71. The pressure traces for M_3 = 0.42 and 0.534 are similar to those of Figure 26b and 26c.

The static pressure traces shown in Figure 26 can be fitted to an exponentially decaying shape represented by $p_e = p_3e^{-At}$, where the characteristic time, A, can itself be a function of t. Based on experimental results, A decreases with time at fixed M_3: at M_3 = 0.71, the value of A at 80 msec is half that at 20 msec. At fixed time, the value of A increases with M_3. If both the value and the change of A are small, then e^{-At} can be expanded to

$$1 - At + \tfrac{1}{2}(At)^2 + \ldots .$$

When $(At)^2$ and higher order terms are neglected, this gives a linear decline in static pressure which agrees with the pressure trace shown in Figure 26a. For each static pressure trace, A was calculated at each 10 milliseconds interval from 20 msec to 80 msec after the opening of the diaphragm. The results are shown in Figure 27, where each vertical bar represents the extreme limits of A based on at least five experiments at fixed M_3.

It should be mentioned that at M_3 = 0.1, the percentage static pressure perturbation at the end of test time based on the result of Chapter III is about 8%, while the experimental results are around 7%. This indicates that for low M_3, the results of Chapter III are still reasonably accurate even for fully-developed pipe flow.

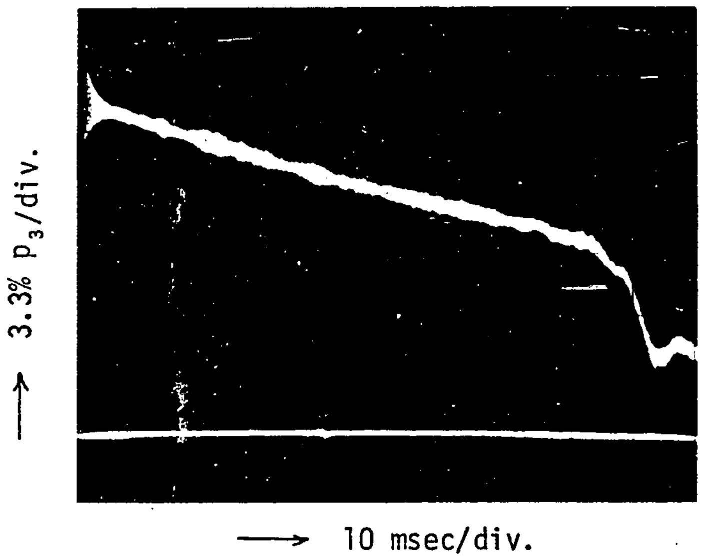

Figure 26a: Static Pressure Decay in the Fully-Developed Pipe Flow, M_3 = 0.1.

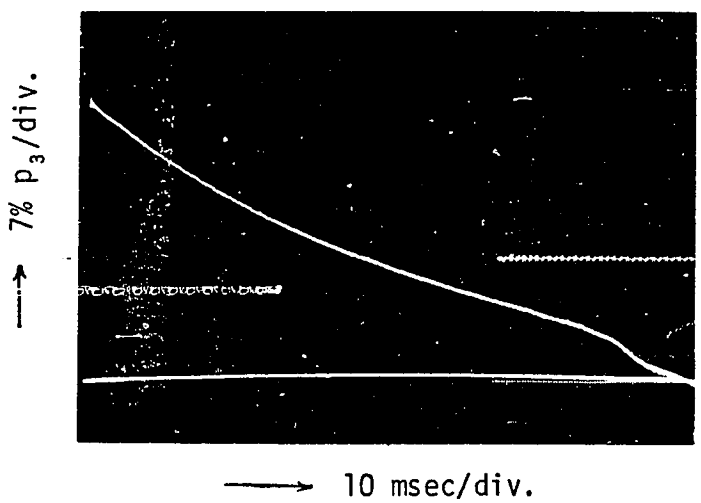

Figure 26b: Static Pressure Decay in the Fully-Developed Pipe Flow, M_3 = 0.235.

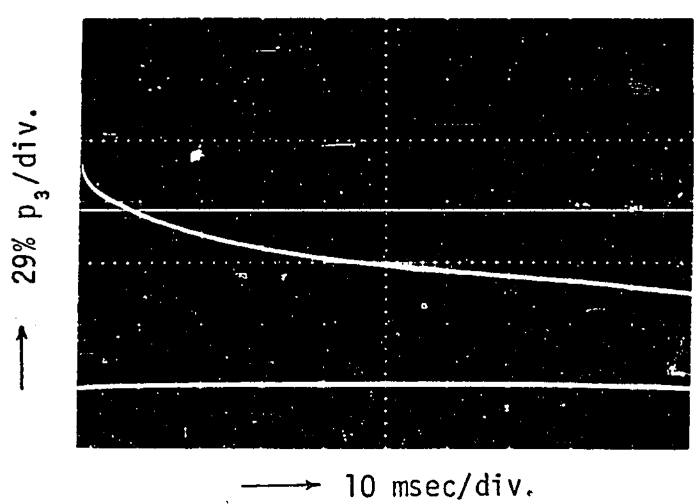

Figure 26c: Static Pressure Decay in the Fully-Developed Pipe Flow, M_3 = 0.71.

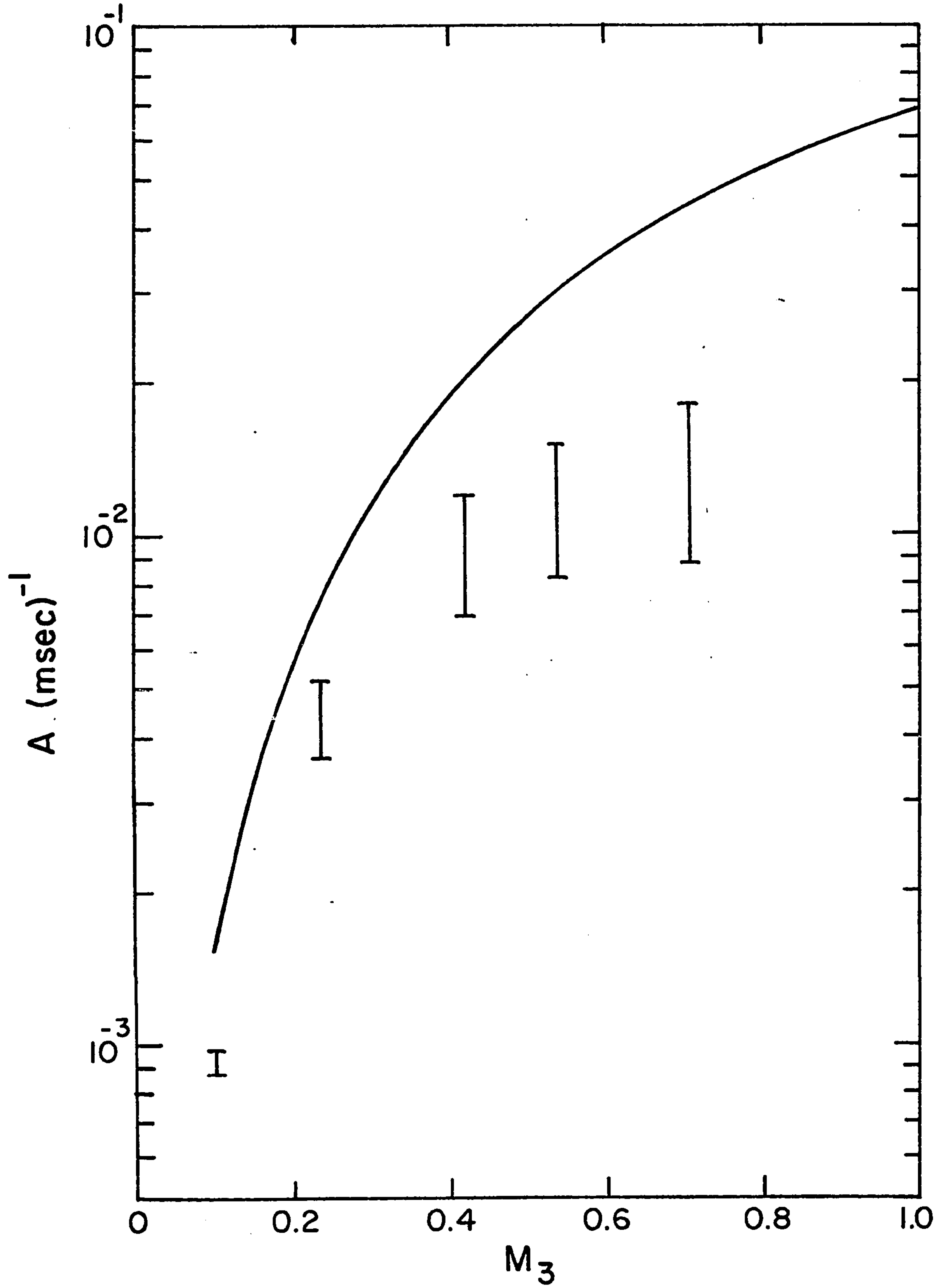

Figure 27: The Characteristic Time of Pressure Decay (A), Nitrogen with T_{40} = 300°K.

VI-2. Analysis

In analyzing the fully-developed pipe flow behind a non-steady expansion wave, the approach used in Chapters III and IV are not appropriate. In that approach, while a source term is introduced in the continuity equation for the displacement effect of the boundary layer, the momentum equation contains no shearing stress term and the entropy of each gas particle is constant. After the boundary layer has filled the tube completely, not only will the shearing stress become important, but the entropy of each gas particle will no longer be constant. Although Trimpi and Cohen (Reference 9) tried to calculate the effect of the boundary layer behind a moving shock wave by introducing a wall shear term in the momentum equation, the assumption that the flow is only perturbed slightly from the ideal condition makes their analysis inapplicable for the fully-developed pipe flow case. Becker (Reference 5) also studied the full-developed pipe flow behind an expansion wave; however, his assumption of small perturbation is questionable.

Since the entropy of the gas is not a constant, the energy equation must be used together with the continuity and momentum equations. Consider a section of the tube of length Δx as the control volume. The conservation equations for the flow within the control volume are

$$\text{Continuity:} \quad \frac{\partial}{\partial t}\int_0^{D/2} 2\pi\rho r\Delta x dr + [\frac{\partial}{\partial x}\int_0^{D/2} 2\pi\rho u r dr]\Delta x = 0,$$

$$\text{or} \qquad \frac{\partial}{\partial t}\int_0^{D/2} \rho r dr + \frac{\partial}{\partial x}\int_0^{D/2} \rho u r dr = 0 \qquad (81)$$

$$\text{Momentum:} \quad \frac{\partial}{\partial t}\int_0^{D/2} 2\pi\rho ur\Delta x dr + [\frac{\partial}{\partial x}\int_0^{D/2} 2\pi\rho u^2 rdr]\Delta x$$

$$= -[\frac{\partial}{\partial x}\int_0^{D/2} 2\pi prdr]\Delta x - \pi D\int \tau_w dx \quad .$$

$$\text{or} \quad \frac{\partial}{\partial t}\int_0^{D/2} \rho urdr + \frac{\partial}{\partial x}\int_0^{D/2} \rho u^2 rdr$$

$$= -\frac{\partial}{\partial x}\int_0^{D/2} prdr - \frac{D}{2}\tau_w \quad , \quad \text{as } \Delta x \to 0 \quad . \tag{82}$$

Here τ_w is the shearing stress at the wall.

$$\text{Energy:} \quad \frac{\partial}{\partial t}\int_0^{D/2} 2\pi(h + \tfrac{1}{2}u^2)\rho r\Delta x dr + [\frac{\partial}{\partial x}\int_0^{D/2} 2\pi\rho u(h$$

$$+ \tfrac{1}{2}u^2) rdr]\Delta x = \frac{\partial}{\partial t}\int_0^{D/2} 2\pi pr\Delta x dr + \pi D\, q_w dx \quad ,$$

$$\text{or} \quad \frac{\partial}{\partial t}\int_0^{D/2} \rho(h + \tfrac{1}{2}u^2) rdr + \frac{\partial}{\partial x}\int_0^{D/2} r\rho u(h + \tfrac{1}{2}u^2) dr$$

$$= \frac{\partial}{\partial t}\int_0^{D/2} prdr + \frac{D}{2} q_w \quad , \quad \text{as } \Delta x \to 0 \quad , \tag{83}$$

here q_w is the heat transfer at the wall. Let F be any property of the gas and define $\bar{F}$ as

$$\bar{F} \equiv \int_0^{D/2} Frdr \Big/ \int_0^{D/2} rdr = \frac{8}{D^2} \int_0^{D/2} Frdr \quad ,$$

then Equations (81), (82) and (83) become

$$\frac{\partial \bar{\rho}}{\partial t} + \frac{\partial}{\partial x} (\overline{\rho u}) = 0 \quad , \tag{84}$$

$$\frac{\partial \overline{\rho u}}{\partial t} + \frac{\partial}{\partial x} (\overline{\rho u^2}) = - \frac{\partial \bar{p}}{\partial x} - \frac{D}{2} \tau_w \quad , \tag{85}$$

$$\frac{\partial}{\partial t} [\overline{\rho h} + \tfrac{1}{2}\overline{\rho u^2}] + \frac{\partial}{\partial x} [\overline{\rho u h} + \tfrac{1}{2} \overline{\rho u^3}] = \frac{\partial \bar{p}}{\partial t} + \frac{D}{2} q_w \quad . \tag{86}$$

If the density, velocity and temperature distribution on the cross-section of the tube are known, then $\overline{\rho u}$, $\overline{\rho u^2}$, $\overline{\rho h}$, $\overline{\rho u h}$, $\overline{\rho u^3}$ can be written in terms of $\bar{\rho}\bar{u}$, $\bar{\rho}\bar{u}^2$, $\bar{\rho}\bar{h}$, $\bar{\rho}\bar{u}\bar{h}$ and $\bar{\rho}\bar{u}^3$, respectively. Combined with the equation of state, Equations (84), (85), and (86) form a set of (4) equations with unknows $\bar{\rho}$, $\bar{u}$, $\bar{h}$ and $\bar{p}$. Since the flow is fully-developed, the condition of the flow will be quite different from the unperturbed condition and the linearizing of the governing equations will not be appropriate. Hence, the governing equations are non-linear and simple closed form solutions are not expected. However, the decay of the static pressure at the nozzle inlet and the characteristic time A may be obtained from the following argument:

$$\text{Let} \quad x^* \equiv x/L \; , \; t^* \equiv (a_3 - |u_3|)t/L \; , \; \rho^* \equiv \bar{\rho}/\rho_3 \quad ,$$

$$u^* \equiv \bar{u}/|u_3| \; , \; p^* \equiv \bar{p}/p_3 \; , \; \tau_w^* \equiv \tau_w/p_3 \; ,$$

and assume that $\overline{\rho u} \approx \bar{\rho}\bar{u}$, $\overline{\rho u^2} \approx \bar{\rho}\bar{u}^2$, then the continuity and momentum equation become

$$(a_3 - |u_3|)\frac{\partial \rho^*}{\partial t^*} + |u_3|\frac{\partial \rho^* u^*}{\partial x^*} = 0 \quad , \tag{87}$$

$$(a_3 - |u_3|)\frac{\partial \rho^* u^*}{\partial t^*} + |u_3|\frac{\partial \rho^* u^{*2}}{\partial x^*} = -\frac{p_3}{\rho_3|u_3|}\left(\frac{\partial p^*}{\partial t} + \frac{4L}{D}\tau_w{}^*\right) . \tag{88}$$

Consider the region far downstream from the tail of the expansion wave, i.e. $x^* = \sigma t^*$ with $\sigma << 1$, then $\frac{\partial}{\partial x^*} \approx \frac{1}{\sigma}\frac{\partial}{\partial t^*}$, and Equations (87) and (88) become

$$(a_3 - |u_3|)\frac{\partial \rho^*}{\partial t^*} + \frac{|u_3|}{\sigma}\frac{\partial \rho^* u^*}{\partial t^*} = 0 \quad ,$$

$$(a_3 - |u_3|)\frac{\partial \rho^* u^*}{\partial t^*} + \frac{|u_3|}{\sigma}\frac{\partial \rho^* u^{*2}}{\partial t^*} = -\frac{p_3}{\rho_3|u_3|}\left(\frac{1}{\sigma}\frac{\partial p^*}{\partial t^*} + \frac{4L}{D}\tau_w{}^*\right) ,$$

or
$$(a_3 - |u_3|)\frac{\partial \rho^*}{\partial t^*} + \frac{|u_3|}{\sigma}u^*\frac{\partial \rho^*}{\partial t^*} + \frac{|u_3|}{\sigma}\rho^*\frac{\partial u^*}{\partial t^*} = 0 \quad ,$$

$$(a_3 - |u_3|)\frac{\partial \rho^* u^*}{\partial t^*} + \frac{|u_3|}{\sigma}u^*\frac{\partial \rho^* u^*}{\partial t^*} + \frac{|u_3|}{\sigma}\rho^* u^*\frac{\partial u^*}{\partial t^*}$$
$$= -\frac{p_3}{\rho_3|u_3|}\left(\frac{1}{\sigma}\frac{\partial p^*}{\partial t^*} + \frac{4L}{D}\tau_w{}^*\right) \quad .$$

Since u^* is of the order of one,

$$\frac{|u_3|}{\sigma}u^*\frac{\partial \rho^*}{\partial t^*} >> (a_3 - |u_3|)\frac{\partial \rho^*}{\partial t^*} \quad ,$$

and $\frac{|u_3|}{\sigma}u^*\frac{\partial \rho^* u^*}{\partial t^*} >> (a_3 - |u_3|)\frac{\partial \rho^* u^*}{\partial t^*}$ as long as $\frac{|u_3|}{\sigma} >> (a_3 - |u_3|)$.

In other words, if $\sigma << \frac{M_3}{1 - M_3}$, the $\frac{\partial}{\partial t}$ terms in the continuity and momentum equations are smaller than the $\frac{\partial}{\partial x}$ terms and can be neglected.

Furthermore, since

$$\frac{\frac{\partial \overline{\rho u^2}}{\partial x}}{\partial \bar{p}/\partial x} \approx \frac{\partial \bar{\rho}\bar{u}^2/\partial x}{\partial \bar{p}/\partial x} = \frac{\rho_3 |u_3|^2}{p_3} \frac{\frac{\partial \rho^* u^{*2}}{\partial x^*}}{\frac{\partial p^*}{\partial x^*}} = \gamma M_3^2 \frac{\frac{\partial \rho^* u^{*2}}{\partial x^*}}{\frac{\partial p^*}{\partial x^*}}$$

For $M_3 << 1$, $\frac{\partial \overline{\rho u^2}}{\partial x} << \frac{\partial \bar{p}}{\partial x}$. Therefore, the momentum equation can be simplified into

$$\frac{\partial p}{\partial x} = -\frac{4}{D}\tau_w = -\frac{2}{D} c_f \bar{\rho}\bar{u}^2 \quad , \tag{89}$$

Here c_f is the drag coefficient defined as

$$\tau_w = c_f \tfrac{1}{2} \bar{\rho}\bar{u}^2 \quad .$$

If Blasius' law of friction is used (Reference 20)

$$c_f = \frac{1}{4} [0.316 \, (Re_D)^{-0.25}] \quad ,$$

where $(Re_D)^{-0.25} = (\frac{\bar{\rho}\bar{u}D}{\bar{\mu}})^{-0.25} \approx (\frac{\rho_3 |u_3| D_0}{\mu_3})^{-0.25} = (Re_{D_0})^{-0.25}$

then $$\frac{\partial p}{\partial x} \approx -\frac{1}{2D_0} [0.316 (Re_{D_0})^{-0.25}] \, \bar{\rho}\bar{u}^2$$

$$= -\frac{1}{2D_0} [0.316 (Re_{D_0})^{-0.25}] \, \gamma \bar{p} \, (\frac{\bar{u}}{\bar{a}})^2 \tag{90}$$

Since $\frac{\partial}{\partial x} \approx \frac{1}{U_0} \frac{\partial}{\partial t}$. Hence,

$$\frac{1}{U_0} \frac{\partial \bar{p}}{\partial t} = -\frac{1}{2D_0} [0.316 \, (Re_{D_0})^{-0.25}] \, \gamma \bar{p} \, (\frac{\bar{u}}{\bar{a}})^2$$

or $$\frac{1}{\bar{p}}\frac{\partial\bar{p}}{\partial t} = -\frac{1}{2D_0}[0.316(Re_{D_0})^{-0.25}]\,\gamma U_0(\frac{\bar{u}}{\bar{a}})^2 \quad . \tag{91}$$

If $\frac{\bar{u}}{\bar{a}} \approx$ constant, then from Equation (91)

$$\bar{p}/p_3 = e^{-\frac{1}{2D_0}[0.316(Re_{D_0})^{-0.25}]\,\gamma U_0(\frac{\bar{u}}{\bar{a}})^2\, t} \quad . \tag{92}$$

Here the boundary condition that at t=0, $\bar{p}=p_3$ has been used. According to Equation (92), the characteristic time for pressure decay A is given by

$$A = -\frac{1}{2D_0}[0.316(Re_{D_0})^{-0.25}]\,\gamma U_0(\frac{\bar{u}}{\bar{a}})^2 \quad . \tag{93}$$

A has a weak dependence on the pressure level through the Reynolds number. Since $\frac{\bar{u}}{\bar{a}}$ is assumed to be approximately constant, the characteristic time A given by Equation (93) is not a function of time.

In order to be consistent with the skin friction law, the distribution of the velocity should be

$$\frac{u}{u_{max}} = (1 - \frac{2r}{D})^{1/7} \quad ,$$

$u_{max}(x,t)$ is the velocity of the gas along the center of the tube. Hence,

$$\bar{u} \equiv \frac{8}{D^2}\int_0^{D/2} urdr = \frac{49}{60}u_{max} \quad ,$$

and A can be written as

$$A = -\frac{1}{2D_0}[0.316(Re_{D_0})^{-0.25}]\,\gamma U_0(\frac{49}{60})^2\,(\frac{u_{max}}{\bar{a}}) \quad . \tag{94}$$

Although the exact value of $\frac{u_{max}}{\bar{a}}$ must be obtained from the solution of the system of non-linear governing equations, it turns out when $\frac{u_{max}}{\bar{a}}$ is calculated by the following method, the values of A given by Equation (94) are in rough agreement with the experimental results:

Let $u_{max} = u_3 + u'$, where u' is the velocity perturbation at the tail of the expansion wave at the instant when the boundary layer thickness at the nozzle inlet equals the radius of the tube. The value of u' can be calculated from Equation (42) in Chapter III. With $\bar{a} \approx a_3$, the values of A for different M_3 are shown in Figure 27. In this figure, the pressure of the supply tube (p_4) is taken to be 81 atm which is the average pressure level used in the experiments. It is seen that the values of A calculated in this manner are in rough agreement with the experimental values of A even at high M_3. Slightly better agreement can be obtained if U_0 is replaced by the velocity V obtained by Becker through the matching of the boundary layer thicknesses at the tail of the expansion wave (see Section II-1).

CHAPTER VII: CONCLUSIONS

The effects of thin boundary layers, of small variations in tube diameter, and of small variations in initial temperature on the perturbations of the core flow behind a non-steady expansion wave have been analyzed using a single basic approach. When the governing equations are linearized, simple closed form solutions have been obtained by applying boundary conditions at the two ends of the gas column. This is done by replacing the expansion wave by a fictitious "expansion shock," and by using the steady boundary condition at the nozzle inlet that the Mach number increases through the displacement effect of the boundary layer. The boundary layer weakens the expansion wave and gives a positive perturbation in the static pressure and velocity at the unperturbed tail of the expansion wave, while the increase in Mach number at the nozzle inlet contributes to negative perturbations in the static pressure and velocity there. At the nozzle inlet, the predicted value of static pressure perturbation at the end of test time changes from $1.25 \times 10^{-4}(p_4 D_0)^{1/5} / (L/D)^{4/5} \cdot (ATM\text{-}M)^{1/5}$ at $M_3 = 0.1$ to a value of one order of magnitude larger at $M_3 = 0.5$. Although the analysis has weakness at high M_3, the measured static pressure perturbations at such Mach numbers can still be predicted with reasonable accuracy by the boundary condition $dA/A = -dM/M_3$. For the effects of variations in tube diameter and initial temperature, the analysis predicts that the percentage perturbations in static pressure, velocity, and static temperature increase with M_3, but are generally of the same order of the percentage change in tube diameter and initial temperature.

The same basic analytical approach has been applied to the effect of the thin boundary layer on the uniformity of the core flow within the non-steady expansion wave. The linearized governing equations yield closed form solutions for the static pressure and velocity perturbations. When evaluated at the unperturbed tail of the expansion wave, these perturbations are in good agreement with the corresponding predictions obtained by using the "expansion shock" model. This supports the experimental finding that, as far as the uniformity of the core flow behind the expansion wave is concerned, the expansion wave can indeed be replaced by the "expansion shock" without introducing a large error.

The decay of static pressure at the nozzle inlet when the flow behind the expansion wave is a fully-developed pipe flow has been measured. The decay of the static pressure can be represented by $\bar{p}/p_3 = e^{-At}$ with A being the characteristic time for the decay of pressure. At a fixed time, the value of A increases with M_3, while for a fixed M_3 the value of A decreases slightly with time. Although a simple method has been established by which the value of A can be estimated within a factor of 2 or 3 accuracy, the governing equations for such flow are non-linear and numerical methods may have to be used for further improvement.

APPENDIX A: SOME USEFUL FORMULAS FOR THE DESIGN OF LUDWIEG TUBE

Since the nozzle is much shorter than the supply tube, the unperturbed Mach number behind the expansion wave (M_3) can be calculated from the ratio of the cross-section area at the nozzle inlet to that at the throat by the one-dimensional steady channel flow relationship. If the nozzle is choked, this becomes

$$\frac{D_o}{D^*} = \frac{1}{\sqrt{M_3}} \left[\frac{2}{\gamma+1} \left(1 + \frac{\gamma-1}{2} M_3^2\right)\right]^{\frac{\gamma+1}{4(\gamma-1)}} \tag{A1}$$

where D* is the diameter at the nozzle throat.

The speed of sound, temperature, density, static pressure, velocity, stagnation temperature and stagnation pressure behind the expansion wave are:

$$\frac{a_3}{a_{40}} = \left(1 + \frac{\gamma-1}{2} M_3\right)^{-1} \tag{A2}$$

$$\frac{T_3}{T_{40}} = \left(1 + \frac{\gamma-1}{2} M_3\right)^{-2} \tag{A3}$$

$$\frac{\rho_3}{\rho_{40}} = \left(1 + \frac{\gamma-1}{2} M_3\right)^{-2/\gamma-1} \tag{A4}$$

$$\frac{p_3}{p_4} = \left(1 + \frac{\gamma-1}{2} M_3\right)^{-2\gamma/\gamma-1} \tag{A5}$$

$$u_3 = -a_{40}M_3/\left(1 + \frac{\gamma-1}{2} M_3\right) \tag{A6}$$

$$\frac{T_{t_3}}{T_{40}} = \left(1 + \frac{\gamma-1}{2} M_3^2\right)\Big/\left(1 + \frac{\gamma-1}{2} M_3\right)^2 \tag{A7}$$

$$\frac{p_{t_2}}{p_4} = \left(1 + \frac{\gamma-1}{2} M_3^2\right)^{\frac{\gamma}{\gamma-1}} \Big/ \left(1 + \frac{\gamma-1}{2} M_3\right)^{2\gamma/\gamma-1} \tag{A8}$$

The test time of Ludwieg tube ($t_{e.w.}$) is

$$t_{e.w.} = \frac{2L}{a_{40}} \frac{1}{1+M_3} \left[1 + \frac{\gamma-1}{2} M_3\right]^{1+\gamma/2(\gamma-1)} \tag{A9}$$

APPENDIX B: THE CHARACTERISTICS AND GENERAL SOLUTIONS OF EQUATIONS (11) AND (12)

Equations (11) and (12) are rewritten as

$$\frac{1}{\rho_3 a_3^2 |u_3|}\left(U_0 \frac{\partial p'}{\partial \bar{t}} - |u_3|\frac{\partial p'}{\partial \bar{x}}\right) + \frac{1}{|u_3|}\frac{\partial u'}{\partial \bar{x}}$$

$$= K(Re_{D_0})^{-1/5}\ (\bar{t}-\bar{x})^{-1/5} + 2\frac{d}{d\bar{x}}\ (D'/D_0) \tag{B1}$$

$$\frac{1}{\rho_3}\frac{\partial p'}{\partial \bar{x}} + U_0 \frac{\partial u'}{\partial \bar{t}} - |u_3|\frac{\partial u'}{\partial \bar{x}} = 0 \quad . \tag{B2}$$

Following the procedure mentioned in Sections 21 and 22 in Reference 14, since

$$\frac{U_0^2}{\rho_3 a_3^2 |u_3|}\left(\frac{|u_3|^2}{\rho_3 a_3^2 |u_3|} - \frac{1}{\rho_3 |u_3|}\right) - \frac{1}{4}\left(-\frac{U_0\ |u_3|}{\rho_3 a_3^2 |u_3|} - \frac{|u_3|\ U_0}{\rho_3 a_3^2 |u_3|}\right)^2$$

$$= \frac{U_0^2}{\rho_3^2 a_3^4} - \frac{U_0^2}{\rho_3 a_3^4 |u_3|^2} - \frac{U_0^2}{\rho_3^2 a_3^4}$$

$$= -\frac{U_0^2}{\rho_3^2 a_3^4 |u_3|^2} < 0 \quad ;$$

Equations (B1) and (B2) form a system of hyperbolic first order partial differential equations.

The slopes of characteristics at any point satisfies the equation

$$\frac{U_0^2}{\rho_3 a_3^2 |u_3|}\zeta^2 + \frac{2U_0}{\rho_3 a_3^2}\zeta + \left(\frac{|u_3|}{\rho_3 a_3^2} - \frac{1}{\rho_3 |u_3|}\right) = 0 \ , \tag{B3}$$

where ζ is the slope of the characteristic in $\bar{t}$-$\bar{x}$ plane. The solutions are

$$\zeta_+ = \frac{a_3 - |u_3|}{U_0} \ , \tag{B4}$$

$$\zeta_- = -\frac{a_3 + |u_3|}{U_0} \ . \tag{B5}$$

In the t-x plane, the slopes become $a_3 - |u_3|$ and $-(a_3 + |u_3|)$, same as the slopes of the characteristics of the unperturbed flow behind the expansion wave. As in Equation (13), the characteristic variables are chosen to be

$$\xi \equiv \bar{t} - \frac{U_0/a_3}{M_0-1}(\bar{t}-\bar{x}) \quad , \quad \eta \equiv \bar{t} - \frac{U_0/a_3}{M_0+1}(\bar{t}-\bar{x}) \quad . \tag{B6}$$

$\bar{x}$ and $\bar{t}$ can then be expressed as

$$\bar{x} = \frac{1}{2U_0}[(M_0+1)(a_3 - |u_3|)\eta + (M_0-1)(a_3 + |u_3|)\xi] \quad , \tag{B7}$$

$$\bar{t} = \tfrac{1}{2}[(M_0+1)\eta - (M_0-1)\xi] \quad . \tag{B8}$$

Equations (B1) and (B2) can be replaced by

$$\frac{U_0}{\rho_3^2 a_3^2 |u_3|} p'_\eta + [\frac{U_0 (a_3 - |u_3|)}{\rho_3 a_3^2 |u_3|} + \frac{U_0}{\rho_3 a_3^2}] u'_\eta$$

$$- \left\{\frac{K}{\rho_3}(Re_{D_0})^{-1/5}(\bar{t}-\bar{x})^{-1/5} + \frac{2}{\rho_3}\frac{d[D'(\bar{x})/D_0]}{dx}\right\}\frac{M_0+1}{2} = 0 \quad , \tag{B9}$$

$$\frac{U_0}{\rho_3^2 a_3^2 |u_3|} p'_\xi + [-\frac{U_0 (a_3 + |u_3|)}{\rho_3 a_3^2 |u_3|} + \frac{U_0}{\rho_3 a_3^2}] u'_\xi$$

$$+ \left\{\frac{K}{\rho_3}(Re_{D_0})^{-1/5}(\bar{t}-\bar{x})^{-1/5} + \frac{2}{\rho_3}\frac{d[D'(\bar{x})/D_0]}{dx}\right\}\frac{M_0-1}{2} = 0 \quad . \tag{B10}$$

If the $\bar{x}$ and $\bar{t}$ are substituted by Equations (B7) and (B8), then Equations (B9) and (B10) can be integrated with the following results:

$$\frac{U_0}{\rho_3^2 a_3^2 |u_3|} p' + \frac{U_0}{\rho_3 a_3 |u_3|} u' = \left\{\frac{K}{\rho_3}(Re_{D_0})^{-1/5}\left[\frac{a_3(M_0^2-1)}{2U_0}\right]^{-1/5}\right.$$

$$\left. \cdot \frac{5}{4}(\xi-\eta)^{4/5} + \frac{4U_0}{(M_0+1)(a_3 - |u_3|)}\frac{D'(\bar{x})}{D_0}\right\}\frac{M_0+1}{2}$$

$$+ \frac{2U_0}{\rho_3 a_3} f(\xi) \quad , \tag{B11}$$

$$\frac{U_0}{\rho_3^2 a_3^2 |u_3|} p' - \frac{U_0 u^1}{\rho_3 a_3 |u_3|} u' = \left\{ \frac{K}{\rho_3} (Re_{D_0})^{-1/5} \left[\frac{a_3(M_0^2-1)}{2U_0} \right]^{-1/5} \frac{5}{4} (\xi - \eta)^{4/5} \right.$$

$$\left. - \frac{4U_0}{\rho_3 (M_0-1)(a_3 + |u_3|)} \frac{D'(\bar{x})}{D_0} \right\} \frac{M_0-1}{2} - \frac{2U_0}{\rho_3 a_3} g(\eta) \quad , \tag{B12}$$

where $f(\xi)$ and $g(\eta)$ are unknown functions resulting from the integrating process. Combining Equations (B11) and (B12) yields

$$\frac{p'}{\rho_3 a_3 |u_3|} = \frac{5}{4} \frac{M_0}{M_0^2 - 1} K(Re_{D_0})^{-1/5} (\bar{t} - \bar{x})^{4/5} + \frac{2M_3}{1 - M_3^2} \frac{D'(\bar{x})}{D_0}$$

$$+ f(\xi) - g(\eta) \quad , \tag{B13}$$

$$\frac{u'}{|u_3|} = \frac{5}{4} \frac{1}{M_0^2 - 1} K(Re_{D_0})^{-1/5} (\bar{t} - \bar{x})^{4/5} + \frac{2}{1 - M_3^2} \frac{D'(\bar{x})}{D_0}$$

$$+ f(\xi) + g(\eta) \quad . \tag{B14}$$

APPENDIX C: CORE FLOW PERTURBATIONS DUE TO THE BOUNDARY LAYER WITH $^1/_n$ th POWER LAW VELOCITY PROFILE

The Thickness of the Boundary Layer Behind a Discontinuity Surface Moving with Velocity V.

In this section, Becker's method for solving the boundary layer behind a discontinuity surface moving with velocity V is applied to the boundary layer with any power law velocity profile. It is assumed that the gas changes from the condition in Region 4 to the condition in Region 3 across the discontinuity surface (see sketch).

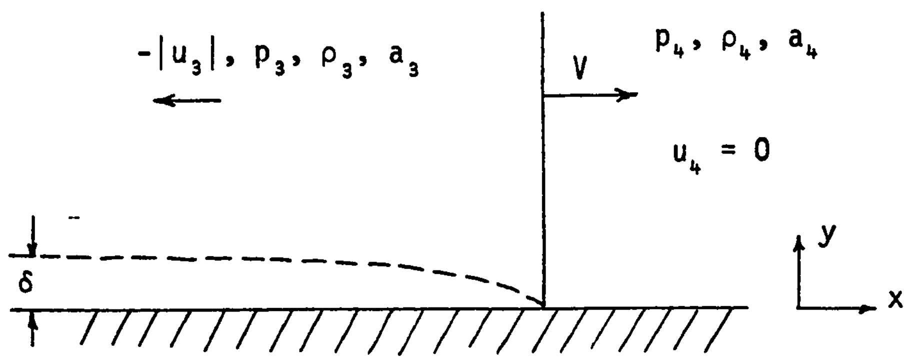

In the laboratory-fixed coordinate, the continuity and momentum equations for the boundary layer are

$$\frac{\partial \rho}{\partial t} + \frac{\partial \rho u}{\partial x} + \frac{\partial \rho v}{\partial y} = 0 \quad , \tag{C1}$$

$$\rho \left(\frac{\partial u}{\partial t} + u \frac{\partial u}{\partial x} + v \frac{\partial u}{\partial y} \right) = -\frac{\partial p_e}{\partial x} + \frac{\partial \tau}{\partial y} \quad , \tag{C2}$$

where u and v are the velocity component in the x and y direction. Integrate Equation (C2) with respect to y from 0 to ∞, then

$$\int_0^\infty (\rho \frac{\partial u}{\partial t} + \rho u \frac{\partial u}{\partial x} + \rho v \frac{\partial u}{\partial y}) dy = -\int_0^\infty \frac{\partial p_e}{\partial x} + \tau \Big|_0^\infty$$

$$= -\int_0^\infty \frac{\partial p_e}{\partial x} - \tau_w \quad , \tag{C3}$$

where τ_w is the wall shear stress. The momentum equation of the flow outside the boundary layer is

$$\rho_e (\frac{\partial u_e}{\partial t} + u_e \frac{\partial u_e}{\partial x}) = -\frac{\partial p_e}{\partial x} \quad . \tag{C4}$$

From Equation (C1)

$$\rho v = -\int_0^y (\frac{\partial \rho}{\partial t} + \frac{\partial \rho u}{\partial x}) dy \quad . \tag{C5}$$

Substitute Equations (C5) and (C4) into (C3) yields

$$\int_0^\infty \left[\rho \frac{\partial u}{\partial t} + \rho u \frac{\partial u}{\partial x} - \frac{\partial u}{\partial y} \int_0^y (\frac{\partial \rho}{\partial t} + \frac{\partial \rho u}{\partial x}) dy\right] dy$$

$$= \int_0^\infty (\rho_e \frac{\partial u_e}{\partial t} + \rho_e u_e \frac{\partial u_e}{\partial x}) dy - \tau_w \quad . \tag{C6}$$

Since

$$\int_0^\infty \left[\frac{\partial u}{\partial y} \int_0^y (\frac{\partial \rho}{\partial t} + \frac{\partial \rho u}{\partial x}) dy\right] dy = u_e \int_0^\infty (\frac{\partial \rho}{\partial t} + \frac{\partial \rho u}{\partial x}) dy$$

$$-\int_0^\infty u (\frac{\partial \rho}{\partial t} + \frac{\partial \rho u}{\partial x}) dy \quad ,$$

Equations (C6) become

$$\int_0^\infty \Big[\rho \frac{\partial u}{\partial t} + \rho u \frac{\partial u}{\partial x} - u_e \left(\frac{\partial \rho}{\partial t} + \frac{\partial \rho u}{\partial x}\right) + u \left(\frac{\partial \rho}{\partial t} + \frac{\partial \rho u}{\partial x}\right)$$

$$- \rho_e \frac{\partial u_e}{\partial t} - \rho_e u_e \frac{\partial u_e}{\partial x}\Big] dy = - \tau_w \quad ,$$

or

$$\int_0^\infty \frac{\partial}{\partial t} (\rho u - \rho_e u_e) dy - \int_0^\infty u_e \frac{\partial}{\partial t} (\rho - \rho_e) dy + \int_0^\infty \frac{\partial}{\partial x} [\rho u (u - u_e)] dy$$

$$+ \int_0^\infty \frac{\partial u_e}{\partial x} (\rho u - \rho_e u_e) dy = - \tau_w \quad .$$

Since ρ_e and u_e are constant, the above equation becomes

$$\rho_e u_e \frac{\partial \delta^*}{\partial t} + u_e \frac{\partial}{\partial t} \int_0^\infty (\rho - \rho_e) dy + \rho_e u_e \frac{\partial \theta}{\partial x} = \tau_w \quad . \tag{C7}$$

δ^* and θ are the displacement and momentum thickness of the boundary layer. Equation (C7) is the non-steady momentum integral equation describing the growth of the boundary layer.

Following Becker's approach, let

$$\frac{u}{u_e} = \left(\frac{y}{\delta}\right)^{1/n} \quad , \tag{C8}$$

and

$$\frac{\rho}{\rho_e} = \frac{\rho_w}{\rho_e} + \left(1 - \frac{\rho_w}{\rho_e}\right)\left(\frac{y}{\delta}\right)^{1/n} \quad ,$$

where ρ_w is the density at the wall. Then

$$\delta^* \equiv \frac{1}{\rho_e u_e} \int_0^\infty (\rho_e u_e - \rho u) \, dy = \int_0^\delta \left(1 - \frac{\rho}{\rho_e} \frac{u}{u_e}\right) dy$$

$$= \left[\frac{2}{n+2} - \frac{\rho_w}{\rho_e} \frac{n}{(n+1)(n+2)}\right] \delta \quad , \tag{C9}$$

$$\theta \equiv \frac{1}{\rho_e u_e^2} \int_0^\infty \rho u (u_e - u)\, dy = \int_0^\delta \frac{\rho u}{\rho_e u_e} \left(1 - \frac{u}{u_e}\right) dy$$

$$= \left[\frac{n}{(n+2)(n+3)} + \frac{\rho_w}{\rho_e} \frac{2n}{(n+1)(n+2)(n+3)} \right] \delta \quad , \tag{C10}$$

and

$$\int_0^\infty (\rho - \rho_e)\, dy = \rho_e \int_0^\infty \left(\frac{\rho}{\rho_e} - 1\right) dy = -\rho_e \left(1 - \frac{\rho_w}{\rho_e}\right) \frac{\delta}{n+1} \tag{C11}$$

The wall shear is assumed to have the following form:

$$\frac{\rho_w}{\rho_e u_e^2} = \tfrac{1}{2} E \left(\frac{\theta}{\delta}\right)^{-m} \left(\frac{|u_e|\delta}{\nu_e}\right)^{-m} \tag{C12}$$

where E and m are constants depending on the value of n. Since the wall temperature is approximate T_4, and the temperature within the boundary layer is nearly constant, the values of E and m for different n can be obtained from Reference 21, and are listed in the following table:

n	7	8	9	10
E	0.0252	0.0206	0.0190	0.0148
m	0.250	0.222	0.200	0.182

Substitute Equations (C9), (C10) and (C11) into Equation (C7), yields

$$\rho_e u_e \left[\frac{2}{n+2} - \frac{\rho_w}{\rho_e} \frac{n}{(n+1)(n+2)}\right] \frac{\partial \delta}{\partial t} - u_e \rho_e \left(1 - \frac{\rho_w}{\rho_e}\right) \frac{1}{n+1} \frac{\partial \delta}{\partial t}$$

$$+ \rho_e u_e^2 \left[\frac{n}{(n+2)(n+3)} + \frac{\rho_w}{\rho_e} \frac{2n}{(n+1)(n+2)(n+3)}\right] \frac{\partial \delta}{\partial x} = \tau_w \quad ,$$

or
$$\frac{1}{u_e}\left[\frac{n}{(n+2)(n+1)}+\frac{2}{(n+1)(n+2)}\ \frac{\rho_w}{\rho_e}\right]\frac{\partial\delta}{\partial t}+\left[\frac{n}{(n+2)(n+3)}\right.$$

$$\left.+\frac{\rho_w}{\rho e}\ \frac{2n}{(n+1)(n+2)(n+3)}\right]\frac{\partial\delta}{\partial x}=\frac{\tau_w}{\rho_e u_e^2}\ . \qquad \text{(C13)}$$

Let $\rho=\rho_3$, $u_e=-|u_3|$, $\nu_e=\nu_3$, and since the direction of the velocity at the edge of the boundary layer is in the -x direction, Equation (C13) can be rewritten as

$$\frac{1}{|u_3|}\left[\frac{n}{(n+2)(n+1)}+\frac{2}{(n+1)(n+2)}\ \frac{\rho_w}{\rho_3}\right]\frac{\partial\delta}{\partial t}-\left[\frac{n}{(n+2)(n+3)}\right.$$

$$\left.+\frac{\rho_w}{\rho_3}\ \frac{2n}{(n+1)(n+2)(n+3)}\right]\frac{\partial\delta}{\partial x}=\tfrac{1}{2}\,E\left(\frac{\theta}{\delta}\right)^{-m}\ \frac{|u_3|\delta}{\nu_3}^{-m}\ ,$$

or
$$\frac{\partial\delta^{1+m}}{\partial t}\ \frac{1}{|u_3|}\ \frac{n+2\ \frac{\rho_w}{\rho_e}}{(n+1)(n+2)}-\frac{\partial\delta^{1+m}}{\partial x}\ \frac{n(n+1)\ -\ 2n\ \frac{\rho_w}{\rho_3}}{(n+1)(n+2)(n+3)}$$

$$=\tfrac{1}{2}\,(1+m)\ E\left(\frac{\theta}{\delta}\right)^{-m}\ \frac{|u_3|}{\nu_3}^{-m}\ . \qquad \text{(C14)}$$

The solution of Equation (C14) is

$$\delta^{1+m}=\tfrac{1}{2}\,(1+m)\ E\left(\frac{\theta}{\delta}\right)^{-m}\left(\frac{|u_3|}{\nu_3}\right)^{-m}\ \frac{|u_3|}{V}\,(Vt-x)$$

$$\cdot\ G\left(\frac{|u_3|}{V}\ ,\ \frac{\rho_w}{\rho_3}\right)\ , \qquad \text{(C15)}$$

where
$$G\left(\frac{|u_3|}{V}\ ,\ \frac{\rho_w}{\rho_3}\right)=\frac{1}{\dfrac{n+2\ \frac{\rho_w}{\rho_3}}{(n+1)(n+2)}+\dfrac{n(n+1)\ +\ 2n\ \frac{\rho_w}{\rho_3}}{(n+1)(n+2)(n+3)}\ \dfrac{|u_3|}{V}}\ . \qquad \text{(C16)}$$

Equation (C15) satisfies the boundary condition that $\delta=0$ at $x=Vt$.

Since $T_W \approx T_4$, therefore $\frac{\rho_W}{\rho_3} = \frac{T_3}{T_4}$. As $0 \le M_3 \le 1$, $1 \ge \frac{\rho_W}{\rho_3} \ge 0.695$. For this range of $\frac{\rho_W}{\rho_3}$ and $n \ge 7$, $G\left(\frac{|u_3|}{V}, \frac{\rho_W}{\rho_3}\right) \approx G\left(\frac{|u_3|}{V}, 1\right)$. In other words, as far as the growth of the boundary layer is concerned, the density can be considered constant across the boundary layer. With this approximation, Equations (C9), (C10), and (C16) become

$$\frac{\delta^*}{\delta} = \frac{1}{(n+1)} \quad , \tag{C17}$$

$$\frac{\theta}{\delta} = \frac{n}{(n+1)(n+2)} \quad , \tag{C18}$$

$$G\left(\frac{|u_3|}{V}, 1\right) = \frac{n+1}{1 + \frac{n}{n+2}\frac{|u_3|}{V}} \quad , \tag{C19}$$

and the thickness of the boundary layer is

$$\delta^{1+m} \approx \tfrac{1}{2}(1+m)\, E\left[\frac{n}{(n+1)(n+2)}\right]^{-m}\left(\frac{|u_3|}{\nu_3}\right)^{-m}\frac{|u_3|}{V}(Vt-x)\; G\left(\frac{|u_3|}{V}, 1\right),$$

or

$$\delta = \left\{\tfrac{1}{2}(1+m)\, E\left[\frac{n}{(n+1)(n+2)}\right]^{-m}\right\}^{1/1+m}\left(\frac{|u_3|}{\nu_3}\right)^{-m/1+m} \cdot \left[\frac{|u_3|}{V}\; G\left(\frac{|u_3|}{V}, 1\right)\right]^{1/1+m}(Vt-x)^{1/1+m} \quad . \tag{C20}$$

Therefore

$$\frac{\delta^*}{D_0} = \frac{1}{4}(1+m)\, K\left(\frac{|u_3|D_0}{\nu_3}\right)^{-m/1+m}\left(\frac{Vt-x}{D_0}\right)^{1/1+m} \quad , \tag{C21}$$

where

$$K = \frac{4}{1+m}\left(\frac{\delta^*}{\delta}\right)\left\{\tfrac{1}{2}(1+m)\, E\left[\frac{n}{(n+1)(n+2)}\right]^{-m}\right\}^{1/1+m} \cdot \left[\frac{|u_3|}{V}\, G\left(\frac{|u_3|}{V}, 1\right)\right]^{1/1+m} \quad , \tag{C22}$$

$\frac{\delta^*}{\delta}$ and $G\left(\frac{|u_3|}{V}, 1\right)$ are given by Equations (C18) and (C19). When n=7, Equation (C20) gives the same expression as obtained by Becker (Reference 5).

Uniformity of the Core Flow Behind the Non-steady Expansion Wave due to the Boundary Layer with 1/n Power Law Velocity Profile

In this section, the analysis used in Chapter III is extended for the boundary layer with 1/n power law velocity profile. The displacement thickness of the boundary layer behind the expansion shock is given by Equation (C21) with V replaced by U_0, and Equation (11) becomes

$$\frac{1}{\rho_3 a_3^2 |u_3|}\left(U_0 \frac{\partial p'}{\partial \bar{t}} - |u_3| \frac{\partial p'}{\partial \bar{x}}\right) + \frac{1}{|u_3|}\frac{\partial u'}{\partial \bar{x}}$$

$$= K(Re_{D_0})^{-m/1+m} \quad (\bar{t}-\bar{x})^{-m/1+m} \quad . \tag{C23}$$

Since only the effect of the boundary layer is considered, the source term due to the variation in diameter has been neglected in Equation (C23). The momentum equation is the same as Equation (12)

$$U_0 \frac{\partial u'}{\partial \bar{t}} - |u_3| \frac{\partial u'}{\partial \bar{x}} + \frac{1}{\rho_3}\frac{\partial p'}{\partial \bar{x}} = 0 \tag{C24}$$

Equations (C21) and (C22) form the set of governing equations of u´ and p´. Since the coefficients are the same as in Equations (11) and (12), the characteristics variables are the same as given by Equation (13). However, the solution to Equations (C23) and (C24) are

$$\frac{p'}{\rho_3 a_3 |u_3|} = (1+m)\, K \frac{M_0}{M_0^2 - 1}(Re_{D_0})^{-m/1+m} \quad (\bar{t}-\bar{x})^{1/1+m}$$

$$+ f(\xi) - g(\eta) \quad , \tag{C25}$$

$$\frac{u'}{|u_3|} = (1+m)\ K \frac{1}{M_0^2 - 1} (Re_{D_0})^{-m/1+m} \ (\bar{t}-\bar{x})^{1/1+m} + f(\xi) + g(\eta) \quad , \qquad \text{(C26)}$$

with $f(\xi)$ and $g(\eta)$ are unknown functions.

Following the same procedure used in Section III-4, $g(\eta)=0$ and Equations (C25) and (C26) become

$$\frac{p'}{\rho_3 a_3 |u_3|} = (1+m)\ K \frac{M_0}{M_0^2 - 1} (Re_{D_0})^{-m/1+m} \ (\bar{t}-\bar{x})^{1/1+m} + f_I(\xi) \quad . \qquad \text{(C27)}$$

$$\frac{u'}{|u_3|} = (1+m)\ K \frac{1}{M_0^2 - 1} (Re_{D_0})^{-m/1+m} \ (\bar{t}-\bar{x})^{1/1+m} + f_I(\xi) \quad . \qquad \text{(C28)}$$

Using the same boundary condition at the nozzle inlet as in Section III-5 yields

$$f_I(\xi) = -(1+m)\ K(Re_{D_0})^{-m/1+m} \left(\frac{\xi}{\alpha}\right)^{1/1+m} \qquad \text{(C29)}$$

$$\cdot \frac{(1 + \frac{\gamma-1}{2} M_3^2)(M_0^2 - 1) + (1 - M_3^2)(1 + \frac{\gamma-1}{2} M_3 M_0)}{(1 + \frac{\gamma-1}{2} M_3)(M_0^2 - 1)(1 - M_3^2)} , \quad \text{for } \xi \le 0,$$

where $\qquad \alpha \equiv - \dfrac{1 - M_3}{M_0 - 1} \quad .$

Therefore, for the boundary layer with $\frac{u}{u_e} = (\frac{y}{\delta})^{1/n}$ velocity profile, the static pressure and velocity perturbations in the core flow behind the expansion wave are

$$\frac{p'}{\rho_3 a_3 |u_3|} = (1+m)\ K(Re_{D_0})^{-m/1+m} \left[\frac{M_0}{M_0^2 - 1} (\bar{t}-\bar{x})^{1/1+m} - \left(\frac{\xi}{\alpha}\right)^{1/1+m} \cdot \frac{(1 + \frac{\gamma-1}{2} M_3^2)(M_0^2 - 1) + (1 - M_3^2)(1 + \frac{\gamma-1}{2} M_3 M_0)}{(1 + \frac{\gamma-1}{2} M_3)(M_0^2 - 1)(1 - M_3^2)} \right] , \qquad \text{(C30)}$$

$$\frac{u'}{|u_3|} = (1+m)\ K(Re_{D_0})^{-m/1+m}\left[\frac{1}{M_0^2 - 1}\ (\bar{t}-\bar{x})^{1/1+m} - (\frac{\xi}{\alpha})^{1/1+m}\right.$$

$$\left.\frac{(1 + \frac{\gamma-1}{2} M_3^2)(M_0^2 - 1) + (1 - M_3^2)(1 + \frac{\gamma-1}{2} M_3 M_0)}{(1 + \frac{\gamma-1}{2} M_3)(M_0^2 - 1)(1 - M_3^2)}\right] . \qquad (C31)$$

The perturbations on speed of sound, Mach number, static temperature, stagnation temperature and stagnation pressure are the same as Equations (43) to (47). When n=7, Equations (C30) and (C-31) are identical to Equations (41) and (42).

APPENDIX D: THE DERIVATION AND SOLUTION OF EQUATIONS (64a) AND (64b)

Equations (61) and (62) in Chapter IV are restated here for convenience,

$$\frac{1}{a_e^2}\left(\frac{\partial p_e}{\partial t} + u_e\frac{\partial p_e}{\partial x}\right) + \rho_e\frac{\partial u_e}{\partial x} = \frac{4}{D_0}\frac{\partial}{\partial t}\left[\rho_e\left(1 - \frac{\rho_w}{\rho_e}\right)\frac{\delta}{8}\right]$$

$$+ \frac{4}{D_0}\frac{\partial}{\partial x}\left[\rho_e u_e\left(\frac{2}{9} - \frac{7}{72}\frac{\rho_w}{\rho_e}\right)\delta\right] \quad , \tag{D1}$$

$$\rho_e\left(\frac{\partial u_e}{\partial t} + u_e\frac{\partial u_e}{\partial x}\right) + \frac{\partial p_e}{\partial x} = 0 \quad . \tag{D2}$$

Since the temperature of wall remains at T_{40} during the whole test time, $\frac{\rho_w}{\rho_e} = \frac{T_e}{T_{40}}$, and Equation (D1) becomes

$$\frac{1}{a_e^2}\left(\frac{\partial p_e}{\partial t} + u_e\frac{\partial p_e}{\partial x}\right) + \rho_e\frac{\partial u_e}{\partial x} = \frac{4}{D_0}\frac{\partial}{\partial t}\left[\rho_e\left(1 - \frac{T_e}{T_{40}}\right)\frac{\delta}{8}\right]$$

$$+ \frac{4}{D_0}\frac{\partial}{\partial x}\left[\rho_e u_e\left(\frac{2}{9} - \frac{7}{72}\frac{T_e}{T_{40}}\right)\delta\right] \quad . \tag{D3}$$

Let $a_e = a_i+a'$, $\rho_e = \rho_i+\rho'$, $p_e = p_i+p'$, and $u_e = u_i+u'$, where a_i, ρ_i, p_i, and u_i are given by Equations (54), (56), (57) and (58). Assuming $\frac{a'}{a_i}$, $\frac{\rho'}{\rho_i}$, $\frac{p'}{p_i}$ and $\frac{u'}{u_i}$ are of the order of δ/D_0, which is smaller than $\frac{\partial p_i}{\partial t}$, $\frac{\partial p_i}{\partial x}$, $\frac{\partial u_i}{\partial t}$, or $\frac{\partial u_i}{\partial x}$, Equations (D3) and (D2) can be simplified into

$$\frac{1}{a_i^2}\left(\frac{\partial p_i}{\partial t} + u_i\frac{\partial p_i}{\partial x}\right) + \rho_i\frac{\partial u_i}{\partial x} + \frac{1}{a_i^2}\left(\frac{\partial p'}{\partial t} + u_i\frac{\partial p'}{\partial x} + u'\frac{\partial p_i}{\partial x}\right)$$

$$- \frac{2}{a_i^{\,2}}\frac{a'}{a_i}\left(\frac{\partial p_i}{\partial t} + u_i\frac{\partial p_i}{\partial x}\right) + \rho'\frac{\partial u_i}{\partial x} + \rho_i\frac{\partial u'}{\partial x}$$

$$= \frac{4}{D_0}\frac{\partial}{\partial t}\left[\rho_i\left(1 - \frac{T_i}{T_{40}}\right)\frac{\delta}{8}\right] + \frac{4}{D_0}\frac{\partial}{\partial x}\left[\rho_i u_i\left(\frac{2}{9} - \frac{7}{72}\frac{T_i}{T_{40}}\right)\delta\right] \quad . \tag{D4}$$

and
$$\rho_i\left(\frac{\partial u_i}{\partial t} + u_i \frac{\partial u_i}{\partial x}\right) + \frac{\partial p_i}{\partial x} + \rho_i\left(\frac{\partial u'}{\partial t} + u_i \frac{\partial u'}{\partial x} + u' \frac{\partial u_i}{\partial x}\right)$$
$$+ \rho'\left(\frac{\partial u_i}{\partial t} + u_i \frac{\partial u_i}{\partial x}\right) + \frac{\partial p'}{\partial x} = 0 \quad . \qquad \text{(D5)}$$

In Equations (D4) and (D5), terms of order $(\frac{\delta}{D_0})^2$ and higher are neglected. Since

$$\frac{1}{a_i^2}\left(\frac{\partial p_i}{\partial t} + u_i \frac{\partial p_i}{\partial x}\right) + \rho_i \frac{\partial u_i}{\partial x} = 0 \quad ,$$

$$\rho_i\left(\frac{\partial u_i}{\partial t} + u_i \frac{\partial u_i}{\partial x}\right) + \frac{\partial p_i}{\partial x} = 0 \quad ,$$

and the entropy of the gas is constant, i.e.

$$\frac{a'}{a_i} = \frac{\gamma-1}{2\gamma}\frac{p'}{p_i} = \frac{\gamma-1}{2}\frac{\rho'}{\rho_i} \quad ,$$

Equations (D4) and (D5) become

$$\frac{1}{a_i^2}\left(\frac{\partial p'}{\partial t} + u_i \frac{\partial p'}{\partial x} + u' \frac{\partial p_i}{\partial x}\right) - \frac{\gamma-1}{\gamma}\frac{1}{a_i^2}\frac{p'}{p_i}\left(\frac{\partial p_i}{\partial t} + u_i \frac{\partial p_i}{\partial x}\right) + \rho_i \frac{\partial u'}{\partial x}$$
$$+ \rho' \frac{\partial u_i}{\partial x} = \frac{4}{D_0}\left\{\frac{1}{8}\frac{\partial}{\partial t}\left[\rho_i\left(1 - \frac{T_i}{T_{40}}\right)\delta\right]\right.$$
$$\left. + \frac{\partial}{\partial x}\left[\rho_i u_i\left(\frac{2}{9} - \frac{7}{72}\frac{T_i}{T_{40}}\right)\delta\right]\right\} \quad , \qquad \text{(D6)}$$

$$\rho_i\left(\frac{\partial u'}{\partial t} + u_i \frac{\partial u'}{\partial x} + u' \frac{\partial u_i}{\partial x}\right) + \frac{p'}{a_i^2}\left(\frac{\partial u_i}{\partial t} + u_i \frac{\partial u_i}{\partial x}\right) + \frac{\partial p'}{\partial x} = 0 \quad . \qquad \text{(D7)}$$

These two equations are the same as Equations (64a) and (64b), respectively. Equations (D6) and (D7) can be rewritten as

$$\frac{1}{a_i^2}\frac{\partial p'}{\partial t} + \frac{\partial u_i}{a_i^2}\frac{\partial p'}{\partial x} + \rho_i \frac{\partial u'}{\partial x} + \gamma\frac{1}{a_i^2}\frac{\partial u_i}{\partial x}p' + \frac{1}{a_i^2}\frac{\partial p_i}{\partial x}u' - \frac{4}{D_0}\left\{\frac{1}{8}\frac{\partial}{\partial t}\right.$$
$$\left.\cdot\left[\rho_i\left(1 - \frac{T_i}{T_{40}}\right)\delta\right] + \frac{\partial}{\partial x}\left[\rho_i u_i\left(\frac{2}{9} - \frac{7}{72}\frac{T_i}{T_{40}}\right)\delta\right]\right\} = 0, \qquad \text{(D8)}$$

$$\frac{\partial p'}{\partial x} + \rho_i \frac{\partial u'}{\partial t} + \rho_i u_i \frac{\partial u'}{\partial x} - \frac{1}{a_i^2}\frac{1}{\rho_i}\frac{\partial p_i}{\partial x} p' + \rho_i \frac{\partial u_i}{\partial x} u' = 0 \quad . \tag{D9}$$

Since p_i, u_i, T_i and δ are given by Equations (57), (58), (55) and (63), respectively, it can be shown that for $\gamma=1.4$,

$$\frac{\partial p_i}{\partial x} = \frac{7}{6}\frac{p_4}{a_{40}}\frac{1}{t}\left(\frac{5}{6} + \frac{x}{6a_{40}t}\right)^6 \quad , \tag{D10}$$

$$\frac{\partial u_i}{\partial x} = -\frac{7}{6}\frac{p_4}{a_{40}}\frac{x}{t^2}\left(\frac{5}{6} + \frac{x}{6a_{40}t}\right)^6 \quad , \tag{D11}$$

$$\frac{\partial}{\partial t}\left[\rho_i\left(1 - \frac{T_i}{T_{40}}\right)\delta\right] = \frac{1}{3}\left(\frac{0.196}{3}\right)^{4/5} \rho_{40}(a_{40}t)^{4/5}\left(\frac{\nu_{40}}{a_{40}}\right)^{1/5}$$

$$\cdot\left(\frac{5}{6} + \frac{x}{6a_{40}t}\right)^4 \frac{1}{t}\left(1 - \frac{x}{a_{40}t}\right)^{7/5}\left(\frac{2}{3} + \frac{19}{30}\frac{x}{a_{40}t} + \frac{11}{10}\frac{x^2}{a_{40}{}^2t^2}\right) , \tag{D12}$$

and

$$\frac{\partial}{\partial x}\left[\rho_i u_i\left(\frac{2}{9} - \frac{7}{72}\frac{T_i}{T_{40}}\right)\delta\right] = -\frac{5}{6}\left(\frac{0.196}{3}\right)^{4/5} \rho_{40}(a_{40}t)^{4/5}$$

$$\frac{\nu_{40}}{a_{40}}^{1/5}\left(\frac{5}{6} + \frac{x}{6a_{40}t}\right)^4 \frac{1}{t}\left(1 - \frac{x}{a_{40}t}\right)^{7/5}\left(-\frac{91}{216 \times 2}\right.$$

$$\left. - \frac{97}{720}\frac{x}{a_{40}t} + \frac{49}{5 \times 216}\frac{x}{a_{40}{}^2t^2}\right) . \tag{D13}$$

Equations (D8) and (D9) form a system of quasi-linear partial differential equations with unknowns p' and u'. Following the procedure mentioned in Section 21 and 22 in Reference 14, it can be shown that Equations (D8) and (D9) form a hyperbolic system of equations with the slopes of characterisitics given by

$$\frac{dx}{dt} = a_i + u_i \quad ,$$

and

$$\frac{dx}{dt} = -a_i + u_i \quad .$$

The two characteristic variables are chosen as

$$\psi = 1 - \frac{x}{a_{40}t} \quad , \tag{D14}$$

$$\omega = t\left(\frac{5}{6} + \frac{x}{6a_{40}t}\right)^3 \quad . \tag{D15}$$

The physical meaning of these two variables has been explained in Chapter IV. In terms of ψ and ω, x and t become

$$x = a_{40}\omega \frac{1-\psi}{(1 - \frac{\psi}{6})^3} \quad , \tag{D16}$$

and

$$t = \frac{\omega}{(1 - \frac{\psi}{6})^3} \quad . \tag{D17}$$

Equations (D8) and (D9) can be replaced by

$$\frac{1}{a_i^2} p'_\omega + \frac{\rho_i}{a_i} u'_\omega + \left[p'\left(\gamma \frac{1}{a_i^2} \frac{\partial u_i}{\partial x} - \frac{1}{a_i^3} \frac{1}{\rho_i} \frac{\partial p_i}{\partial x}\right) + u'\left(\frac{\rho_i}{a_i} \frac{\partial u_i}{\partial x} + \frac{1}{a_i^2} \frac{\partial p_i}{\partial x}\right)\right] t_\omega - \frac{4}{D_0}\left\{\frac{1}{8} \frac{\partial}{\partial t}\left[\rho_i \left(1 - \frac{T_i}{T_{40}}\right) \delta\right] + \frac{\partial}{\partial x}\left[\rho_i u_i \left(\frac{2}{9} - \frac{7}{72} \frac{T_i}{T_{40}}\right) \delta\right]\right\} t_\omega = 0 \quad , \tag{D18}$$

$$\frac{1}{a_i} p'_\psi - \frac{\rho_i}{a_i} u'_\psi + \left[p'\left(\gamma \frac{1}{a_i} \frac{\partial u_i}{\partial x} + \frac{1}{a_i^3} \frac{1}{\rho_i} \frac{\partial p_i}{\partial x}\right) + u'\left(- \frac{\rho_i}{a_i} \frac{\partial u_i}{\partial x} + \frac{1}{a_i^2} \frac{\partial p_i}{\partial x}\right)\right] t_\psi - \frac{4}{D_0}\left\{\frac{1}{8} \frac{\partial}{\partial t}\left[\rho_i \left(1 - \frac{T_i}{T_{40}}\right) \delta\right] + \frac{\partial}{\partial x}\left[\rho_i u_i \left(\frac{2}{9} - \frac{7}{72} \frac{T_i}{T_{40}}\right) \delta\right]\right\} t_\psi = 0 \quad . \tag{D19}$$

When a_i, ρ_i, $\frac{\partial p_i}{\partial x}$, and $\frac{\partial u_i}{\partial x}$ on the left-hand side of Equation (D18), are substituted by Equations (54), (56), (D10), and (D11), Equation (D18) becomes

$$\frac{1}{a_{40}} p'_\omega + \rho_{40}(1 - \tfrac{\psi}{6})^6 \quad u'_\omega + \left[\frac{5}{3}\frac{\rho_{40}}{t}(1 - \tfrac{\psi}{6})^6 \quad u' + \frac{1}{3}\frac{1}{a_{40}t} p'\right]t_\omega$$

$$- 4\,\frac{a_{40}}{D_0}\left\{\frac{1}{8}\frac{\partial}{\partial t}\left[\rho_i \;(1 - \frac{T_i}{T_{40}})\delta\right] + \frac{\partial}{\partial x}\left[\rho_i u_i\;(\tfrac{2}{9} - \tfrac{7}{72}\frac{T_i}{T_{40}})\,\delta\right]\right\}t_\omega \;=\; 0,$$

or

$$\left[\rho_{40}(1 - \tfrac{\psi}{6})^6 \; t\; u' + \frac{t}{a_{40}} p'\right]_\omega + \frac{2}{3}\left[\rho_{40}(1 - \tfrac{\psi}{6})^6 \; u' - \frac{p'}{a_{40}}\right]t_\omega$$

$$- 4\,\frac{a_{40}}{D_0}\,(1 - \tfrac{\psi}{6})^2\left\{\frac{1}{8}\frac{\partial}{\partial t}\left[\rho_i\;(1 - \frac{T_i}{T_{40}})\delta\right] + \frac{\partial}{\partial x}\left[\rho_i u_i\,(\tfrac{2}{9}\right.\right.$$

$$\left.\left. - \tfrac{7}{72}\frac{T_i}{T_{40}})\,\delta\right]\right\}t_\omega \;=\; 0 \quad . \tag{D20}$$

Similarly, Equation (D19) becomes

$$-\left[\rho_{40}(1 - \tfrac{\psi}{6})^6 \; t\; u' - \frac{t}{a_{40}} p'\right]_\psi + \left[\rho_{40}(1 - \tfrac{\psi}{6})^6 \; u' + \frac{p'}{a_{40}}\right]t_\psi$$

$$- \rho_{40}(1 - \tfrac{\psi}{6})^5 \; tu' - 4\,\frac{a_{40}}{D_0}\,(1 - \tfrac{\psi}{6})^2\left\{\frac{1}{8}\frac{\partial}{\partial t}\left[\rho_i\;(1 - \frac{T_i}{T_{40}})\,\delta\right]\right.$$

$$\left. + \frac{\partial}{\partial x}\left[\rho_i u_i\,(\tfrac{2}{9} - \tfrac{7}{72}\frac{T_i}{T_{40}})\,\delta\right]\right\}t_\psi \;=\; 0 \quad . \tag{D21}$$

Substitute $\frac{\partial}{\partial t}\left[\rho_i\left(1 - \frac{T_i}{T_{40}}\right)\delta\right]$, $\frac{\partial}{\partial x}\left[\rho_i u_i\left(\frac{2}{9} - \frac{7}{72}\,\frac{T_i}{T_{40}}\right)\delta\right]$, t_ω and t_ψ with the appropriate functions of ψ and ω, and define

$$\Lambda \;\equiv\; \rho_{40}(1 - \tfrac{\psi}{6})^6 \; tu' + \frac{t}{a_{40}} p' \quad , \tag{D22}$$

$$\Delta \;\equiv\; \rho_{40}(1 - \tfrac{\psi}{6})^6 \; tu' - \frac{t}{a_{40}} p' \quad , \tag{D23}$$

Equations (D20) and (D21) become

$$\Lambda_\omega + \frac{2}{3}\frac{\Delta}{\omega} - \frac{4a_{40}}{D_0}\left(\frac{0.196}{3}\right)^{4/5} \rho_{40}a_{40}{}^{4/5} \left(\frac{\nu_{40}}{a_{40}}\right)^{1/5} \omega^{4/5} \left(1 - \frac{\psi}{6}\right)^{3/5}$$

$$\cdot\ \psi^{7/5} \left[\frac{7}{20} - \frac{401}{72 \times 36}\psi + \frac{13}{60 \times 27}\psi^2\right] = 0 \quad , \qquad \text{(D24)}$$

$$\Delta_\psi + \frac{\Delta}{2}\frac{1}{1 - \frac{\psi}{6}} + \frac{2a_{40}}{D_0}\left(\frac{0.196}{3}\right)^{4/5} \rho_{40}a_{40}{}^{4/5} \left(\frac{\nu_{40}}{a_{40}}\right)^{1/5} \omega^{9/5} \left(1 - \frac{\psi}{6}\right)^{-2/5}$$

$$\cdot\ \psi^{7/5} \left[\frac{7}{20} - \frac{401}{72 \times 36}\psi + \frac{13}{60 \times 27}\psi^2\right] = 0 \quad . \qquad \text{(D25)}$$

Equation (D25) yields

$$\Delta = -\frac{2a_{40}}{D_0}\left(\frac{0.196}{3}\right)^{4/5} \rho_{40}a_{40}{}^{4/5} \left(\frac{\nu_{40}}{a_{40}}\right)^{1/5} \omega^{9/5} \left(1 - \frac{\psi}{6}\right)^{3}$$

$$\cdot \int \left(1 - \frac{\psi}{6}\right)^{-17/5} \psi^{7/5} \left[\frac{7}{20} - \frac{401}{72 \times 36}\psi + \frac{13}{60 \times 27}\psi^2\right] d\psi \quad ,$$

satisfying the boundary condition that at the head of expansion wave (i.e. ψ=0) u' and p' are both zero. If $(1 - \frac{\psi}{6})^{-17/5}$ is expanded by the binomial series, then the above equation becomes

$$\Delta = -\frac{10a_{40}}{D_0}\left(\frac{0.196}{3}\right)^{4/5} \rho_{40}a_{40}{}^{4/5} \left(\frac{\nu_{40}}{a_{40}}\right)^{1/5} \omega^{9/5} \left(1 - \frac{\psi}{6}\right)^{3}$$

$$\cdot\ \psi^{12/5} \left[\frac{0.35}{12} + \frac{0.04363}{17}\psi - \frac{0.00692}{22}\psi^2\right] \quad . \qquad \text{(D26)}$$

Combining Equation (D24) and (D26) yields

$$\Lambda = \frac{20}{9}\frac{a_{40}}{D_0}\left(\frac{0.196}{3}\right)^{4/5} \rho_{40}a_{40}{}^{4/5} \left(\frac{\nu_{40}}{a_{40}}\right)^{1/5} \omega^{9/5} \left\{\frac{5}{3}\left(1 - \frac{\psi}{6}\right)^{3}\right.$$

$$\cdot\ \psi^{12/5} \left[\frac{0.35}{12} + \frac{0.04363}{17}\psi - \frac{0.00692}{22}\psi^2\right] + \left(1 - \frac{\psi}{6}\right)^{3/5} \psi^{7/5}$$

$$\left.\cdot \left[\frac{7}{20} - \frac{401}{72 \times 36}\psi + \frac{13}{60 \times 27}\psi^2\right]\right\} \quad , \qquad \text{(D27)}$$

satisfying the boundary condition that at t=0 (i.e. ω=0), u' and p' are both zero.

From Equations (D26) and (D27) it can be shown that

$$\frac{p'}{p_4} = 14\left(\frac{0.196}{3}\right)^{4/5}\left(\frac{a_{40}t}{D_0}\right)^{4/5}\left(\frac{\nu_{40}}{a_{40}D_0}\right)^{1/5}\left(1-\frac{\psi}{6}\right)^6 \psi^{7/5}$$
$$\cdot\left\{\frac{37}{54}\left(1-\frac{\psi}{6}\right)^{12/5}\psi\left[\frac{0.35}{12}+\frac{0.04363}{17}\psi-\frac{0.00692}{22}\psi^2\right]\right.$$
$$\left.+\frac{1}{9}\left[\frac{7}{20}-\frac{401}{72\times 36}\psi+\frac{13}{60\times 27}\psi^2\right]\right\}, \qquad \text{(D28)}$$

and

$$\frac{u'}{a_{40}} = 10\left(\frac{0.196}{3}\right)^{4/5}\left(\frac{a_{40}t}{D_0}\right)^{4/5}\left(\frac{\nu_{40}}{a_{40}D_0}\right)^{1/5}\psi^{7/5}$$
$$\cdot\left\{-\frac{17}{54}\left(1-\frac{\psi}{6}\right)^{12/5}\psi\left[\frac{0.35}{12}+\frac{0.04363}{17}\psi-\frac{0.00692}{22}\psi^2\right]\right.$$
$$\left.+\frac{1}{9}\left[\frac{7}{20}-\frac{401}{72\times 36}\psi+\frac{13}{60\times 27}\psi^2\right]\right\}, \qquad \text{(D29)}$$

the same as Equations (72) and (73) in Chapter IV.

REFERENCES

1. Whitfield, J.D., Schueler, C.J., and Starr, R.F., "High Reynolds Number Transonic Wind Tunnels -- Blowdown or Ludwieg Tube," Facilities and Techniques for Aerodynamic Testing at Transonic Speeds and High Reynolds Number, AGARD-CP-83-71, 1971.

2. Enkenhus, K.R. and Merritt, D.L., "Evaluation of Two Types of Facilities to Fulfill the Need for High Reynolds Number Transonic Testing," NOLTR71-147, July 1971, Naval Ordnance Laboratory, White Oak, Silver Spring, MD.

3. Ludwieg, H., "Der Rohrwindkanal," Zeitschrift für Flugwisserschaften, Vol. 3, No. 7, July 1955, pp. 206-216.

4. Mirels, H., "Boundary Layer Behind Shock or Thin Expansion Waves Moving into Stationary Fluid," TN3712, 1956, NACA.

5. Becker, E., "Reibungswirkungen beim Rohrwindkanal," Mitt. aus dem Max-Planck-Institut fuer Stroemungsforschung u.d. Aerodynamischen Versuchsanstalt, No. 20, 1958.

6. Becker, E., "Instationäre Grenzschichten Hinter Verdichtungsstössen und Expansionswellen," Progress in Aeronautical Sciences, Vol. 1, 1961, pp. 104-173.

7. Cable, A.J. and Cox, R.N., "The Ludwieg Pressure Tube Supersonic Wind Tunnel," Aeronautical Quarterly, Vol 14, Part 2, May 1963, pp. 143-157.

8. Starr, R.F. and Schuler, C.J., "Experimental Studies of a Ludwieg Tube High Reynolds Number Transonic Tunnel," AIAA Paper No. 73-212, 1973.

9. Trimpi, R.L. and Cohen, N.B., "A Theory for Predicting the Flow of Real Gases in Shock Tubes, with Experimental Verification," TN3375, 1955, NACA.

10. Mirels, H. and Braun, W.H., "Nonuniformities in Shock-Tube Flow Due to Unsteady-Boundary-Layer Action," TN4021, 1957, NACA.

11. Demyanov, Yu A., "The Influence of the Boundary Layer on the Character of the Flow of Gas in a Tube Behind a Moving Shock Wave," Prikladnaia Mathematika i Mekhanika, Vol. 21, No. 4, 1957. pp. 473-477; also Translation 796, 1959, R.A.E. Library.

12. Spence, D.A. and Woods, B.A., "Boundary Layer and Combustion Effects in Shock Tube Flows," Colston Papers, Vol. 11, Proceedings of the Eleventh Symposium of the Colston Research Society, Butterworths, London, April 1959.

13. Spence, D.A. and Woods, B.A., "A Review of Theoretical Treatments of Shock-Tube Attenuation," Journal of Fluid Mechanics, Vol. 19, June 1964, pp. 161-174.

14. Courant, R. and Friedrichs, K.O., Supersonic Flow and Shock Waves, Interscience, New York, 1948.

15. Sasman, P.K. and Cresci, R.J., "Compressible Turbulent Boundary Layer with Pressure Gradient and Heat Transfer," AIAA Journal, Vol. 4, No. 1, January 1966, pp. 19-25.

16. Russell, D.A. and Tong, K.-O., "Aerodynamics of High-Performance Ludwieg Tubes," AIAA Journal, Vol. 11, No. 5, May 1973, pp. 642-648.

17. Liepmann, H.W. and Roshko, A., Elements of Gasdynamics, John Wiley & Sons, New York, 1957.

18. Hall, J.G., "Laminar Boundary Layers Developed Within Unsteady Expansion and Compression Waves," AIAA Journal, Vol. 10, No. 4, 1972, pp. 499-505.

19. Chester, W., "The Propagation of Shock Waves along Ducts of Varying Cross-Section," Advance in Applied Mechanics, Vol. 6, 1960, pp. 119-152.

20. Schlichting, H., Boundary-Layer Theory, McGraw-Hill, New York, 1968.

21. Kutateladze, S.S. and Leont'ev, A.I., Turbulent Boundary Layers in Compressible Gases, Edward Arnold, London, 1964.

BIOGRAPHICAL DATA

Name:	Kwok-On Tong
Date of Birth:	February 10, 1945
Place of Birth:	Canton, China
Parentage:	Mr. and Mrs. Fai-Chow Tong Hong Kong
Secondary Education:	Clementi Middle School Hong Kong (1957 - 1963)
Degrees:	B.S.E. in Mechanical Engineering Cheng Kung University Tainan, Taiwan, China 1967
	M.S. in Aeronautics and Astronautics University of Washington Seattle, Washington 1969